1989

Rotoreflected Double-Beam Thermal Lens Spectrometry and Simultaneous Thermal Lens and Fluorescence Detection for High Performance Microbore Liquid Chromatography

Steven Craig Hall
Loyola University Chicago

ROTOREFLECTED DOUBLE-BEAM THERMAL LENS SPECTROMETRY AND SIMULTANEOUS THERMAL LENS AND FLUORESCENCE DETECTION FOR HIGH PERFORMANCE MICROBORE LIQUID CHROMATOGRAPHY

by

Steven Craig Hall

A Dissertation Submitted to the Faculty of the Graduate School of Loyola University of Chicago in Partial Fulfillment of the Requirements For the Degree of Doctor of Philosophy

May

1989

ACKNOWLEDGMENTS

The author would like to thank his research advisor Dr. Yen Yang for providing guidance and exercising patience throughout the course of this project. Gratitude is extended to Dr. Alanah Fitch for use of her digital storage oscilloscope, Dr. A. K. Jameson for use of his argon-ion laser, Mr. Eugene Zaluzec for his electronics expertise, and Dr. Stephen White and the National Bureau of Standards for providing the SRC II sample. Without these contributions this work would not have been possible.

The author thanks the Loyola University Department of Chemistry and Graduate School for providing financial assistance throughout his tenure at the university in the form of teaching and research assistantships and a Dissertation Fellowship.

The author thanks his parents for sacrifices they have made on behalf of their son pursuing this degree and for never doubting he could accomplish it. In addition, the author thanks his many friends for their support and numerous meals they have furnished over the years.

A special thanks is extended to Marijo De La Cruz and Pamela Schrock for their constant humor and emotional support provided throughout this endeavor.

VITA

The author, Steven Craig Hall, is the son of Chester Leigh Hall, II and Esther Yoshioka Hall. He was born November 29, 1956, in Fort Worth, Texas.

His elementary and junior high school education was obtained in the public schools of Jefferson County, Colorado. His secondary education was completed in 1975 at Lakewood Senior High School in Lakewood, Colorado.

In August, 1975, Mr. Hall entered Grinnell College in Grinnell, Iowa, receiving the degree of Bachelor of Arts with a major in Chemistry in May, 1979. He was awarded a Grinnell Honor Scholarship during his tenure at Grinnell College. In 1977, he became a student affiliate member of the American Chemical Society and became a full member in 1979.

In March 1980, Mr. Hall became employed as a Research Assistant in the Analytical and Technical Services Laboratory at Baxter-Travenol Laboratories, Inc. in Morton Grove, Illinois. In 1982, he was promoted to Research Associate in the Trace Organic Analysis and Mass Spectrometry Laboratory at Baxter-Travenol.

In August 1984, Mr. Hall became a graduate assistant in the chemistry department of Loyola University of Chicago. He was awarded a Loyola University Dissertation Fellowship in August 1987.

Mr. Hall has coauthored a publication with Yen Yang and Marijo S. De La Cruz entitled "Pump/Probe Thermal Lens Spectrometry with Oppositely Propagated Beams for Liquid Chromatography". This paper appeared in Analytical Chemistry, volume 54, 1986. He has also coauthored a publication with Yen Yang entitled "Differential Thermal Lens Spectrometry Based on High Frequency Modulation and Rotoreflective Double-Beam Configuration". This paper appeared in Applied Spectroscopy, volume 43, 1988.

TABLE OF CONTENTS

LIST OF TABLES

LIST OF ILLUSTRATIONS

CONTENTS FOR APPENDICES

CHAPTER 1

INTRODUCTION

EARLY DEVELOPMENT OF THE THERMAL LENS AS AN ANALYTICAL TOOL

The thermal lens effect was first reported by J. P. Gordon et al. in 1965 (1). While performing experiments to enhance Raman scattering, Gordon and his coworkers observed several unexpected phenomena after positioning cells containing polar and non-polar liquids inside the resonator of a helium-neon laser. The laser was operated at a wavelength of 632.8 nm. Using a shutter to turn on and off the laser beam, transients were observed on an oscilloscope which showed an initial increase in power density at the beam center followed by gradual decrease to a steady state. Formation of these transients was observed to be time dependent with time constants on the order of seconds. Observation of the beam spot size on the mirror of the cell side of the resonator showed it to be larger than the spot size on the mirror at the opposite end of the resonator. Without the cell present in the cavity, the two spot sizes were the same. This led Gordon et al. to postulate that as the beam passed through the cell it was experiencing a

lens-like effect. Specifically, by estimating the spot sizes and knowing the cell path lengths, it was shown that the cell acted as a diverging lens possessing a focal length equal to approximately that of the resonator mirrors.

The formation of this diverging lens was hypothesized to originate from a change in the dielectric constant of the liquid medium near the beam. It was also speculated that the heat required to form the temperature gradients necessary for this change to occur originated from the heat produced through absorption of the laser light by the liquid medium; thus the term "thermal lens." A model was then proposed to explain this effect.

For the sake of simplicity, this model was based on the assumption that the change in refractive index of the liquid medium around the laser beam center is parabolic in nature, although it is in fact Gaussian because the laser beam intensity profile is Gaussian. Also, parabolic the assumption is a valid approximation for the refractive index gradient profile at the beam center. The model showed that the total change in refractive index from the beam center to the beam edge was 7.5×10^{-5} and that this change required a temperature differential of approximately 0.0075°. The amount of heat necessary to produce this temperature change can be generated by an absorption of 10^{-3} to 10^{-4} cm^{-1}. From their model, Gordon et al. derived

the following equation to describe the time dependent focal length of the thermal lens:

$$F(t) = \frac{\pi k \omega^2 (1+t_c/2t)}{Pbl(dn/dT)} \qquad (1)$$

where

k = thermal conductivity (watts $cm^{-1} \cdot C^{-1}$)
ω = laser beam radius (cm)
P = laser power (watts)
l = path length (cm)
b = absorption coefficient (cm^{-1})
dn/dT = refractive index variation with temperature

and

$$t_c = \frac{\rho \omega^2 C}{4k} \qquad (2)$$

where

ρ = density (g cm^{-3})
C = specific heat (joule $g^{-1} \cdot C^{-1}$).

Thus, the thermal lens effect is simply a heat induced phenomenon. When a laser beam possessing a Gaussian intensity profile passes through a solution which absorbs at the laser wavelength the solution is heated. This heat is produced by non-radiative relaxation of molecules in excited electronic states and is most intense at locations closest to the beam. As a result, expansion of the solution produces temperature, density, and refractive index profiles illustrated in Figure 1. Since most liquids have a positive coefficient of thermal expansion and a negative refractive index with temperature change, the absorbing solution behaves as a diverging lens.

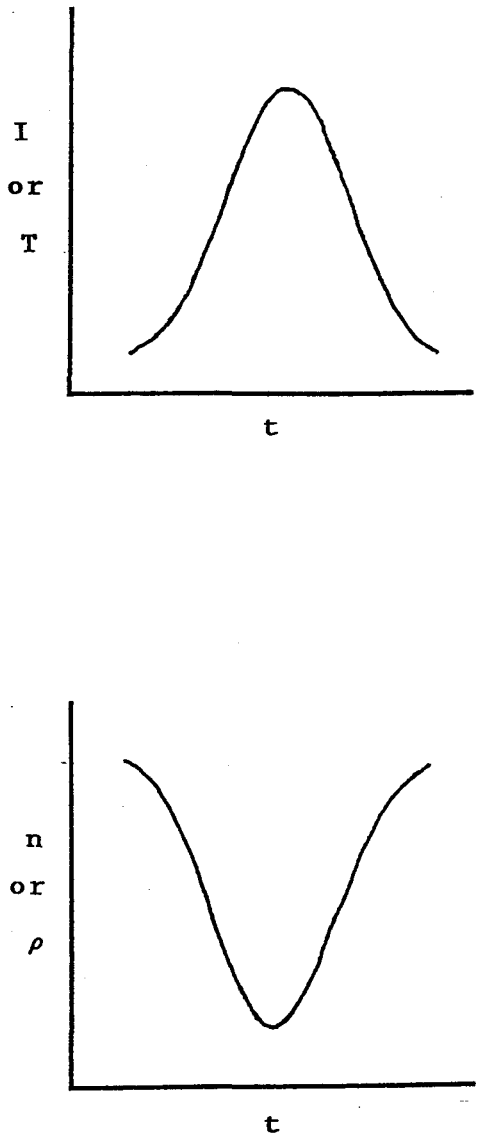

Figure 1. Density, $\rho(t)$; refractive index, n(t) and temperature, T(t) profiles created by a laser beam with a Gaussian intensity profile, I(t), traveling through an absorbing solution, t = time.

Thus, an increase in laser beam spot size is observed in the far-field due to thermal lens formation. Equation 1 demonstrates that thermal lens formation is enhanced in solvents having a low thermal conductivity and a large refractive index with temperature change. These two parameters are satisfied by non-polar solvents, notably carbon tetrachloride and benzene. Equation 1 also indicates that thermal lens formation is time dependent. When a shutter is used to turn on and off the laser beam, this time dependency becomes evident by observing the thermal lens transient. Once the laser is turned on (t=0), an instantaneous temperature rise takes place in the absorbing solution followed by a gradual decay to a steady state (t=∞). The steady state focal length, f(∞), is simply defined as

$$f(\infty) = -\frac{\pi k \omega^2}{P b I (dn/dT)} \qquad (3)$$

Alternatively, expressed in terms of absorbance A, Equation (3) becomes

$$f(\infty) = -\frac{\pi k \omega^2}{2.303 P (dn/dT) A} \qquad (4)$$

At steady state the rate of heat gained by the solution equals the rate of heat lost. The amount of time required to reach thermal lens steady state is dictated by the thermal lens time constant, t_c. As shown in Equation 2, t_c values vary with solution density, laser beam spot size,

solvent heat capacity, and thermal conductivity. Values for t_c can range from less than a microsecond to a few seconds (2).

After the thermal lens effect was first reported, various methods were developed to measure it. These methods relied upon observing physical changes in the properties of the laser beam once it had passed through an absorbing medium. Leite, Moore, and Whinnery used an intracavity technique. By placing a cell containing an absorbing medium at one end of the laser tube they measured the growth in spot size on the mirror located at the opposite tube end. The growth in spot size was an indirect measure of how much light the medium had absorbed. Absorbances of benzene, carbon disulfide, toluene, nitrobenzene, and carbon tetrachloride were reported (3).

Solimini expanded on this technique by incorporating a scanning spherical mirror interferometer (SSMI) into the experimental arrangement of Leite, Moore, and Whinnery. The purpose of the SSMI was to eliminate higher laser modes that were not visible by the eye. Thus, the purity of the Gaussian beam was guaranteed. It also permitted observation of the liquid's spectrum when the sample was placed inside the laser cavity. The absorbances of 29 low loss organic liquids as well as water were measured and reported (4).

In 1972 Stone reported an extra-cavity technique where the refractive index change produced by a temperature rise due to absorption causes the laser beam path to alter as the beam travels through an absorbing medium. This path change can be detected, with an interferometer, as a small phase shift in the laser beam as it emerges from the medium. Stone constructed a very sensitive interferometer which allowed for the measurement of the thermally induced phase shift for several low loss organic liquids. An attractive feature of this interferometer was that both interferometer beams passed through the sample cell. Thus, any changes in the ambient temperature, causing thermal drift, would not affect the measurement (5).

Furthermore, Dabby et al. demonstrated that in addition to phase modulation, the laser beam also undergoes a slight frequency shift as a result of the medium's refractive index change. The magnitude of the frequency shift is proportional to the amount of lensing taking place in solution. Dabby was able to measure the shift by monitoring the beam center intensity change in the far-field with an intensity-dependent detector. His rationale was that a small shift in frequency would create a large change in the far-field beam center intensity profile. Dabby demonstrated the feasibility of this technique by measuring the absorption coefficient of methylene blue dissolved in methanol (6).

Despite their reasonable accuracy and sensitivity, the methods developed to measure the thermal lens effect, prior to 1973, were not easily adaptable to most analytical applications. In 1973 Hu and Whinnery ascertained the need for a simple and sensitive method for measuring the thermal lens effect (7). They developed a method that was based on the measurement of the far-field expansion of a laser beam created by the formation of an extracavity thermal lens. The goal of their work was to test their new method by measuring the absorption coefficients of some low absorbing organic solvents and then compare their results to those obtained by the previously developed methods. Thus, they were in need of an equation that would define the absorption coefficient as a function of the fractional change in the far-field laser beam center intensity.

The derivation of this equation was based on two premises; the first being that a laser beam is completely defined, at any position, by its beam radius, ω, and its radius of curvature, R (refer to Appendix IV). Second, if a thin, diverging lens is placed at some distance beyond the beam waist then the beam is defocused beyond this lens. It was necessary to choose values of ω and R so that the fractional change in the far-field beam due to lens formation would be a maximum. In the course of their derivation Hu and Whinnery were able to show that a weak thermal lens does not diverge the beam when it is located at the beam

waist. They also demonstrated a very unique property regarding the thermal lens. Unlike conventional absorption measurements, the thermal lens signal magnitude is dependent upon the location of the sample relative to the laser beam waist. They found that maximum beam expansion occurred when the thermal lens is positioned at a point beyond the beam waist where R is a minimum. This distance is defined as, z, the confocal distance. When a thermal lens is placed at one confocal distance beyond the beam waist the following definitions applied:

$$z = \frac{\pi \omega_o^2}{\lambda} \tag{5}$$

and

$$R = \frac{2\pi \omega_o^2}{\lambda} \tag{6}$$

where ω_o = laser beam waist radius (cm)
λ = wavelength of laser (cm).

Knowing these two facts allowed Hu and Whinnery to arrive at the following equation describing the absorption coefficient, b, as a function of the change in far-field beam center intensity:

$$b = - \frac{\Delta I_{bc}}{I_{bc}(t=\infty)} \left\{ \frac{\pi k}{P l (dn/dT)} \right\} \tag{7}$$

$\Delta I_{bc} = I_{bc}(t=0) - I_{bc}(t=\infty)$
$I_{bc}(t=0)$ = far-field beam center intensity at t=0
$I_{bc}(t=\infty)$ = far-field beam center intensity at t=∞.

Thus, all that was required to obtain a thermal lens measurement was to measure the change in the far-field beam size by monitoring the light intensity at the beam center.

The experimental arrangement used by Hu and Whinnery was quite simple. After passing through a focusing lens, the beam from a He-Ne laser traveled through a cell containing an absorbing liquid. The cell was placed such that its center was one confocal distance beyond the laser beam waist. A shutter, positioned at the beam waist for sharpest chopping, acted as a switch to turn the beam on and off. A pinhole, placed in the far-field, served as a limiting aperture while a photomultiplier behind the pinhole detected any light passing through. Thermal lens transients were observed on an oscilloscope. Hu and Whinnery used this single-beam arrangement to measure the fractional beam center intensity change produced by carbon tetrachloride, cyclohexane, acetone, hexane, ethanol and methanol. From these measurements they calculated the absorption coefficients of these solvents using their newly derived equation. Their results were in general agreement with those obtained with the other thermooptical methods developed prior to 1973. Discrepancies between their results and others were attributed to variations in sample impurities.

In 1976 Swofford, Long, and Albrecht introduced a new optical arrangement for measuring the thermal lens

effect (8, 9). Their research involved measuring very weak C-H stretch vibrational transitions induced by visible light, on benzene, methyl substituted benzenes, naphthalene, and anthracene. Since these stretching vibrations have absorption coefficients on the order of 10^{-6} cm^{-1}, thermal lensing was well suited to their purpose. Swofford's dual-beam approach used two lasers. A modulated cw dye laser, serving as a heating (pump) beam, formed a pulsating thermal lens in the sample. An unmodulated beam from a HeCd laser (442nm), aligned collinearly with the pump beam, acted as a probe. The probe beam's function was to monitor the formation and deformation of the thermal lens created by the pump beam. Both beams propagated in the same direction. A bandpass filter placed before the aperture to a photomultiplier blocked the pump beam and only allowed the probe beam to pass. Synchronous detection was used to monitor the modulated probe beam. Output from the lock-in amplifier could then be recorded on a strip-chart recorder.

Figure 2 illustrates a schematic representation of the modulated pump and probe beam center intensity profiles created with the dual-beam arrangement. During the pump beam "on time" a thermal lens forms in the solution. The probe beam center intensity gradually decreases during this time interval. In the interval that the pump beam is turned off, the probe beam center intensity rises in

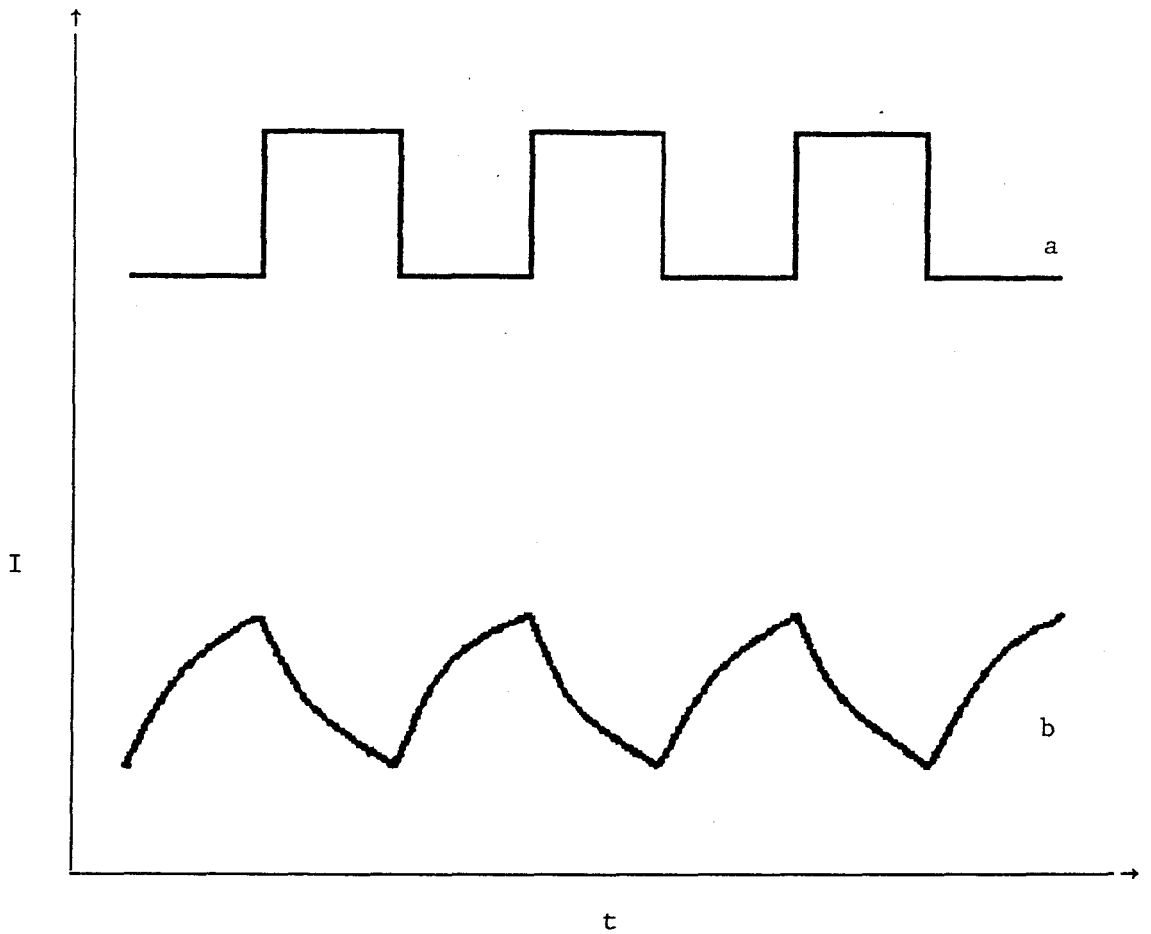

Figure 2. Pump (a) and probe (b) beam intensity profiles observed in a dual-beam thermal lens configuration; I = beam center intensity, t = time.

response to the thermal lens deformation. The observed probe beam center intensity versus time profile correlated very well with that predicted by Swofford's theoretical analysis of the dual-beam arrangement (10).

In 1979 and 1980 Dovichi and Harris expanded on the theoretical development, originally started by Hu and Whinnery, concerning the effect a thermal lens has on a laser beam depending upon where the lens was placed relative to the beam waist (2). They derived the following equation which describes the relative change in the far field laser beam spot size induced by positioning a thermal lens beyond the beam waist:

$$\frac{\Delta\omega^2}{\omega^2} = \frac{-2z_1}{f(\infty)} + \frac{(z_1^2 + z_c^2)}{(f(\infty))^2} \qquad (8)$$

where ω = far field beam spot size
$\Delta w = \omega(0) - \omega(t)$
z_1 = distance from beam waist to thermal lens
z_c = confocal distance.

This equation told them that in the case of a weak lens, $(f(\infty)^2 >> z_1 + z_c)$, the thermal lens effect depended linearly on the inverse focal length. Limiting themselves to the weak thermal lens case, they further went on to mathematically describe the positional dependence of the weak thermal lens response in terms of z_1 and z_c as:

$$\frac{\Delta\omega^2}{\omega^2} = \frac{-2.303P(dn/dT)A}{\lambda k}\left\{\frac{2z_1z_c}{z_c^2 + z_1^2}\right\} \qquad (9).$$

If Equation 9 is plotted as $\Delta I_{bc}/I_{bc}$ versus z_1, then a curve, asymmetric about the beam waist, similar to that shown in Figure 3, is obtained. Positioned before the beam waist a diverging thermal lens reduces the beam convergence thereby reducing the amount of divergence once the beam has traveled through its waist. A thermal lens placed after the beam waist serves only to enhance the divergence of the beam. Figure 3 also shows that there exists a finite distance before and after the beam waist at which a maximum thermal lens response is obtained. This is the confocal distance as was defined earlier (subsequent work, discussed later in this chapter, showed this to be incorrect). In order to obtain the largest thermal lens possible the sample must be positioned one confocal distance on either side of the beam waist. Thus, allowing z_1 to equal z_c in Equation 9, Dovichi and Harris arrived at the following expression describing the relative change in the far field beam center intensity as a function of sample absorbance:

$$\frac{\Delta I_{bc}}{I_{bc}} = \frac{-2.303P(dn/dT)A}{\lambda k} \qquad (10)$$

$$= 2.303EA \qquad (11)$$

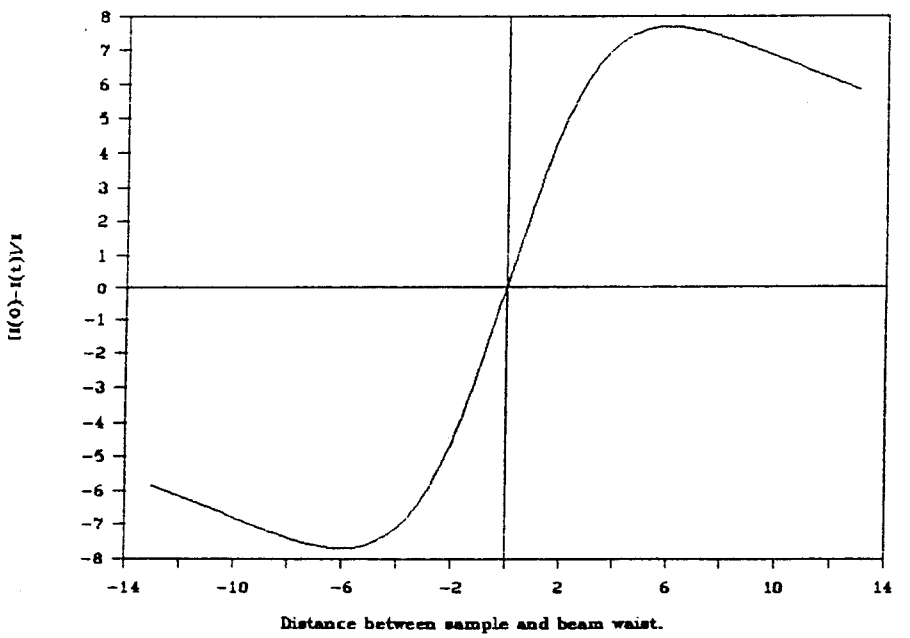

Figure 3. Thermal lens magnitude as a function of z_1, the distance between the sample and the laser beam waist.

This equation assumes that all absorbed energy is lost as heat and no fluorescence occurs. If fluorescence is present a correction term incorporating quantum yield must be added.

Equation 10 predicts an enhancement, E, for thermal lens absorption measurements relative to conventional Beer's law measurements. The magnitude of this enhancement is governed by judicious choice of a solvent with low thermal conductivity and large refractive index change with temperature. Typical enhancement values per unit of laser power range from 3.88 for carbon tetrachloride to 0.09 for water (2). Also, Equation 10 shows a linear increase in response with laser power supplied to the sample. Consequently, the ability to measure smaller than conventional absorbances should be realized by increasing the laser power. These two factors promised an excellent improvement in minimum measurable absorbances relative to those obtained with conventional techniques.

As of 1979, the thermal lens effect had not been used to quantitate any analyte in solution. All samples had been neat solvents or solutions and experimentation was mainly restricted to demonstrating the properties of the thermal lens or measuring absorption coefficients of weakly absorbing solutions (1, 4-8). Two qualitative applications of the thermal lens effect had been reported. The first involved using the thermal lens effect for measuring C-H

vibrational overtones of benzene, naphthalene, and anthracene (11). The second application demonstrated that multiphoton absorption spectra could be recorded using a thermal lens method (12, 13). Realizing the analytical significance for the quantitation of trace solutes in solution offered by Equation 10, as well as the opportunity to introduce lasers as practical tools for analytical chemists, Dovichi and Harris reported, in 1979, the first use of the thermal lens effect for analytical purposes (14).

The experimental arrangement used by Dovichi and Harris was identical to that used by Hu and Whinnery. However, instead of observing thermal lens transients on an oscilloscope, an electronic signal processor hooked to a computer was used to measure $[I(0)-I(\infty)]/I(\infty)$. Using methylene blue in methanol:water (2:1) and a helium-neon laser the confocal distance was determined by translating the sample along the beam path, after the waist, and taking thermal lens measurements. The confocal distance was obtained by plotting $[I(0)-I(\infty)]/I(\infty)$ versus the sample distance from the beam focus. The observed maximum in this curve was taken as the confocal distance. Once the confocal distance was known the sample cell was fixed at that point. A copper(II) determination was then performed by measuring the thermal lens signals produced by solutions of Cu-EDTA complex. The determination was done in water, 1:1 acetone:water and 3:1 acetone:water in order to demonstrate

the enhancement achieved by using increasingly nonpolar solvent systems. The minimum measurable absorbances obtained for each solvent system were $5.1x10^{-3}$ (5.5 μg/mL), $3.5x10^{-3}$ (3.7 μg/mL) and $1.0x10^{-3}$ (1.0 μg/mL), respectively.

Subsequent to Dovichi and Harris' work, the first analytical applications of the pump/probe thermal lens technique were reported by Ishibashi, et al. (15, 16). Using an Ar^{+}-ion pump and a HeNe probe they quantitated iron through complexation with 1,10-orthophenathroline. Minimum measurable absorbances of $6x10^{-3}$ absorbance units (AU) for an aqueous buffer solution and $1.9x10^{-5}$ AU by ion-pair solvent extraction of the complex into chloroform were reported. Other analytical applications for the determination of phosphorus in solution (17) and nitrogen dioxide in gaseous mixtures (18, 19) soon followed. All used visible wavelength lasers. In turn, an application was reported which used an infrared laser to quantitate condensed phase hydrocarbons (20).

Once the potential for using the thermal lens effect for quantitative solution analysis had been demonstrated, many contributions to the refinement of this new analytical technique were made by several researchers. These refinements generally fell into three categories: new theoretical approaches, novel optical configurations, and application of the technique as a detection method for high

performance liquid chromatography. The remainder of this chapter will be devoted to summarizing the highlights from these three categories followed by a discussion of the application of laser-induced fluorescence to HPLC detection and concluding with a statement of purpose for this dissertation.

NEW THEORETICAL APPROACHES

In 1982, Sheldon, Knight, and Thorne developed a new theory to describe the effect a thermal lens has on the far-field beam center intensity (21). Up to this point, researchers had accepted the parabolic thin lens model as an accurate theoretical model of the thermal lens effect. However, this model was based on the assumption that the refractive index gradient around the beam center was parabolic. Assuming a parabolic refractive index gradient implies that the thermal lens behaves as a "perfect lens" in that aberrant lens effects are non-existent. However, in reality, the refractive index gradient around the beam center is Gaussian which means aberrations are present to some extent. Thus, the thin lens model provided only a qualitative description of the thermal lens since it did not take into consideration the lens' aberrant nature. Taking this into consideration, Sheldon et al. ascertained the need for a more rigorous theory that would better describe the thermal lens quantitatively. Their new theory stated that, if the sample is located at the position for optimum thermal lens signal, the fractional change in far-field beam center intensity would be described by the following equation:

$$\frac{I(t) - I(\infty)}{I(\infty)} = \frac{1 - \theta \tan^{-1}\left\{\frac{0.577}{1 + t_c/t}\right\}}{1 - \theta(0.524)} \qquad (12)$$

where

$$\theta = \frac{0.24 P l b (dn/dT)}{\lambda k}. \qquad (13)$$

Equation 12 predicted that maximum thermal lens response was achieved by placing the sample, not at the confocal distance as the parabolic thin lens model predicts, but at a distance of $3^{1/2} z_c$ relative to the beam waist.

Carter and Harris developed a theory which applied to measuring the thermal lens effect using long path length cells (22). Their integrated positional dependence theory relies upon integrating the thin lens positional dependence equation over the distance of the sample path. This would account for the non-uniform beam divergence in a long path sample. However, this theory assumes that the beam spot size across the sample is uniform when, in fact, it is not because of the different refractive index boundaries the beam crosses as it travels through the sample. Realizing this, they developed a second theory based on numerical modeling which accounts for the non-uniform beam profile across the sample.

In 1985 Berthoud, Delorme, and Mauchien made a significant contribution to dual-beam thermal lens theory (23). They reported the first systematic study of the relative positions of the pump and probe beam waists and their effects on thermal lens measurements. They demonstr-

ated, experimentally and theoretically, that for a dual-beam system maximum, sensitivity occurs when the sample is placed at the focal point of the pump beam, allowing for the strongest thermal lens possible to be formed, and when the probe beam is focused at $3^{\frac{1}{2}}z_c$ before or after the pump beam waist.

NOVEL OPTICAL CONFIGURATIONS

Realizing that the lower limit of detection for the thermal lens technique was dominated by background solvent absorbance, Dovichi and Harris designed an optical arrangement whereby the background signal could automatically be subtracted from the sample (24). This single-beam differential thermal lens spectrometer was based on the antisymmetric dependence of the thermal lens response relative to the lens position with respect to the beam waist (see Figure 3, page 15). A differential response was created by placing the sample and reference cells one confocal distance before and after the beam waist. Since the reference cell contained only solvent any signal due to solvent absorbance produce in the sample cell was cancelled by that produced in the reference cell as long as the two cells were positioned symmetrically about the laser beam waist. This system was unique since subtraction of laser intensity fluctuations and solvent absorption was produced optically as opposed to electronically. A detection limit of 6.3×10^{-7} AU was observed using a laser power of 200 mW. Subsequent applications for the determination of phosphorous (25) and lanthanides (26) have been reported using this differential technique.

Alternatively, a differential response can be produced electronically rather than optically. A dual laser

double-beam thermal lens spectrometer based on photo-differential detection has been reported by Termae and Winefordner (27). In their configuration collinear argon-ion pump and HeNe probe beams were split into sample and reference beams which passed through respective sample and reference cuvettes. A variable neutral density filter was positioned in the reference beam to match the intensity of the sample beam. After blocking the pump beams with colored filters the sample and reference beams centers struck respective photodiodes. By electronically subtracting the sample and reference beam center intensities, a modulated signal was produced which represented only thermal lens formation and deformation. In this manner, the background signal due to solvent absorption was compensated for. A detection limit of $4x10^{-10}$ M amaranth in methanol was achieved using this configuration.

In addition, a single laser double-beam thermal lens spectrometer has been reported by Jansen and Harris (28) which combines the advantages of the single-beam and pump/probe designs. Their configuration was similar to Termae and Winefordner's however a single laser beam was split into sample and reference beams. A variable neutral density filter was positioned in the reference beam, to match the intensity of the sample beam. By electronically subtracting the average sample and reference beam intensities a modulated signal characteristic of only the ana-

lyte thermal lens formation and deformation was produced. Lower detection limits compared to the single-beam configuration and a reduction of short term laser intensity fluctuations were the most significant advantages of this configuration. Since no reference cuvette was used a differential response reflecting solvent absorption cancellation was not reported.

Several unique optical configurations have been developed by taking advantage of laser beam polarization properties (29-32). In 1984, Yang introduced a dual-beam thermal lens spectrometer which used a single laser (29). Prior to this, all dual-beam thermal lens spectrometers reported required the use of two lasers. A polarizing beam splitter cube was used to split a randomly polarized HeNe laser beam into pump and probe beams of orthogonal polarization. The modulated pump beam was recombined, collinearly, with the unmodulated probe beam before passing through the sample. Separation of the two beams was accomplished by placing a dichroic sheet polarizer before the photodiode aperture. A minimum measurable absorbance of 2.5×10^{-4} was observed.

A single-laser/dual-beam configuration based on polarization encoding was developed by Pang and Morris (30). After splitting the beam with a glass plate splitter, the pump beam was passed through a Fresnel rhomb which rotated its plane of polarization perpendicular to that of

the probe beam. A Glan prism positioned before a fiber optic aperture allowed optical separation of the two beams. The prism passed only light polarized in the direction of the probe beam.

A fundamentally different approach to polarization encoding was developed by Yang, Hall and De La Cruz (31). Their propagation encoded configuration utilized orthogonally polarized pump and probe beams which traveled collinearly in opposite directions through the sample. The pump and probe beams were separated spatially and no optical rejection device was necessary for the pump beam. Thus, the emergent probe beam was devoid of pump radiation which resulted in an over all reduction in signal noise.

A unique single-beam pump/probe thermal lens spectrometer developed for sensitivity enhancement has been reported by Yang (32). The rotoreflected laser beam thermal lens configuration allowed the sample to be placed at the laser focal point for maximum thermal lens formation while being probed at $3^{\frac{1}{2}}z_c$ for optimum probing effect. This was accomplished by placing the sample at the laser waist and positioning a quarter-wave retarder/mirror combination at a distance of one-half z_{opt} ($3^{\frac{1}{2}}z_c/2$) behind the cell. A sensitivity enhancement of three times that of the conventional single-beam arrangement was observed. This agreed well with the proposed theory. Yang predicted an absolute sensitivity increase of 12-fold, based on mass,

since the excited sample volume was four times smaller than in a conventional single beam arrangement. A detection limit of $5x10^{-7}$ AU was obtained with the rotoreflected beam system.

One other single-laser, single beam pump/probe thermal lens spectrometer has been reported by Bobbitt, Erskine, and Foley (33). In their configuration modulation was accomplished by passing the laser beam through an acousto-optic modulator (AOM). After exiting the sample cell the beam was split into its first and zero order Bragg components by traveling through a second AOM. The first order beam, acting as the probe, was centered onto an aperture positioned before a photodiode. Thus, the pump and probe beams were separated temporally rather than spatially. The most significant advantage of this configuration was the reduction of laser alignment noise caused by trying to overlap two beams inside the sample cell.

Two unique variations on the pump/probe thermal lens concept were introduced by Yang and Hairrell (34) and Dovichi, Nolan and Weimer (35,36) in 1984. Both concepts were based on crossing the pump and probe beams in the sample instead of having them propagate collinearly. Yang and Hairrell used a single-laser/dual beam configuration and crossed the pump and probe beams inside the sample at an angle of approximately 1°. Since the pump and probe beams were spatially separated, noise due to optical inter-

ference from collinear beams was avoided. Also, no rejection device was needed to block the pump beam from the detector, thus eliminating another system noise source. Applying their system to flow injection analysis, a minimum measurable absorbance of 2.0×10^{-4} AU was observed. In the static mode a minimum measurable absorbance of 7.2×10^{-5} AU was achieved. This represented a factor of 3 lower than the detection limit obtained with their collinear pump/probe configuration (29).

Photothermal refraction, the term used by Dovichi, Nolan and Weimer to describe their crossed-beam method, involved crossing the pump and probe beams in the sample at a right angle. This allowed for very high spatial resolution. The heated sample acted as a cylindrical lens and defocused the probe beam along the axis perpendicular to the beam plane. In addition, photothermal refraction theory demonstrated that the sensitivity of the technique was not dependent on path length and was also inversely proportional to the pump beam spot size (35). Thus, the more tightly focused the pump beam, the greater the sensitivity of the technique. Consequently, photothermal refraction was very amenable to small volume situations. Dovichi et al. were able to quantitate 0.4 femtograms of iron in a probe volume of 25 picoliters (36). An absorbance detection limit of 1.1×10^{-7} AU was achieved using CCl_4 as a solvent (36).

In 1982, Ishibashi, Imasada, and Miyaishi introduced a new type of thermal lens spectrometer based on image detection (37). They noted that in a pump/probe configuration inhomogeneities in the probe beam Gaussian intensity profile, produced by the beam passing through the various optical elements in the configuration, were a source of spatial noise. Also, slight misalignment of the pump beam could deflect the probe beam center away from the pinhole aperture, causing serious error in measuring weak thermal lens signals. In order to alleviate both of these problems, Ishibashi et al. used a photodiode array to sample the entire probe beam profile and subsequently, with a microcomputer, least-square fitted the profile to a Gaussian curve. The change in far-field spot size was then calculated. In this manner spatial noise was effectively averaged out and, since no pinhole aperture was used, improper measurements were avoided. By complexing Fe(II) with 1,10-orthophenanthroline a minimum measurable absorbance of 6×10^{-7} AU was obtained which represented a two order of magnitude decrease over a previous determination using conventional pinhole aperture and photodiode detection (16).

Jansen and Harris were able to improve upon the image detection method by employing a parabolic transmission mask for the purpose of optically computing the far-field beam spot size (38). This allowed the spatial noise

to be averaged over two dimensions rather than one as was the case with the photodiode array method. Combining the effects of signal averaging in both time and two spatial dimensions produced detection limits which were 24 times lower than those obtained with photodiode array imaging.

APPLICATION TO HIGH PERFORMANCE LIQUID CHROMATOGRAPHY

Once the thermal lens technique had become established as a convenient method for measuring small absorbance in solution, application to high performance liquid chromatography (HPLC) soon followed. The enhancement over conventional absorbance measurements inherent to the thermal lens signal, coupled with the coherent nature of a laser beam, made this technique extremely well suited for liquid chromatographic detection in small volume flow cells. This was especially significant to microbore and capillary column detection where submicroliter sample volumes are typical.

Dovichi and Harris were the first researchers to study the effect of flow on the thermal lens signal (39). Their investigation revealed that the overall effect of flow was to decrease the thermal lens strength. This was explained by the fact that a constant flow continually removes heat from the sample producing a cooling effect, which decreases the temperature gradient at the beam axis, resulting in a loss of signal enhancement. They concluded that the primary cause of the enhancement loss was due to perturbations in the thermal lens induced by sample mixing taking place inside the flow cell, as well as pump pulsations from the mobile phase pump. However, this enhancement loss was not severe enough to rule out using the ther-

mal lens as a detection method at flow rates typically used in HPLC analysis.

The first application of the thermal lens effect for HPLC detection was reported by Leach and Harris in 1981 (40). Using a single-beam configuration they positioned a flow cell beyond the beam waist, where maximum thermal lens signal was observed, and demonstrated a reverse phase separation of nitroaniline isomers. Beam center intensity changes were monitored using transient signal recording (41). Soon to follow was the first dual-beam application to HPLC detection by Buffet and Morris in 1982 (42). An Ar^+-ion pump and HeNe probe beams were used to detect a reverse phase separation of o-nitroaniline and N,N-dimethyl-3-nitroaniline. Subsequently, application of the thermal lens effect to liquid chromatographic detection has been demonstrated for the polarization (30) and propagation encoding (31) optical configurations, in addition to Bobbitt's acousto-optic arrangement (33).

In 1984, Pang and Morris reported a very unique development in single-beam thermal lens detection applied to liquid chromatography (43). By mathematical derivation they demonstrated that the thermal lens response contained a component, $R(t) = K''\alpha P^2(\cos 2\omega t)$ (K'' is a constant; α, P, t as previously defined), at twice the modulation frequency, ω. By monitoring the thermal lens signal at twice the modulation frequency and using lock-in amplification

detection they were able to extract the second harmonic component of the thermal lens signal. A notch filter was installed in their lock-in to suppress the large fundamental signal component. This approach represented a major simplification for single-beam thermal lens detection since sophisticated signal processing electronics, unavailable in many analytical laboratories, was not necessary to detect the beam center intensity change. However, a loss in signal-to-noise ratio was observed with the second harmonic method compared to a conventional pump/probe arrangement. This was attributed to residual fundamental present in the signal due to the less than 100% efficiency of the notch filter.

Another innovative contribution to the development of thermal lens detection for HPLC was also demonstrated by Pang and Morris when they successfully applied Dovichi and Harris's differential thermal lens configuration (44). The size of the optics did not allow direct application to a flow cell situation because it required tightly focused beams and confocal parameters less than one millimeter. To overcome this problem a 1:1 telescope was incorporated into the configuration, between the sample and reference cells, which created enough space for convenient positioning of the reference cell. Using second harmonic detection they achieved solvent absorbance compensation of 98%. A two-fold increase in thermal lens signal, over the single cell

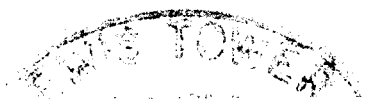

configuration, was attributed to compensation of the cylindrical lens effect on the beam as it passed through a single flow cell. The signal-to-noise ratio was also increased by a factor of 2.5-4 compared to the single cell arrangement. This was due to partial flow fluctuation compensation in the two cell system.

Pang and Morris have also reported a unique thermal lens liquid chromatography detector using a retroreflective array (45). By incorporating a retroreflective array into their single-beam configuration they were able to compensate for aberrations caused by thermally induced refractive index gradients plus perform a double pass through the sample cell. They observed absorbances twice as great with the retroreflective array system and a signal-to-noise enhancement of 6:1 compared to a conventional single-beam arrangement.

The first use of thermal lens for detecting components eluting from a microbore liquid chromatography column was demonstrated by Buffet and Morris (46). Using the same dual-beam optical configuration as in reference 43 they replaced the 8 μL volume, 1 cm path length flow cell with one having a 0.5 μL volume and 1-mm pathlength. A 250 mm x 1-mm i.d. reverse phase microbore column replaced the standard analytical column. Their microbore system performance was similar to that of the analytical column system. They also demonstrated that using pump laser powers below

10 mW was feasible as long as a 60:1 pump/probe power ratio was maintained.

Photothermal refraction has proven to be an ideal technique for detecting components separated on microbore and capillary columns. As stated earlier (pg. 28), the photothermal refraction signal magnitude is independent of path length and inversely proportional to pump beam spot size, allowing the use of tightly focused beams. Using a 10 cm x 1-mm i.d. reverse phase microbore column Nolan, Hart, and Dovichi separated a mixture of (dimethylamino)azobenzenesulfonyl (DABSY) derivatized amino acids (47). A mass detection limit of 5 femtomoles was observed. This corresponded to a glycine concentration detection limit of $8x10^{-8}$ M or a minimum measurable absorbance of $1x10^{-7}$ AU. By changing to a 80 cm x 0.25 mm i.d. capillary column they reported a detection limit of 750 atomoles (48). Femtomole detection limits have also been reported using the same system for the quantitation of 2,4-dinitophenylhydrazones (49).

Skogerboe and Yeung have demonstrated a single laser thermal lens detector for microbore liquid chromatography based on high frequency modulation (50). In order to obtain maximum signal strength an acoustooptical modulator was used to modulate the beam at 150 kHz, thereby forming a steady-state thermal lens in the sample cell. Noise due to laser intensity fluctuations was also reduced as a

result of the high modulation frequency. A detection limit (S/N=3) of 0.3 picograms of benzopurpurin was achieved which corresponded to a minimum measurable absorbance of $4x10^{-6}$ AU.

APPLICATION OF LASER-INDUCED FLUORESCENCE AS A DETECTION METHOD FOR HIGH PERFORMANCE LIQUID CHROMATOGRAPHY

Quantitation of analytes in the condensed phase by molecular fluorescence, utilizing an incoherent excitation source, is a well established analytical technique. Rigorous treatment of this subject regarding theory and instrumentation is found in the literature (51, 52). In general, when a molecule absorbs electromagnetic radiation at a specific wavelength, it is promoted from the singlet ground state to the first excited singlet state. Providing that intersystem crossing and radiationless relaxation are minimal the molecule will return to the ground state by emitting light at a longer wavelength than at which it was excited. Measuring the amount of light emitted, which is proportional to the number of molecules in solution, makes quantitation possible.

Direct excitation of a fluorescing substance leads to a fluorescence intensity, F, whose magnitude is described by the following equation,

$$F = 2.303 Q_f K I_o \epsilon C L \qquad (14)$$

where Q_f = fluorescence quantum efficiency
K = collection efficiency
I_o = excitation wavelength intensity
ϵ = analyte molar absorptivity
C = analyte molar concentration
L = pathlength.

Assuming that intersystem crossing and inner-filter effects are minimal this equation will be valid (53).

Equation 14 demonstrates that total observed fluorescence is directly proportional to the incident photon flux. Thus, theoretically, equation 14 predicts that lower analyte concentrations can be detected by increasing the excitation intensity. For ultimate sensitivity, quantitation by fluorescence becomes the method of choice since achievable detection limits, routinely, are 1000 to 10,000 times lower than those observed with conventional absorption techniques (54).

In addition to increased sensitivity, fluorescence offers a high degree of selectivity over absorption spectroscopy, which makes it an attractive method for mixture analysis. Two obvious experimental situations are immediately realized. First, numerous components in a mixture may absorb at the same excitation wavelength where only a select few fluoresce. Monitoring emission allows for analysis of the fluorescing components without interference from the non-fluorescing compounds. Second, components in a mixture which absorb at the same excitation wavelength can be resolved spectrally or temporally providing they have different spectral emission profiles or fluorescence lifetimes. Spectral resolution is accomplished by adjusting the emission monochromator or creating an appropriate optical window with filters to selectively block unwanted emission. With temporal resolution, emission possessing

shorter lifetimes is allowed to dissipate before the desired emission is measured.

Unfortunately, not all molecules naturally fluoresce. However, this is not a disadvantage since many molecules can be made to fluoresce, through chemical modification, by attachment of an appropriate fluorotag. Numerous fluorescent derivatization reagents have been developed for this purpose (55-59). Chemical derivatization imparts an additional degree of selectivity to an analysis by turning a non-fluorescing molecule into one that fluoresces. In addition, sensitivity increases since the analyte is converted to a form that produces a larger detector response (60).

Replacing the incoherent excitation source with a laser makes fluorescence analysis an even more powerful tool for the analytical chemist. Specifically, laser-induced fluorescence offers several advantages, in terms of selectivity and background noise reduction, compared to conventional fluorescence methods (61). As stated earlier, the fluorescence signal magnitude is proportional to incident photon flux. Typical incoherent excitation sources and their operating wattages are the mercury arc lamp (100 W), deuterium lamp (50 W), and tungsten lamp (100 W). On the average, these three sources deliver 4.5 mW (254 nm), 0.9 mW (230 nm), and 17.3 mW (600 nm), respectively, to the sample cell (61). In contrast, depending on the type used,

continuous laser sources can deliver anywhere from a few milliwatts up to 20 watts, directly, to the sample due to their monochromatic nature. Thus, a higher photon flux per unit detection volume is realized compared to conventional incoherent excitation sources and theoretically, this should lead to lower detection limits. However, detection limits are ultimately limited by the background noise magnitude. Three sources of background noise inherent in fluorescence measurements are elastic Rayleigh scattering of the excitation wavelength by reflection and refraction from the cell walls; inelastic Raman scattering from the solvent and cell walls; and fluorescence from impurities, optics, and cell walls. Stray light must be kept to a minimum if optimum detection limits are desired.

In addition to a high photon flux delivered to the sample, the laser beam monochromaticity allows these background effects to be addressed more easily. Excitation bandwidths of conventional incoherent sources are on the order of 10 nm which means the Rayleigh and Raman bands will have the same width. However, a corresponding 10-fold reduction in the Rayleigh and Raman band widths is achieved by using a monochromatic source (61). Therefore, employing a laser as an excitation source expands the spectral range over which fluorescence emission can be collected. Furthermore, use of a pulsed laser with gated detection allows for temporal resolution of fluorescence intensity from

Raman scatter. Since fluorescence decay has a longer lifetime than Raman scatter, time gating allows the fluorescence signal to be measured after the Raman intensity has diminished to a minimal level (61, 62). Also, laser light possesses inherent polarization. Rayleigh and Raman lines are polarized too, and can be filtered out from fluorescence intensity by using appropriate filters positioned before the detector (61). Finally, observation of two-photon molecular fluorescence offers an additional degree of analytical selectivity when lasers are used as excitation sources (63-65). The ability to deliver high average powers in a minimal sample volume greatly increases the probability of simultaneous two photon absorption. Interference from stray light and solvent Raman bands is no longer a problem since two-photon fluorescence is observed at twice the excitation wavelength.

No where have the advantages of laser-induced fluorescence been more evident than in its application as a detection method for high performance liquid chromatography. Laser beams are easy to manipulate and their directionality allows for highly colliminated beams, with low divergence angles (0.5 to 1 milliradian) to be focused into small volumes (66). This is especially advantageous for microbore and capillary column detection where microliter and submicroliter flow cell volumes are necessary to preserve component resolution (67). For on-column fluores-

cence detection, Guthrie pointed out that the excitation energy delivered to the sample with a laser decreases proportionate to the column diameter (68). The power delivered with an incoherent source decreases proportional to the square of the column diameter. Thus, as the column diameter decreases, the laser detection limit should improve over that for an incoherent source in a fashion inversely proportional to the column diameter (68).

Several different designs for HPLC flow cells have evolved out of a need to compensate for stray light reduction, volume minimization, and proper imaging onto the detector (61). Diebold and Zare created a windowless flow-cell by gravity suspending the column effluent, as a flowing drop, between a stainless steel tube, inserted into the column end, and a stainless steel rod (69). The laser beam was focused into the center of the free flowing drop which had a volume range of 4 to 5 microliters. Since the flow cell was windowless, extraneous fluorescence from cell walls was avoided. This flow cell type has been applied to the separation of antibody bound insulin from free insulin (70) and to the determination of aflatoxins and mycotoxins in corn on analytical liquid chromatography columns (69, 71).

A simple variation on the suspended droplet flow cell has been demonstrated by Joseffson et al. (72). They replaced the stainless steel tube at the end of the column

with one having capillary dimensions. Thus, the column effluent exited the tube in the form of a free falling jet as long as the mobile phase flow rate was at least 1mL/min. This windowless flow cell was used to demonstrated a separation of twelve aldehydes derivatized with (dimethylamino)naphthalenesulfonylhydrazine.

Another type of windowless flow cell has been designed by Callis et al. based on the sheath flow principal (73). In their design, column effluent is injected into the center of an ensheathing mobile phase stream. Since laminar flow conditions are maintained, mixing between the solvent and sample streams does not occur. The mobile phase sheath and sample stream flow rates are variable, resulting in effective sample volumes ranging from 6 to 150 microliters. Besides a small optical dead volume this flow cell offers a reduction in stray light since the quartz cell windows are placed 5 mm away from the sample flow where the laser is focused. Also, extraneous fluorescence from impurities adhering to the flow cell wall is avoided. A detection limit (S/N=3) of 1.2×10^{-9} M mesoporphyrin IX dimethyl ester eluting from an reverse phase analytical column has been reported with this flow cell design (73).

A simple and effective means for monitoring fluorescent components separated with open tubular and capillary HPLC columns is by on-column detection (68, 74). This method involves scraping off a section of the protective poly-

amide coating to expose the underlying fused silica column. The laser beam is then focused into the column center and emitted light collected using appropriate optics. Essentially the flow cell becomes an extension of the column and peak band broadening is eliminated since excess volume due to connections to an independent flow cell are absent. However, background fluorescence due to trace amounts of natural quartz can restrict detection limits (68). Separation of a mixture of oxadiazoles using on-column laser two-photon fluorescence detection has also been reported (75).

Another unique method for detecting fluorescing components eluting from an HPLC column has been demonstrated by Sepaniak and Yeung (76). Instead of using conventional optics for collecting fluorescence emission they attached a quartz capillary tube to the column end into which the laser beam was focused. Then a fiber optic was inserted inside the capillary, just below the beam, to collect emitted light. By proper positioning of the fiber optic, sample fluorescence emission emanating from the capillary center was selectively transmitted over light originating from the capillary walls. Thus, scattered light and extraneous fluorescence from the cell walls were reduced. Separation and quantitation of two antitumor drugs, in urine, on an analytical column was demonstrated using their flow cell. Subsequently, this detector design has been applied to bile acid and plasma steroid separa-

tions on capillary columns (77), detection of subfemtomole amounts of primary amino acids (78), and for analysis of liquified coal by two-photon fluorescence (79).

Laser-induced fluorescence can also be used to detect non-emitting compounds, namely inorganic ions, eluting from an HPLC column. Mho and Yeung have developed a double-beam ion chromatography detector which operates on the principle of indirect fluorimetry (80). Salicylate ion, used as the eluent, produced a constant high fluorescent background signal such that when non-fluorescing anions passed through the detector cell a decrease in fluorescence was monitored. A 1 mm i.d. quartz tube attached to the column end served as the sample flow cell while the reference flow cell consisted of an identical tube with only eluent flowing through pumped by a separate peristaltic pump. A separation of iodate and chloride ions was demonstrated.

STATEMENT OF PURPOSE

The purpose of this dissertation is three fold. First, a rotoreflective double-beam thermal lens spectrometer based on incorporation of high frequency modulation and the conventional double-beam approach into the rotoreflective single-beam thermal lens configuration is presented. The rotoreflective single-beam thermal lens spectrometer is designed for sensitivity enhancement and its simple optical configuration allows for optimum pumping and probing of the thermal lens as well as performing a double pass (32). However, the chief disadvantage of the single-beam configuration is the inability to adopt the differential thermal lens technique (24) for the purpose of background solvent absorption cancellation (32). The rotoreflective double-beam thermal lens spectrometer is designed to compensate for solvent absorption while incorporating the advantages of the rotoreflective single-beam configuration. Also, high frequency modulation is added to create a steady state thermal lens allowing for the largest possible signal to be recorded.

The second purpose of this dissertation is to describe a microbore high performance liquid chromatography (HPLC) detection system which will simultaneously detect via thermal lens absorption and laser-induced fluorescence. This idea was first proposed by Buffett and Morris (42).

It is designed to exploit the complementary relationship between the thermal lens effect and fluorescence. This relationship becomes evident by examining, more closely, the variables that are responsible for creating the two signals. Equations 15 and 16 describe the thermal lens and fluorescence signals, ΔI and I_f respectively, which are measured by lock-in detection:

$$\Delta I = 2.303E\epsilon bcI_o \quad (15)$$

$$I_F = 2.303KI_o\epsilon bcQ_f \quad (16)$$

The extinction coefficient of the absorbing or fluorescing species is represented by ϵ and all other variables have been previously defined. Even though both effects originate from different photophysical processes, their magnitudes depend on several of the same variables.

Specifically, equations 15 and 16 illustrate that for sufficiently dilute solutions, both effects are proportional to cell pathlength, solute concentration, solute extinction coefficient, and incident power delivered to the sample. However, equation 15 only applies to excited molecules in which relaxation is dominated by radiationless pathways. If an excited molecule relaxes by radiative and as well as non-radiative processes then equation 15 must be altered by a factor of $1-Q_f$. This factor can be thought of as the efficiency of radiationless relaxation.

On the other hand, the fluorescence signal magnitude will be constrained by the width of the optical

window created by whatever means is used to block Raman and spurious excitation radiation. Accordingly, equation 16 must be altered by factor of T which accounts for the percentage of total fluorescence passed through the optical window before the photomultiplier. With these considerations in mind, equations 15 and 16 can be written as

$$\Delta I = 2.303E\epsilon bcI_o(1-Q_f) \quad (17)$$

$$I_F = 2.303KI_o\epsilon bcQ_fT \quad (18).$$

Equations 17 and 18 point out the limitations that the thermal lens effect and fluorescence have when they are applied separately as detection methods for HPLC, especially for mixture analyses. For example, if a mixture contains components possessing large extinction coefficients at the designated analysis wavelength and Q_f's which approach 1 then these components most likely would not produce a thermal lens signal and peaks indicating their presence would not appear in the chromatogram if thermal lensing is the detection method of choice. Conversely, the mixture may contain components such that Q_f or T approaches zero resulting in no response if fluorescence detection is used. In addition, since both effects are wavelength dependent, the appearance of the thermal lens and fluorescence chromatograms will change according to the extinction coefficient values the mixture components possess for the chosen wavelength. Clearly, both detection methods should be utilized at different excitation wavelengths to obtain a

the most complete characterization of the mixture. Recording of the two effects simultaneously will produce thermal lens and fluorescence chromatograms without resorting to several separate experiments. More importantly, understanding the variables which account for the complementary nature between the thermal lens effect and fluorescence should allow for a deeper insight into interpretation of the chromatograms obtained for complex mixtures. This is demonstrated by using the dual detector to obtain simultaneous thermal lens and fluorescence chromatograms of a standard solution of polynuclear aromatic hydrocarbons and the neutral PAH fraction of solvent refined coal using laser excitation wavelengths ranging from the ultraviolet to the visible.

The third purpose of this dissertation is to demonstrate that it is now possible to obtain thermal lens chromatograms using ultraviolet wavelengths. Historically, the number of compounds which can be analyzed for using conventional laser-based HPLC detectors has been limited to those which absorb or can be chemically modified to absorb at a single wavelength, mainly in the visible portion of the electromagnetic spectrum. Generally, one laser has been required for each analysis wavelength desired. The availability of ultraviolet laser lines having intensities on the order of hundreds of milliwatts allows for the routine thermal lens detection of organic compounds which otherwise

would have to be chemically modified to absorb at a visible wavelength or not be detected at all. Chromatograms recorded using ultraviolet excitation are presented which represent applications to pharmaceutical, chemical and environmental analysis.

CHAPTER 2

ROTOREFLECTIVE DOUBLE-BEAM THERMAL LENS SPECTROMETER EXPERIMENTAL SECTION

Apparatus

An optical diagram for the rotoreflective double-beam thermal lens spectrometer is shown in Figure 4. All optical components are mounted on a 2 ft x 4 ft x 2 in optical breadboard (Newport Research Corporation, Model LS-24). A linearly polarized beam, 514.5 nm (P=200 mW), from an argon-ion laser (Spectra Physics, Model 171) passes through a Glan-Thompson polarizer (Ealing, Model 34-5207, not pictured) to insure polarity purity, followed by a zero order half-wave retardation plate (Ealing, Model 34-5827). The half-wave plate is mounted on a rotation stage (Newport Research Corporation, Model RSA-1T) so that the polarization content of the laser beam can be varied. It is rotated with respect to the incident beam polarization, such that the emerging beam contains equal amounts of vertically and horizontally polarized light. After traveling through an achromatic biconvex lens (Oriel, 400 mm focal length) the beam is split into equally intense, sample and refer-

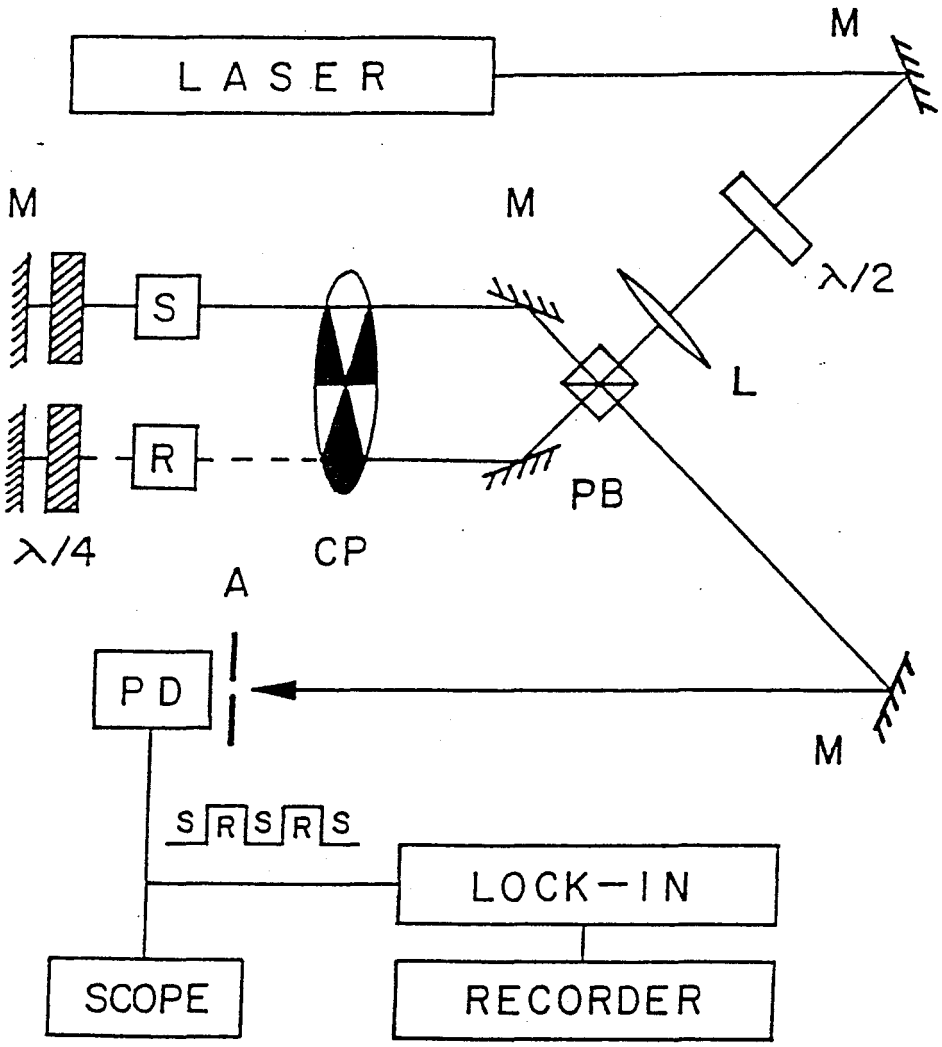

Figure 4. Rotoreflected double-beam thermal lens optical configuration: M, mirror; 1/2, half-wave retarder;, L, lens; PB, polarizing beam splitter; CP, mechanical chopper; S, sample cuvette; R, reference cuvette; 1/4, quarter-wave retarder; A, aperture; and PD, photodiode.

ence beams by a polarizing beam splitter cube. The beam-splitter cube is mounted on an adjustable tilt table (National Research Corporation, Model MM-2). Then, both beams are alternately chopped at 1.5 kHz with a variable speed chopper having a duty cycle of 42% (Princeton Applied Research, Model 222). A modulation frequency with a period much shorter than the thermal lens deformation time constant is deliberately chosen in order to form a steady state thermal lens in the sample and reference cell. Also, alternate chopping of both beams allows the thermal lens in both solutions to be probed alternately in time, thus forming a modulated differential response at the detector. The speed of the chopper is controlled by a function generator (Hewlett-Packard, Model 3310A). Once the two beams pass through standard 1 cm quartz cuvettes, positioned at the lens focal point, rotoreflection is accomplished by two, zero order, quarter-wave retarder (Ealing, Model 34-5819)/-mirror couples mounted on the same translational stage. Maximum rotoreflection is realized by orienting each quarter-wave retardation plate 45 degrees with respect to the incident beam polarization. The quarter-wave/mirror couples are positioned at the optimum sample-to-mirror distance of 3 cm (32). Rotoreflection of the sample and reference beams allows them to recombine, collinearly, and exit the polarizing cube face 90 degrees from which they entered. Optical feedback into the laser cavity is also avoided.

The collinear, alternately chopped rotoreflected sample and reference beams are centered onto a fiber optic (A), which serves as the limiting aperture, connected to a photodiode (EG&G Electro-Optics, Model FND-100). A digital storage oscilloscope (Nicolet Instrument Co., Model 2090) is used to monitor and store the modulated signals received at the detector, followed by plotting on an x-y recorder (IBM Instruments, Inc., Model 7424 M-T).

For the detection limit studies a lock-in amplifier (Princeton Applied Research, Model 5101) operating in the fundamental mode is used to demodulate the signal. A narrow bandpass filter installed inside the lock-in and centered at 1.5 kHz, allows undesirable system noise to be filtered. Pre- and post-filter time constants are set at 1 s. The lock-in output is recorded on a stripchart recorder (Cole-Parmer, Model 8373-20).

Laser beam power is measured with a power meter (Scientech, 360203).

Reagents

A 1.5×10^{-3} M stock solution is prepared from reagent grade iodine and Spectrograde carbon tetrachloride (Aldrich Chemical Company, Inc.). Working standards are diluted from this solution. In addition, two other sets of working standards are prepared by diluting a 1.0×10^{-3} M aqueous cobalt complex, $[Co(en)_2CO_3]ClO_4$, with HPLC grade methanol (Fisher) and high purity water (Syron/Barnstead,

Nanopure II System). Prior to analysis, all solutions are filtered through a 0.45 μm Nylon 66 membrane filter.

Procedures

Construction of the differential spectrometer. Since proper beam alignment and positioning of all optical components is crucial for optimum performance, the following procedure is used in the construction of the differential spectrometer. First, the Glan-Thompson polarizer is positioned in the beam path a few centimeters beyond the laser head, and rotated until a maximum intensity reading is observed on the power meter, thus insuring that the beam is essentially vertically polarized. Then the beam is aligned parallel to the optical breadboard using two matched pinholes. One pinhole is placed before the first steering mirror and the other one is positioned at a distance beyond the point where the polarizing beam splitter cube will be placed. The beam is aligned through the second pinhole by fine adjustment of the first steering mirror. Then, the half-wave retarder and focusing lens are put into place. Proper alignment is maintained by subsequent fine adjustment of the steering mirror after positioning each optical component. After the beam has been aligned the pinholes are removed. Next, the polarizing beam splitter cube is positioned in the beam path to produce the sample and reference beams, followed by the mechanical chopper. The two beams are steered with the sample and reference steering

mirrors such that they remain parallel to each other as well as in proper position to be alternately chopped.

At this point, the sample and reference cuvettes are introduced into the configuration. The rotoreflection arrangement requires that these two components be placed at the laser waist. In order to insure that the cuvettes are properly positioned the following procedure is used. First, the reference beam is blocked. Then the sample beam, modulated at approximately 60 Hz, is centered onto the fiber optic limiting aperture positioned in the far field. The sample cuvette is filled with a solution of I_2/CCl_4 (1.6×10^{-6} M) or cobalt complex/MeOH (1.5×10^{-4} M). Starting at a point before the laser waist the sample cuvette is translated along the beam path until a thermal lens transient is no longer observed on the oscilloscope. This point is taken as the laser waist and the sample cuvette is fastened to the breadboard. The procedure is repeated to position the reference cuvette.

Once the sample and reference cuvettes are properly positioned they are filled with solvent (CCl_4, MeOH, or H_2O). The intensities of the two beams are then balanced by rotating the half-wave plate. The power meter is used to monitor each beam's intensity. Then the quarter-wave mirror couples are positioned into the configuration such that the sample-to-mirror distance is 3 cm. The quarter-wave retarders are oriented approximately 45 degrees with

respect to the incident beam polarization to provide maximum rotoreflection. Coaxial alignment of the forward and rotoreflected beams is accomplished by positioning a pinhole between the sample/reference cuvette and the polarizing beam splitter. The pinhole is adjusted for maximum forward throughput. Then the rotoreflected beam is adjusted using the fine positioning knobs on the quarter-wave/mirror mounts, for maximum transmission back through the pinhole.

Finally, the rotoreflected sample and reference "probe" beams are recombined and spatially isolated from their respective "pump" beams by the polarizing beamsplitter. The emerging beam is centered onto the fiber optic aperture in order to facilitate signal processing of the modulated differential response.

Recording of oscilloscope tracings of modulated transients. The sample and reference cuvettes are filled with CCl_4. A modulated sample beam transient is obtained by blocking the reference beam. Similarly, blocking the sample beam allows for a reference modulated transient to be acquired. A signal representative of only solvent in the cuvettes is obtained by unblocking both beams. Then a solution of I_2/CCl_4 (7.4×10^{-6} M) is introduced into the sample cuvette to obtain the modulated transient signal characteristic of an absorbing species. All transients are collected and

stored on a digital storage oscilloscope and plotted on an x-y recorder.

Detection limit studies. The chosen solvent (CCl_4, H_2O, or MeOH) is placed in both cuvettes. Output from the lock-in amplifier is recorded on a stripchart recorder until a stable baseline is achieved. Then the sample cuvette is filled with a solution having a known concentration of absorbing species. Again, the output from the lock-in amplifier is recorded until a stable signal is obtained. The difference between the solvent baseline and sample response is taken as a measure of the sample solution absorbance. The limit of detection is calculated as the signal observable at twice the magnitude of the baseline noise.

Comparison between the steady state thermal lens magnitude produced with the double-beam system and the thermal lens magnitude produced with the single-beam rotoreflection system. Three types of beam center intensity measurements are recorded using a solution of cobalt complex in methanol (2.4×10^{-5} M). First, the magnitude of the thermal lens produced in the single-beam case under continuous illumination, $I(\infty)$, is measured. The sample beam quarter-wave/mirror couple is removed and replaced by the fiber optic aperture in the far field. Then a value for $I(\infty)$ is obtained

by measuring, off the oscilloscope, the height of the DC signal produced by an unmodulated sample beam.

Next, the initial beam center intensity, I(0), is measured. The chopper is turned on for a few seconds and then turned off and I(0) is measured directly from the oscilloscope during the final rotations of the chopper blade. Lastly, the strength of the steady-state thermal lens, I(ss), formed with high frequency modulation is obtained by measuring the height of the waveform produced by chopping the sample beam at 1.5 kHz. Twenty measurements of each beam center intensity type are measured. Using the average measurement of each beam center intensity type, the percentage of the maximum thermal lens strength, %MTLS (obtainable with the single-beam system under continuous illumination) observed with the double-beam system using high frequency modulation was calculated using the following equation:

$$\%MTLS = \left\{ \frac{I(0)}{I(0)} - \frac{I(ss)}{I(\infty)} \right\} \times 100 \qquad (15)$$

Linearity study. Standard solutions of iodine in CCl_4 are prepared at molar concentrations of 2.4×10^{-6}, 4.8×10^{-6}, 7.2×10^{-6}, and 9.6×10^{-6}. The sample and reference cuvettes are replaced with one millimeter path length flow cells in order to facilitate easier solution transfer. Starting with the least concentrated solution, differential thermal

lens measurements of each I_2/CCl_4 solution are made with CCl_4 in the reference flow cell. Three runs of the standard series are made. Sample response versus concentration is plotted followed by a linear regression analysis of the data.

Common mode response study. Each of the above standards are introduced into the sample and reference flow cells. The common mode response is recorded on a strip chart recorder and compared to the response obtained with CCl_4 in both flow cells.

Extinction coefficient determinations. Extinction coefficients for $[Co(en)_2CO_3]ClO_4$ in water and methanol at a wavelength of 514.5 nm are determined experimentally. Aliquots of the $1.0x10^{-3}$ M aqueous cobalt complex solution are diluted with high purity water to form working standards having molar concentrations of $1.0x10^{-4}$, $2.0x10^{-4}$, $3.0x10^{-4}$, and $5.1x10^{-4}$. The stock solution is also used as a working standard.

A 0.0245 g sample of the cobalt complex is dissolved and quantitatively diluted to 100 mL with HPLC grade methanol. Aliquots of this stock solution are diluted with methanol to form working standards having molar concentrations of $1.0x10^{-4}$, $2.1x10^{-4}$, $3.1x10^{-4}$, $4.2x10^{-4}$, and $5.2x10^{-4}$.

Triplicate absorbance readings of each working standard are measured on a double-beam spectrophotometer (Perkin Elmer, Coleman Model 5274). The spectrophotometer is calibrated using a 632.8 nm interference filter. Linear regression analysis is used to calculate the extinction coefficient of the cobalt complex in water and methanol at the designated wavelength. A value of 860 $Lmol^{-1}cm^{-1}$ for the extinction coefficient of I_2/CCl_4 is adapted from the literature (81).

RESULTS AND DISCUSSION

Figure 5 demonstrates the operating principles of the rotoreflective double-beam spectrometer by illustrating four types of modulated transient signals recorded with it at a chopping frequency of 1.5 kHz. With CCl_4, a low absorbing solvent, in both cuvettes sample and reference square waves (tracings 5a and 5b) are recorded by blocking one of the beams from the detector. Note that the sample and reference square waves are 180° out of phase which is expected if the two beams are properly aligned. Allowing both beams to strike the detector produces the transient illustrated in Figure 5c. Rotating the half-wave retarder to equalize the sample and reference square wave heights produces a null signal at the lock-in amplifier. This allows for automatic cancellation of the thermal lens signal produced by the solvent in both cuvettes. Ideally, with the system properly nulled Figure 5d should be a horizontal line; however, negative spikes appear at regular intervals throughout the signal. These spikes are a consequence of the duty cycle of the chopper being only 42%. A more precisely cut chopper blade should give a duty cycle which approaches 50% thus alleviating the negative spikes. Initial observation of the transient indicates that the negative spikes are a potential noise source. However, closer inspection of the transient reveals that the spikes

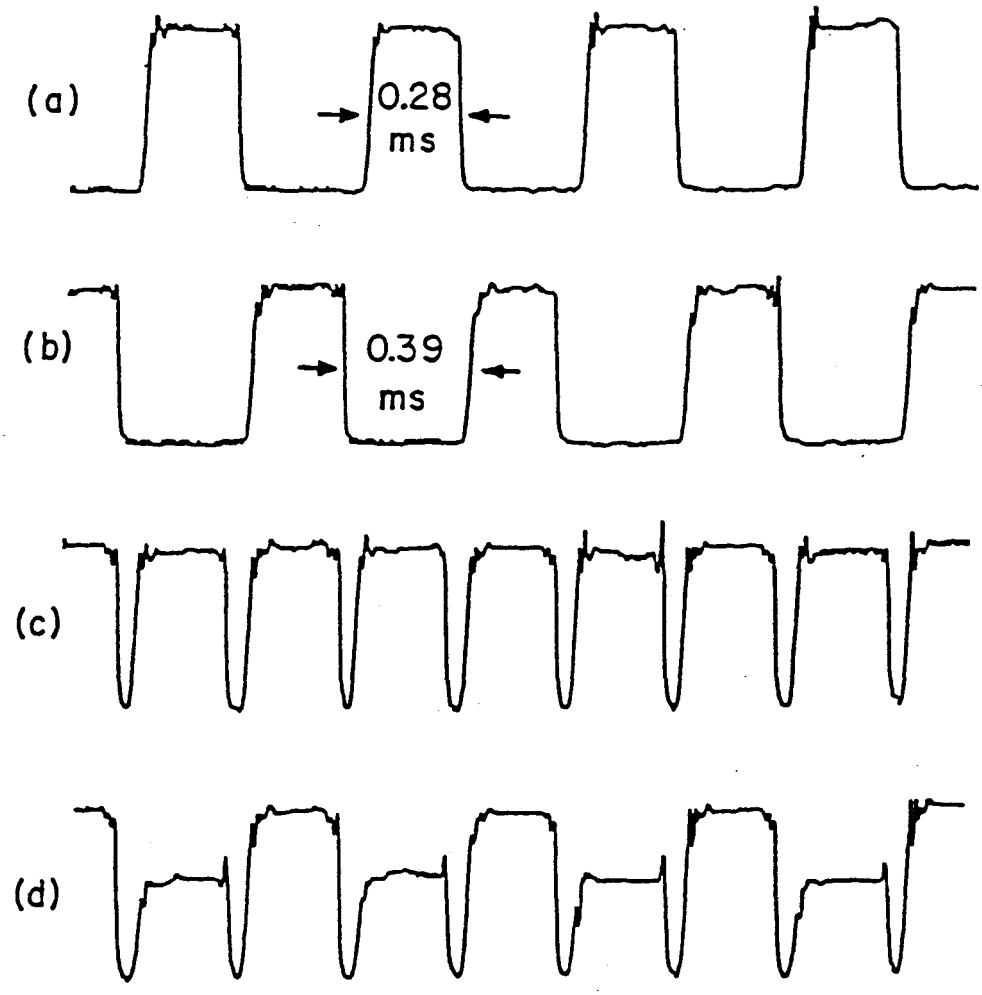

Figure 5. Oscilloscope tracings of the modulated transient signals obtained with (a) CCl_4 in sample cuvette and reference beam blocked, (b) CCl_4 in reference cuvette and sample beam blocked, (c) CCl_4 in both cuvettes and no beam blocked, and (d) sample cuvette containing 7.4×10^{-6}M I_2/CCl_4 solution and reference containing only CCl_4.

occur at twice the modulation frequency. Since a narrow bandpass filter installed in the lock-in amplifier only allows signals modulated at 1.5 kHz to pass, the signal component generated by the negative spikes at 3.0 kHz is filtered out at the lock-in amplification stage. Thus, the presence of the negative spikes is not detrimental to the desired signal.

Introduction of a 7.4×10^{-6} M I_2/CCl_4 solution into the sample cuvette produces the signal transient observed in Figure 5d. A decrease in the sample portion of the signal reflects the stronger steady-state thermal lens formed in the sample cuvette due to absorption by I_2. If the negative spikes are ignored then the transient is seen as a modulated differential response which is generated as a consequence of the difference between thermal lens magnitudes in the two cuvettes. Thus, the signal observed at the lock-in amplifier is only indicative of the analyte concentration present in the sample cuvette and is free of signal component due to solvent absorbance.

Since the magnitude of the beam center intensity change determines the sensitivity of the double-beam configuration it is necessary to compare the strength of the steady state thermal lens formed at high modulation frequency to that produced with continuous excitation. The results of this experiment are illustrated in Figure 6. This figure depicts the time dependent thermal lens signals

produced by the rotoreflected single-beam configuration under continuous illumination, curve a, and that for the double-beam case at a modulation frequency of 1.5 kHz, curve b. The strongest possible thermal lens formed, $I_{bc}(\infty)$, is normalized to $\Delta I=1.0$. Figure 6 demonstrates that the steady state thermal lens strength formed at a modulation frequency of 1.5 kHz corresponds to one-third the magnitude of the strongest possible thermal lens. Presently, 1.5 kHz is the fastest chopping frequency available in our laboratory. Thus, in order to increase the sensitivity of the double-beam system employment of a modulation frequency greater than 1.5 kHz is necessary in order to obtain a steady state thermal lens whose strength approaches that at $I_{bc}=(\infty)$. However, the steady state thermal lens magnitude is controlled by the amount of power delivered to the sample which, in turn is limited by the chopper duty cycle. Hence, a mechanical chopper which combines a high duty cycle and a modulation frequency greater than 1.5 kHz should produce a steady state thermal lens strength greater than 30% of that produced in the single-beam system under continuous illumination.

The analytical detection limits, in terms of minimum measurable absorbance and concentration, obtained with the double-beam configuration, are presented in Table 1. Three solvent systems were studied: Co(III)/H_2O,

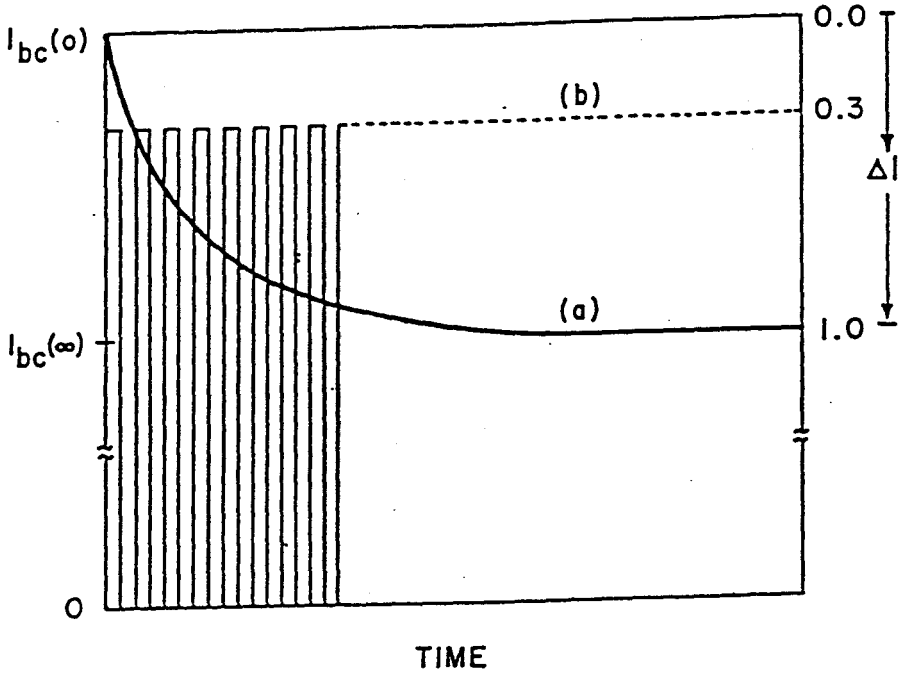

Figure 6. Time-dependent signals from rotoreflective (a) single-beam system with continuous excitation, and (b) double-beam system with chopped excitation at 1.5 kHz.

Table 1. Analytical Results of Detection Limits and Minimum Measurable Absorbances

Solution System	Molar[a] Absorptivity ($M^{-1}cm^{-1}$)	Detection[b] Limit (M)	Minimum Measurable Absorbance
Co(III) complex[c]/H_2O	94	2×10^{-6}	2×10^{-4}
Co(III) complex/MeOH	97	4×10^{-7}	4×10^{-4}
I_2/CCl_4	860	1×10^{-8}	9×10^{-6}

[a] At 514.5 nm [b] at S/N = 2 [c] $Co(en)_2CO_3^+$

Co(III)/MeOH, and I_2/CCl_4. As expected the I_2/CCl_4 system gave the lowest detection limit owing to the superior thermo-optical properties of CCl_4 compared to water and methanol. The minimum measurable absorbance obtained in methanol compares well with that obtained by Winefordner and Teramae, $5x10^{-6}$ AU, using their double-beam photodifferential configuration (27). However, the detection limit obtained in carbon tetrachloride is 14 times greater than that measured by Dovichi and Harris, $6.3x10^{-7}$ AU, with their single-beam differential spectrometer (24).

In order to account for the marginal detection limits observed with the rotoreflected double-beam configuration it is necessary to discuss the possible sources of noise inherent in the instrumental design. First, from a qualitative stand point, the double-beam system is optically more complicated than the Dovichi and Harris configuration. This requires a much tighter control over positioning the optical elements in order to achieve proper beam alignment. Due to the increased number of optical components chances for alignment error, which translates into added background noise, are enhanced.

Furthermore, by examining the equation which describes the differential signal, it becomes clearer how a power imbalance between the sample and reference beams can produce a measurement at the lock-in amplification stage

which does not solely represent the difference in sample and reference absorbance. If there is a power offset between the sample and reference beams then the differential signal is described by the following equation:

$$\Delta I = -2.303E[A_s \Delta I_o + 2.303 I_o A_s \Delta A + \Delta A I_o] + \Delta I(0) \qquad (16)$$

where

I_o = initial laser power

$\Delta I_o = I_{o,s} - I_{o,r}$

$\Delta I(0) = I_s(0) - I_r(0)$

$\Delta A = A_s - A_r$

with $I_{o,s}$ = sample beam center intensity before entering the cuvette

$I_{o,r}$ = reference beam center intensity before entering the cuvette

$I_s(0)$ = sample beam center intensity immediately after exiting the cuvette (t = 0)

$I_r(0)$ = reference beam center intensity immediately after exiting the cuvette (t = 0)

A_s = sample absorbance

A_r = reference absorbance

Refer to Appendix I for the derivation of this equation. Equation 16 demonstrates that if an offset is present, then ΔI_o and $\Delta I(0)$ contribute to the lock-in signal as well as ΔA and could explain why only marginal detection limits are observed with the current system.

If no offset occurs between the sample and reference beams then $\Delta I_o = 0$ and $\Delta I(0) = 0$ and equation 16 reduces to:

$$\Delta I = 2.303 E I_o \Delta A \quad (17)$$

in which the lock-in signal is only a function of the absorbance difference between the sample and reference cuvettes (See Appendix I).

Second, a source of noise was found to be due to the mechanical chopper employed. Using a modulation frequency of 1.5 kHz required the chopper to operate at its upper frequency limit which imposed substantial vibration throughout the optical configuration. This vibration coupled with imperfections in the chopping blade contributed a phase jitter noise component of approximately 10% of the chopper "on time". The phase jitter was seen visually on the oscilloscope screen by observing rapid horizontal shaking of the signal square wave. Vibrations present in the optical system could be eliminated by employing a better quality chopper and mounting the entire configuration on a vibration free optical table.

Third, Buffett and Morris have shown that the signal-to-noise ratio for a dual-beam configuration is severely degraded when a low pump:probe power ratio is maintained (46). Typical dual-laser pump/probe thermal lens spectrometers use a pump laser power on the order of hundreds of milliwatts with a HeNe probe laser on the order of 2-3 milliwatts, resulting in high pump/probe power ratios at the sample. On the other hand, in a single-laser dual-beam configuration, a high pump:probe power ratio is not in-

herent since the same laser serves as the source for both beams. If a high pump:probe power ratio is desired in this situation then it must be created by employing a beam splitter which creates two beams of unequal intensity or by attenuating that portion of the beam designated as the probe before it enters the sample cell. The rotoreflected double-beam system is a variation on the single-laser dual-beam thermal lens spectrometer and presently is not configured to induce a high pump:probe power ratio. However, it can easily be altered to achieve a high pump:probe power ratio through attenuation of the rotoreflected probe beams by locating identical neutral density filters between the quarter-wave/mirror couples and the cuvettes. The optical density of the filters would be chosen in order to create a pump:probe power ratio on the order of that used in a typical dual-laser pump/probe thermal lens spectrometer. Consequently, an improvement in the detection limits for the system may be observed.

The differential and common mode responses of the rotoreflected double-beam system are presented in Table 2. The differential responses, obtained by measuring a series of standards against a solvent, were linear with concentration from the detection limit up to 9.6×10^{-6} M, with a correlation coefficient of 0.986. Ideally, the common mode response for each standard should be 0.0 mv, however the data indicates a slight signal is observed for each stan-

Table 2. Differential and Common Mode Responses.

Concentration[a] (M)	Differential Response (mv)	Common-Mode Response (mv)
Solvent	0.000[b]	0.00[b]
2.4×10^{-6}	0.067	0.05
4.8×10^{-6}	0.193	0.03
7.2×10^{-6}	0.363	0.06
9.6×10^{-6}	0.453	0.04

[a] I_2/CCl_4. [b] Designated reference point.

dard solution. This signal originates from a laser power imbalance between the sample and reference channels which is brought about by uncertainties in beam alignment and an optics mismatch.

The optics mismatch originates from the polarizing beam splitter cube because it has different extinction ratios for vertically and horizontally polarized light. Vertically polarized light is reflected by the cube while horizontally polarized light is transmitted with respective extinction ratios of 10^{-3} and 500. Simply stated, for every 1000 photons of vertically polarized light that enters the beam splitter one will not be reflected. Similarly, for every 1000 photons of horizontally polarized light entering the cube two will not be transmitted. Thus, when the laser beam is split by the beam splitter cube the emergent sample and reference pump beams are not equal. Balancing the intensity of these two beams is accomplished through appropriate rotation of the half-wave retarder. On the contrary, when the rotoreflected probe beams recombine there is no mechanism available to compensate for the intensity imbalance created by their second pass through the cube. Thus, a slight intensity imbalance between the sample and reference beams is sensed by the detector which is reflected in the common mode response. Nevertheless, despite the power imbalance caused by alignment uncertainties and the optics mismatch, the marginal chopper quality and

the less than optimum chopping frequency the noise level remains fairly constant over the common mode concentration range which indicates that the system is fairly resistant to background fluctuations due to concentration change.

To illustrate the advantages of the rotoreflected double-beam thermal lens spectrometer a comparison between it and the differential spectrometer of Dovichi and Harris and the dual-laser double-beam photodifferential spectrometer of Teramae and Winefordner is in order. Unlike the Dovichi and Harris set-up, the rotoreflective and dual-laser configurations allow for the sample to be positioned at the laser waist creating the strongest possible thermal lens. In addition, the rotoreflective arrangement also places the sample at the optimum probing distance, thus offering the greatest sensitivity possible of the three configurations.

Although optically more simple, the Dovichi and Harris set-up has one major constraint. In order for the beam divergence to respond linearly to absorbance in both cells, their configuration requires that the thermal lenses formed in both cuvettes have focal lengths longer than the confocal distance. This requirement is necessary so that the focal length of the thermal lens formed in the cuvette between the focusing lens and the beam waist has negligible effect on the spot size of the laser beam in the cuvette after the waist. A focusing lens having a long focal

length is needed in order to satisfy this condition. However, the use of long focal length lenses lowers the dynamic range of the Dovichi and Harris arrangement, since greater values of $\Delta I/I$ are obtained with shorter focal length lenses. No restriction is placed on the rotoreflective double-beam focussing lens focal length since separate beams are used for the sample and reference cuvettes, thus theoretically, dynamic range is not compromised.

The principle difference between the rotoreflective and dual-laser photodifferential spectrometers is that the former uses a single laser which eliminates pointing errors and alignment complexities inherent with two laser systems. More importantly, a differential response is achieved by different means in both configurations. The photodifferential set-up accomplishes background correction by electronically subtracting sample and reference signals, whereas in the rotoreflective system a differential response is achieved through high frequency and alternate modulation of the sample and reference beams. The differential response is produced in real time which eliminates the need for ancillary electronics to create it.

CONCLUSIONS

A unique double-beam thermal lens spectrometer has been developed which possesses a number of attributes innate to an ideal thermal lens spectrometer. These include:

1. Use of a single laser which eliminates alignment difficulties and pointing error associated with dual-laser configurations.
2. Incorporation of the rotoreflective concept which allows for the sample to be placed at the laser focal point to produce the strongest possible thermal lens while probing at the optimum waist-to-sample distance for maximum sensitivity.
3. Alternate high frequency modulation of the sample and reference beams producing a modulated differential response which allows for automatic subtraction of background absorbance through lock-in detection.
4. The differential response is produced in real time eliminating the need for added electronics to create it.

The strength of the steady state thermal lens produced with a modulation frequency of 1.5 kHz corresponded to only 30% of that produced with the single-beam rotoreflec-

tive technique under continuous illumination. Using a higher modulation frequency and chopper with greater duty cycle should produce a stronger thermal lens therefore increasing the detection capability of the instrument. Also, employing a higher quality chopper will diminish chopper-induced vibrations.

The equation derived for the differential response indicated that if a power offset exists between the sample and reference beams then the lock-in response will not solely reflect the difference in absorption between the sample and reference cuvettes. A power imbalance between the sample and reference beams created by alignment uncertainties most likely contributed to the observed marginal detection limits.

Also, the common mode responses indicated good immunity to background fluctuations from concentration change despite the optics mismatch, marginal chopper used and the less than optimal modulation frequency.

CHAPTER 3

SIMULTANEOUS THERMAL LENS AND FLUORESCENCE DETECTION FOR LIQUID CHROMATOGRAPHY

EXPERIMENTAL SECTION

Apparatus

A. Optical Configuration. Figure 7 illustrates an optical diagram for the liquid chromatography detector capable of detecting simultaneously in two modes: absorption via the thermal lens effect and fluorescence. All optical components are mounted on a 2 ft x 4 ft x 2 in optical breadboard (Newport Research Corporation, Model LS-24). The pump beam originates from an argon-ion laser, (Spectra Physics, Model 2030-15) and is composed of one of the following three wavelength combinations:

1. Deep UV: 275.4, 305.5 nanometers, P=100-310 mW
2. Near UV: 334.0, 351.1, 363.8 nanometers, P=100 mW-1 W
3. 457.9 nanometers, P=150, 700 mW.

It is modulated by a mechanical chopper (Stanford Research Systems, Model SR540) operating at a chopping frequency of 20 or 100 Hz. The chopper provides reference signals to lock-in amplifiers #1 and #2 (EG&G Princeton Applied

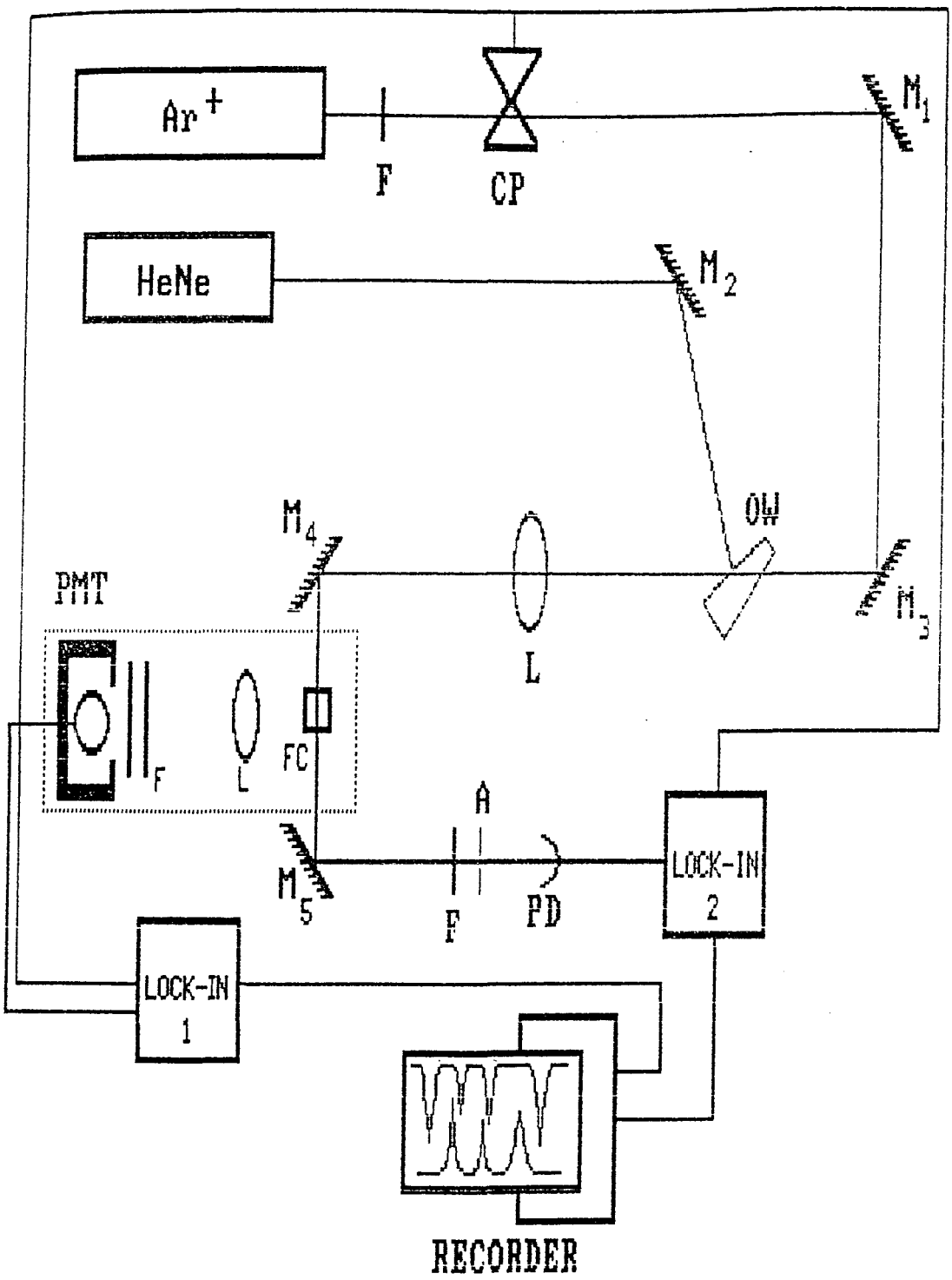

Figure 7. Optical diagram of the HPLC dual detector: CP, chopper; M, mirror; OW, optical wedge; L, lens; F, filter; PMT, photomultiplier tube; FC, flow cell; A, limiting aperture; PD, photodiode.

Research Model 7424 M-T and Model 5208). When the UV lines are in use, an UV bandpass filter (Color Specification Numbers 7-54 and 7-60 for deep and near UV, respectively) is placed before the chopper in order to maintain optical purity of the pump beam. The probe beam consists of a helium neon laser, 632.8 nanometers, P=3 mW (Coherent, Model 80). A fused silica wedge angled beam-splitter (Oriel, Model 44870) which transmits UV light and reflects visible light is used to combine the pump and probe beams collinearly. The beams then pass through a fused silica biconvex focussing lens (Oriel, 200 mm focal length) mounted on a translational stage such that the lens can be moved parallel to the beam direction.

Next, the beam passes through a 0.5 mm x 0.5 mm square fused quartz capillary (Vitro Dynamics), which serves as the detector flow cell, placed at the appropriate distance beyond the focussing lens. The flow cell is connected to the end of the column by a 5 cm x 0.005 in piece of stainless steel tubing. A small piece of tygon tubing joins the flow cell to the end of the connecting tubing. The tygon tubing connection is sealed with cyanoacrylate polymer. The total volume from the end of the column to the point at which the laser beam probes the cell is approximately 4.4 μL. Each end of the capillary is inserted into a threaded polypropylene male tubing connector. The female tubing connector parts are screwed onto each end and

the flow cell is then fastened between the posts of a "goal post" variable lens holder (Newport Research Corporation, Model VLH-3) by clamping the tubing connectors between four aluminum strips. Use of the tubing connectors permits fine rotational movement of the flow cell. A post holder (Newport Research Corporation, Model VPT-3) that allows for fine vertical movement is used to hold the mounted capillary and the entire set-up is fastened to the optical breadboard on a translational stage such that the flow cell can be moved perpendicular to the beam direction. This flow cell is used to obtain all the simultaneous thermal lens/fluorescence chromatograms. A Kratos 1 mm pathlength, 1.1 μL flow cell mounted on a tilt table (Newport, Model MM-2) is used to obtain all other thermal lens chromatograms.

After exiting the flow cell the pump beam is blocked by positioning a red glass filter in the beam path. The transmitted probe beam is then centered onto a 1 mm diameter pinhole serving as a limiting aperture and then strikes a position sensitive photodetector (United Detector Technology, Model 301-DIV) operating in the sum mode. The amplified signal is demodulated by lock-in amplifier #1 operating in the fundamental mode.

Fluorescence emission emanating from the flow cell is collected 90 degrees from the excitation beam using a biconvex quartz lens, f/#=2.1. The emission then passes

through one of the interference filter (Twardy Technology, Inc.) and colored glass filter combinations, described in Table 3, depending on which excitation wavelength is utilized. Emission amplification is accomplished with a RCA, IP28A photomultiplier tube operating at an applied voltage between -900 and -1000 V. The photomultiplier tube is positioned such that an image of the flow cell fills the PMT aperture in order to illuminate as great an area possible of the photocathode. The fluorescence signal is then demodulated by lock-in amplifier #2 operating in the fundamental mode with a time constant of 1 s. A light tight box encloses the photomultiplier tube, collection optics and flow cell.

Outputs from the lock-in amplifiers are recorded on a dual channel strip chart recorder (Cole-Parmer, Model 8373-20). Laser beam power is measured with a power meter (Scientech, Model 360203).

B. Liquid Chromatography Equipment. Microbore separations are performed on a 250 mm x 1 mm i.d. column (Alltech) packed with 5 μm octadecylsilane. A Beckman Model 114M single piston pump regulates the mobile phase delivery while sample injection volumes of 1 μL are delivered to the column with a Rheodyne Model 7520 microbore injector. Unless otherwise stated all microbore chromatograms are obtained using a mobile phase flow rate of 30 μL/min. The polynuclear aromatic hydrocarbon (PAH) stan-

Table 3. Bandpass and Glass Filter Combinations Used To Isolate Fluorescence Emission.

Excitation Wavelength (nm)	Interference Filter Bandpass Center (nm)	Colored Glass* Filters
275.4, 305.5	450 ± 70	GG-400, CS: 4-96, CS: 3-73 (2)
334.0, 351.1, 363.8	500 ± 70	GG-420, CS: 4-96, CS: 3-73 (2)
457.9	550 ± 70	GG-495, CS: 4-96

*Colored glass filters are designated by their Color Specification (CS) Number or their Schott Glass Number.

dard mixture and the solvent refined coal (SRC II) neutral PAH fraction are separated using a mobile phase of 100% methanol. A mixture mobile phase of methanol/water is used to separate the pharmaceutical and substituted benzene mixtures at respective volume ratios of 70:30 and 60:40.

C. Spectrophotometers and Fluorimeter. Absorption spectra are obtained using a Perkin Elmer Coleman 575 spectrophotometer. Transmittance spectra of interference and glass cutoff filters are recorded with a IBM 9420 UV-Visible spectrophotometer. A Perkin Elmer LS-5 spectrofluorimeter is used to record emission spectra of the SRC II neutral PAH fraction and selected individual PAH's.

Reagents

All chemicals are reagent grade quality and used without further purification and all solvents are HPLC grade. High purity water is obtained from a Syron/Barnstead, Nanopure II System. Chemicals and solvents used in this study are listed in Table 4. The commercial standard PAH mixture contains each of the following compounds at a concentration of 0.5 mg/mL: phenanthrene, anthracene, fluoranthene, pyrene, triphenylene, benzo[a]anthracene, chrysene, benzo[e]pyrene, perylene and benzo[a]pyrene. Appropriate working standards are prepared from it by dilution with methanol. Individual PAH standards are prepared in methanol. Minimum amounts of toluene are used to aid dissolution of some PAH's.

Table 4. Chemicals and Solvents Used For the Microbore Dual HPLC Detector

Chemical/Solvent	Source
Tetrahydrofuran	Aldrich Chemical Co.
Benzene	
Hexane	
Chloroform	
o-nitroaniline	
Aluminum oxide	
Fluoranthene	
Chrysene	
Triphenylene	
Perylene	
Benzo[a]pyrene	
Benzo[e]pyrene	
Theophylline	
Caffeine	
4-Acetamidophenol (acetaminophen)	
p-Acetophenetidide (phenacetin)	
Acetylsalicylic acid	
Standard polynuclear aromatic hydrocarbon mixture	Supelco
Benzo[a]anthracene	
Nitrobenzene	Fisher
Anisole	
Acetophenone	Kodak
Pyrene	
Anthracene	
Phenol	Mallinckrodt
Phenanthrene	Dr. Yen Yang

The substituted benzene mixture is prepared by diluting aliquots of toluene, benzaldehyde, acetophenone, anisole, nitrobenzene and phenol with methanol to form stock and working standard solutions.

Individual stock solutions of theophylline, caffeine, acetylsalicylic acid, 4-acetamidophenol (acetaminophen) and p-acetophenetidide (phenacetin) are prepared by dissolving appropriate weights of each compound in methanol. Aliquots of each stock solution are diluted with methanol to form the pharmaceutical mixture.

The SRC II heavy distillate is obtained from the National Bureau of Standards in Bethesda, Maryland.

Procedures

Collinear alignment of the pump and probe beams (Refer to Figure 7). First, the flow cell and M_5 are removed from the configuration. Then, collinear alignment of the pump and probe beams is accomplished by observing their spots on targets positioned in the far-field at two different points outside the optical path. The first target is placed at a point several feet beyond the position of M_5. The second target is placed such that the spots created by the "wedge transmitted" HeNe and "wedge reflected" UV beams can be observed. Alignment of the beams is achieved by keeping the pump beam stationary while the probe beam is manipulated by adjusting the fine positioning controls on the optical wedge and M_2 mirror mounts. When the pump and

probe beam spots at both far-field points appear to be perfectly overlapped the beams are taken to be aligned collinearly. In addition, the alignment is checked by placing a stationary mounted, thin piece of paper in the optical path approximately where the flow cell is to be positioned. If the HeNe probe beam travels cleanly through the hole burned by the pump beam then no further adjustments are made. Next, the flow cell and M_5 are put back into position and the peak due to an eluting component is recorded. Fine adjustment of the probe beam positioning mirrors are made until the peak height is maximized. At this point the beams are considered to be aligned and no further adjustments are made. It is necessary to perform this procedure daily due to the argon-ion laser's pointing instability.

Determination of z_{opt} for a 200 mm focal length lens. Figure 8 illustrates an optical diagram for the single-beam configuration used to determine z_{opt}, the lens to sample cell distance which would produce the greatest thermal lens signal. Output (442 nm, P=10 mW) from a HeCd laser (Liconix, Model 4210NB) is modulated at 80 Hz by a mechanical chopper and passed through an achromatic biconvex lens (Oriel, f=200 mm) followed by a 1 cm quartz cuvette. The focussing lens is mounted on a translational stage which allows the lens to be moved parallel to the laser beam direction. After passing through a sample cell filled with 3.5×10^{-6}M o-nitroaniline, the beam is centered on a limit-

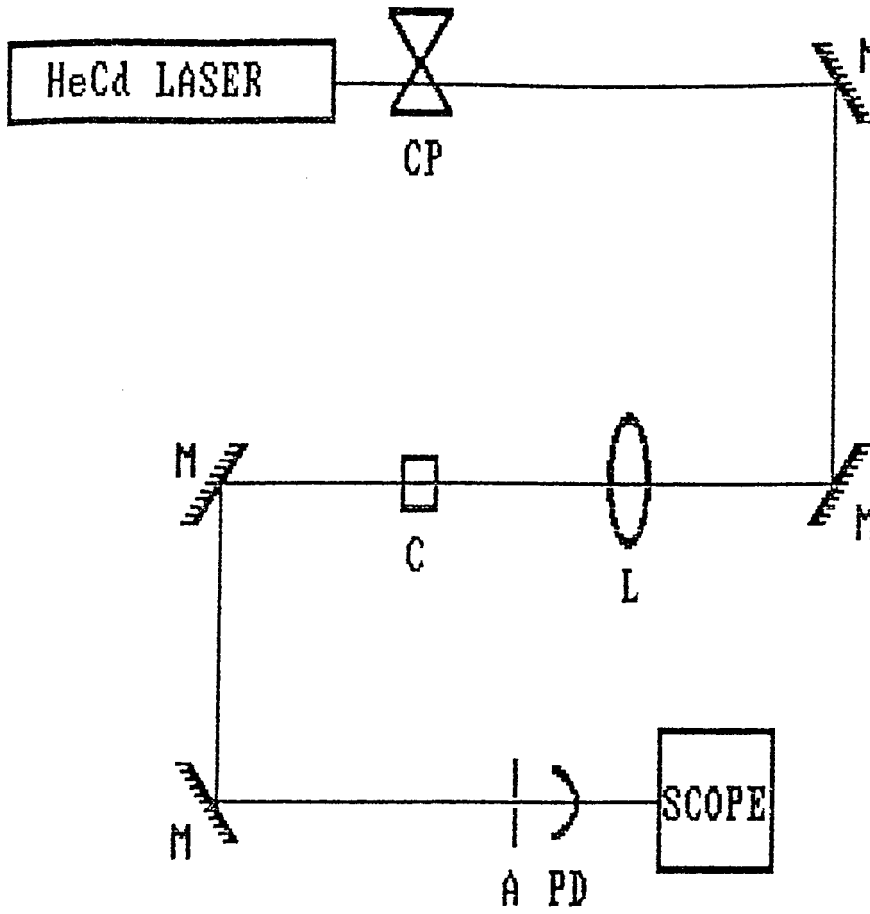

Figure 8. Optical configuration for z_{opt} determination: CP; chopper, M; mirror, L; lens mounted on translational stage, C; sample cuvette, A; aperture, PD; photodiode, OS; oscilloscope.

ing aperture followed by a photodiode. The sample cuvette is positioned in the beam path at a point beyond the lens focal point. Signals from the photodiode are fed directly into a digital storage oscilloscope (Nicolet, Model 4094A).

The focussing lens is moved at 1 mm increments along the beam path. At each position the thermal lens transient was averaged for one minute and stored by the oscilloscope. Measurements of I(0) and I(t) are read directly from the oscilloscope screen. The thermal lens signal, [I(o)-I(t)]/I(t), at each lens position are calculated and plotted against the lens to sample cuvette distance. The maximum of the resulting curve is taken as z_{opt}.

Thermal Lens Response Linearity Study. Standard solutions of benzo[a]anthracene in methanol are prepared at molar concentrations ranging from 7.5×10^{-6} to 2.4×10^{-4}. Starting with the least concentrated solution, triplicate injections of each standard are made. Deep UV detection is used at a power of 115 mW. The benzo[a]anthracene peak height is plotted as a function of concentration and the data is subjected to linear regression analysis. Five linearity studies are done on different days and the results compared in Figure 21. The Kratos flow cell is used for the study.

Isolation of the PAH fraction from solvent refined coal. The PAH fraction from a sample of solvent refined coal (SRC-II, National Bureau of Standards) is isolated using the procedure developed by Vassilaros et al. (82). First, a 20 cm x 1.1 cm i.d. glass column filled with hexane is slurry packed with 6 g of aluminum oxide (neutral, activated, mesh 200). Then, 0.28 g of the SRC-II sample is dissolved in chloroform and adsorbed onto 3.5 g of alumina. The chloroform is evaporated under a gentle stream of nitrogen and the adsorbed sample is dry packed onto the top of the alumina column. A 25 mL aliquot of hexane is then used to elute the hydrocarbon fraction from the adsorbed sample. This fraction is discarded. Next, the PAH fraction is eluted with 50 mL of benzene and collected in a 100 mL round bottom flask. The benzene is rotary evaporated and the remaining residue is dissolved with the aid of sonication and diluted to 25 mL with methanol.

Emission spectra of the SRC II neutral PAH fraction. Emission spectra of the SRC II neutral PAH fraction diluted with methanol/water (80:20, v/v) are recorded between the ranges of 300-530 nm and 320-540 nm using respective excitation wavelengths of 275 and 306 nm.

Methanol and methanol/water Raman shift determination. Emission spectra of methanol and a methanol/water solution

(80:20) are recorded between the ranges of 290-530 nm and 300-530 nm using respective excitation wavelengths of 275 nm and 290 nm. An excitation wavelength of 306 nm is also used to record the emission spectrum of the methanol/water solution between 320 and 540 nm. Peaks due to Raman scattering are identified by noting peaks which maintain a constant wavelength shift when the excitation wavelength is changed.

RESULTS AND DISCUSSION

Dual detector optimization. Before simultaneous thermal lens/fluorescence chromatograms can be recorded the dual detector must be optimized with respect to the proper flow cell position for obtaining maximum thermal lens response plus selection of appropriate optical windows for gathering fluorescence emission while eliminating scatter from mobile phase Raman emission and extraneous source excitation.

Unlike conventional HPLC absorption detectors location of the flow cell in a thermal lens detector is critical if maximum sensitivity is desired. Thermal lens theory predicts that maximum response occurs at a distance z_{opt} along the beam path before and after the pump beam waist. Accordingly, the detector flow cell can be placed at either of these positions for optimum thermal lens response. Due to size constraints imposed by the optics the capillary flow cell is positioned at z_{opt} after the beam waist. Figure 9 illustrates the results obtained for determining z_{opt} after the beam waist for a 200 mm focal length lens. Each point represents the average of two thermal lens measurements $\Delta I/I$, plotted as a function of sample to lens distance z, while the solid curve represents a least squares fit of the data (83). This curve indicates that the focal point of the lens is 20.0 cm since no

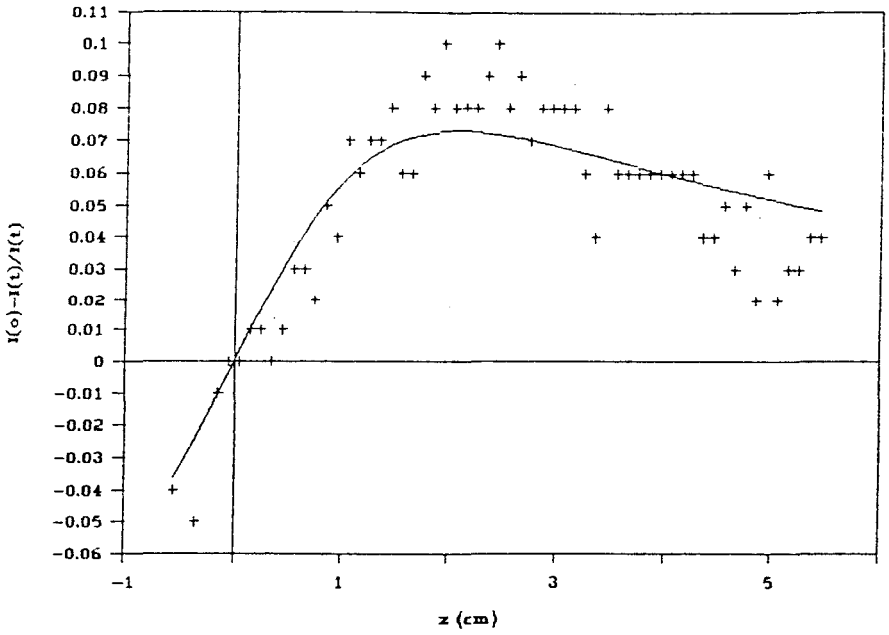

Figure 9. Thermal lens response as a function of distance beyond a 200 mm focal length lens.

thermal lens response is observed at this value of z. Also, the curve maximum indicates that the greatest thermal lens response should be realized if the flow cell is positioned 22.5 cm after the focussing lens meaning that z_{opt} equals 2.5 cm.

After incorporating the flow cell into the optical configuration at z_{opt} and attaching the microbore column the flow cell position is "fine tuned". This is accomplished by using fine increments to change z, through movement of the focussing lens closer or further away from the flow cell, until the peak height produced by an absorbing species eluting off the column is a maximum. The greatest peak height recorded occurs at z equal to 22.5 cm corresponding to the value of z_{opt} = 2.5 cm determined above.

Once the flow cell position and pump/probe alignment are optimized thermal lens detection of components eluting from the microbore column can proceed. Figure 10 illustrates a thermal lens chromatogram of the standard PAH mixture obtained with the deep UV laser line (P = 100 mW) and the Kratos flow cell. Each peak corresponds to 20 ng of injected component. Peak identities are assigned by matching retention times with individually injected standards and by observing relative peak height changes when the standard is spiked with a known compound. Peak assignments and component retention times are listed in Table 5. In addition to the compounds listed in Table 5 the PAH

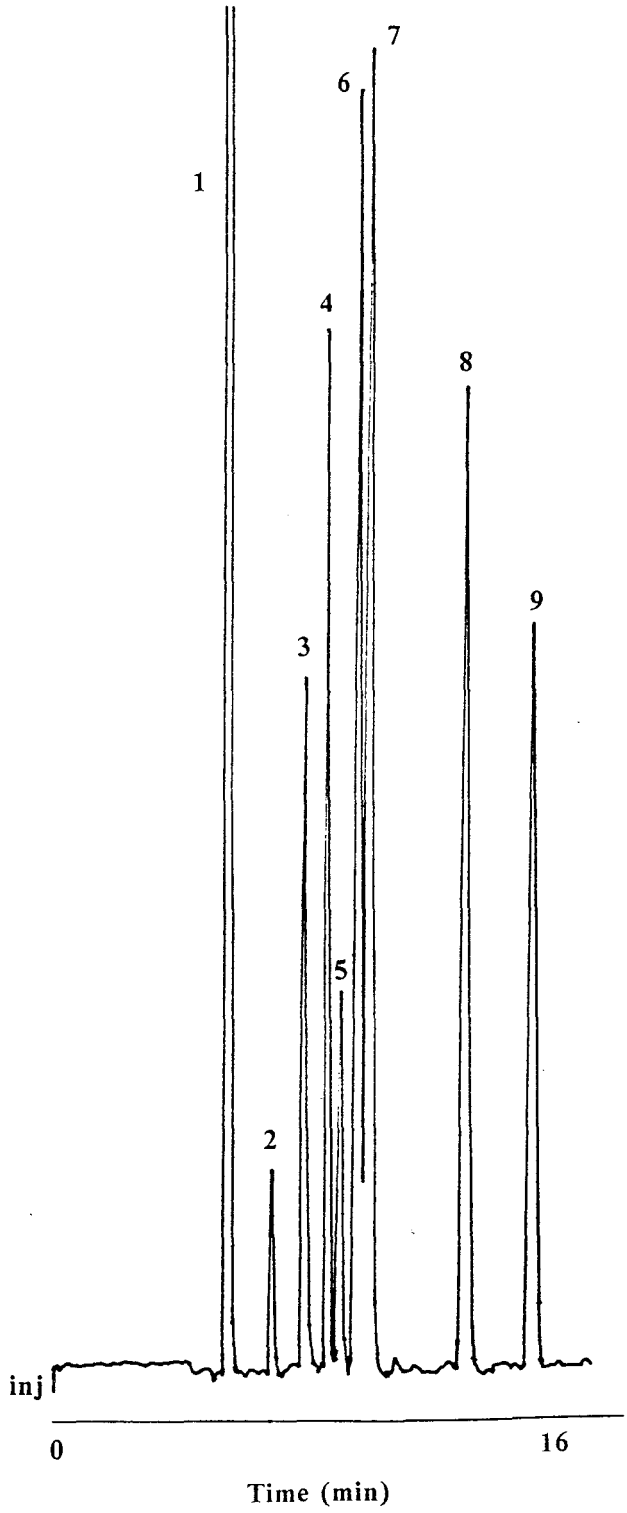

Figure 10. Deep UV thermal lens chromatogram of the standard PAH mixture. Mobile phase: methanol (100%), flow rate: 30 μL/min, 20 ng of each component injected, P=100 mW.

Table 5. Deep UV Thermal Lens Chromatogram Peak Assignments and Retention Times for the Standard PAH Mixture Separation

Peak No.	Compound	Retention Time (min)
1	toluene (solvent)	5.4
2	phenanthrene/ anthracene	7.3
3	fluoranthene	8.3
4	pyrene	9.0
5	triphenylene	9.6
6	benzo[a]anthracene	10.1
7	chrysene	10.5
8	benzo[e]pyrene	13.7
9	benzo[a]pyrene	15.8

standard mixture also contains anthracene and perylene. Anthracene and phenanthrene coelute using the given chromatographic conditions whereas perylene does not produce a detectable thermal lens signal at the chosen wavelength. Note that the peaks in Figure 10 are very sharp and except for benzo[a]anthracene and chrysene baseline resolution is achieved for all detected components. Given the complexity of the mixture and that the separation is performed isocratically without a mixed solvent mobile phase such resolution is outstanding compared to results obtained on an analytical column. To achieve comparable resolution on a reverse phase analytical column requires, upon injection, starting with a water/acetonitrile (35:65) mixed mobile phase for 2 minutes followed by a linear gradient to 100% acetonitrile (84). Clearly, the microbore system is the system of choice for performing this type of separation.

In addition, the components elute from the column according to the number of aromatic rings they possess; the smaller compounds eluting before the larger ones. Since the mixture is composed of compounds containing from one to five aromatic rings it can be used as a standard to ascertain the relative ring composition of a unknown mixture of neutral PAH's provided that the standard and unknown are separated using identical chromatographic conditions. Figure 10 indicates that single membered rings start eluting at approximately 5 minutes followed by three membered

rings at 7 minutes, four membered rings between 8 and 11 minutes, and five membered rings between 14 and 16 minutes.

Figure 11 illustrates a separation of the standard PAH mixture done under identical conditions as that shown in Figure 10 except the near UV laser line is used at a power of 600 mW. Each peak represents 2 ng of injected component. Peak assignment and component retention times are listed in Table 6. The most noticeable difference between the two chromatograms is their appearance. The relative peak heights for the eluting components produced with deep UV excitation are different from those recorded with near UV excitation. Specifically, in the near UV chromatogram the triphenylene and toluene peaks have disappeared and the intensities of chrysene, benzo[a]anthracene and benzo[e]pyrene peaks have decreased to barely above the baseline noise. Also, a peak corresponding to perylene appears between the benzo[e]- and benzo[a]pyrene peaks in the near UV chromatogram. This illustrates an obvious advantage to obtaining mixture chromatograms at more than one excitation wavelength in that most likely not all components of the mixture produce thermal lens signals at a single laser line. More than one wavelength should be use so that the most complete profile of the mixture can be obtained.

At this point the differences between the relative peak heights between the two chromatograms can be explained

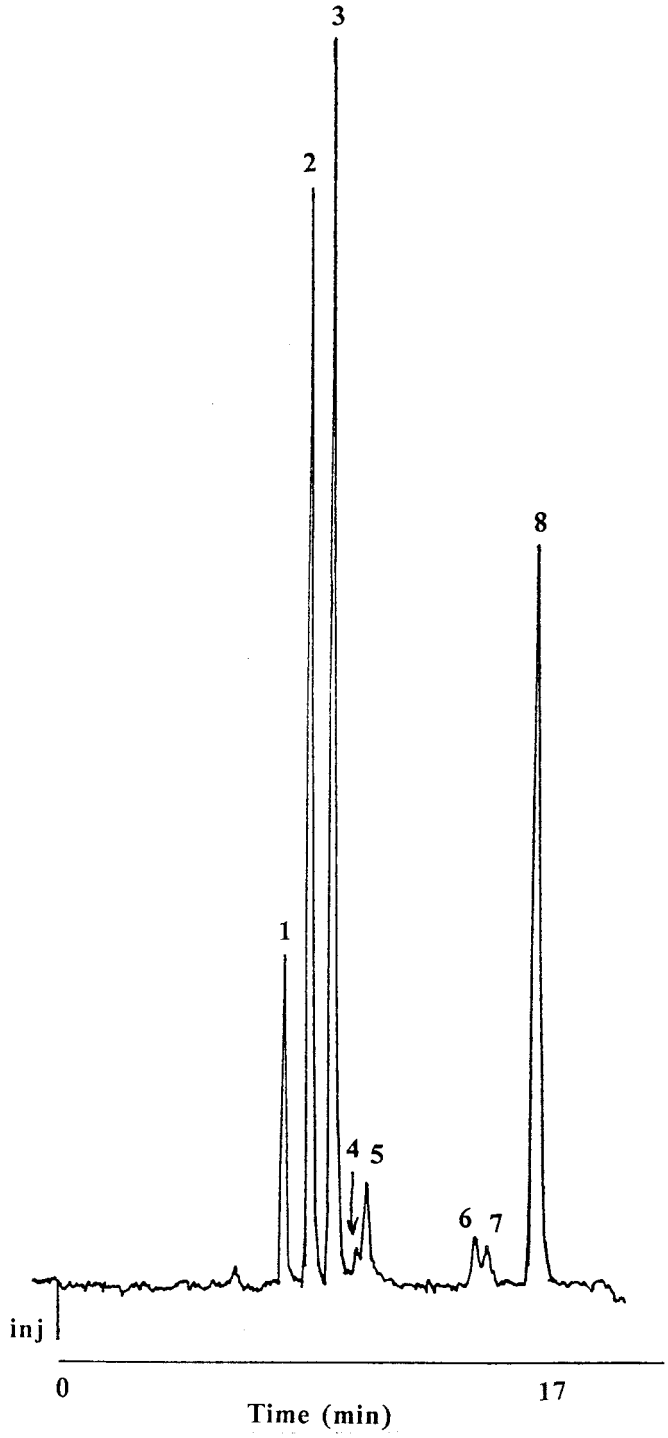

Figure 11. Near UV thermal lens chromatogram of the standard PAH mixture. Mobile phase: methanol (100%), flow rate: 30 μL/min, 2 ng of each component injected, P=600 mW.

Table 6. Near UV Thermal Lens Chromatogram Peak Assignments and Retention Times for the Standard PAH Mixture Separation

Peak No.	Compound	Retention Time (min)
1	phenanthrene	8.0
2	fluoranthene	8.8
3	pyrene	9.5
4	benzo[a]anthracene	10.6
5	chrysene	10.9
6	benzo[e]pyrene	14.7
7	perylene	15.2
8	benzo[a]pyrene	16.8

by two possible reasons. First, for any component in the mixture, if only non-radiative relaxation is taking place then the relative difference in its peak height between the two chromatograms reflects the difference in extinction coefficients the component possesses for the deep and near UV laser lines. However, if a component fluoresces as well as produces a thermal lens then the relative peak height difference between the two chromatograms represents the differences in Q_f and $1-Q_f$ (see equations 17 and 18, page 48) the component has for the two laser lines in addition to the dissimilar extinction coefficients. In order to distinguish which case is relevant a fluorescence chromatogram should be obtained along with the thermal lens profile. This will be elaborated upon when the simultaneous thermal lens/fluorescence chromatograms are discussed.

The other notable difference between the two chromatograms is the non-uniformity in retention times between like components. This discrepancy can arise from mobile phase flow rate drift, an unequilibrated column, or a faulty recorder chart drive. The later is suspect since fluctuations in column back pressure are not observed and the column is allowed to equilibrate at the desired flow rate for up to two hours before any injections are made.

Before fluorescence chromatograms can be recorded appropriate optical windows for emission collection must be determined based on the three excitation laser lines emplo-

yed: deep UV, near UV and 457.9 nm. The windows are chosen based on the SRC II neutral PAH fraction emission spectra so that mobile phase Raman scatter and source excitation, are effectively blocked from the photomultiplier tube, thus keeping the background signal to a minimum.

Figure 12 illustrates the emission profile of the SRC II neutral PAH fraction obtained using the deep UV excitation wavelengths 275 nm (a) and 306 nm (b). All emission produced by the two excitation wavelengths occurs between 280 nm and 520 nm. Emission profiles of methanol recorded at different excitation wavelengths showed the Raman shift of methanol to range between 30 nm and 36 nm. Thus, the peaks appearing in the 275 nm and 306 nm profiles at 305 nm and 342 nm, respectively are due to Raman shifted excitation. Figure 13 illustrates the optical windows, created by the filter combinations listed in Table 3, used to collect fluorescence emission produced by the three excitation wavelengths. In Figure 13a the optical window chosen for deep UV excitation allows radiation to be transmitted between 420 nm and 520 nm (represented by the shaded portions of the deep UV emission profiles in Figure 12) while effectively blocking the Raman and source wavelengths as well as the HeNe probe wavelength of 632.8 nm. Accordingly, the optical windows used with the near UV and 457.9 nm laser lines are selected so that Raman shifted and source excitation and the probe laser wavelength are

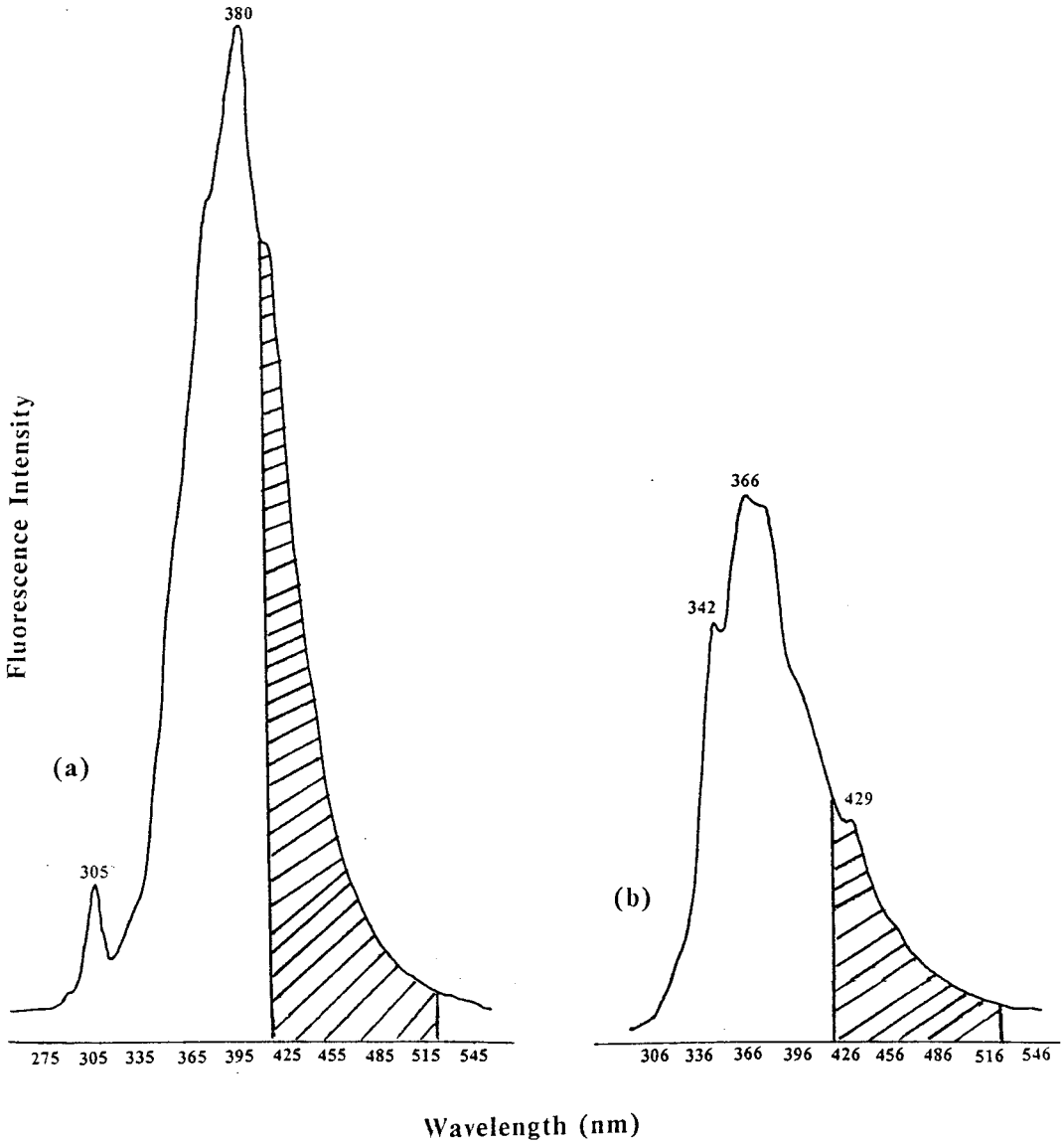

Figure 12. Emission profile of the SRC II neutral PAH fraction. (a) excitation wavelength = 275 nm. (b) excitation wavelength = 306 nm. Solvent: methanol/water (80:20).

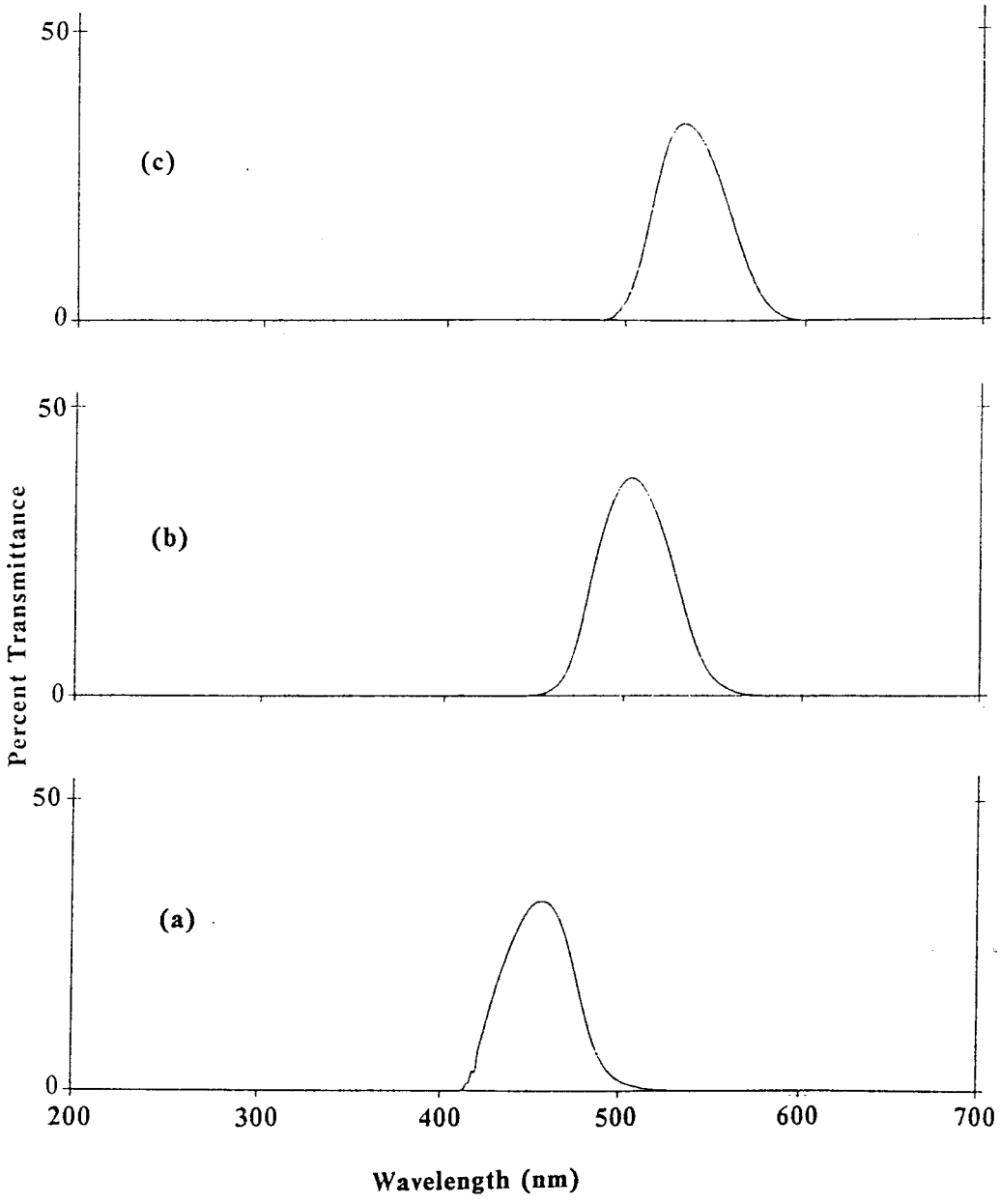

Figure 13. Optical windows used to collect fluorescence emission using excitation wavelengths of (a) deep UV, FWHM=48 nm, %T=16%, (b) near UV, FWHM=50 nm, %T=19%, and (c) 458 nm, FWHM=46 nm, %T=19%.

effectively blocked while also allowing a total transmittance range of 100 nm.

Simultaneous thermal lens and fluorescence detection of the standard PAH mixture. Once the dual detector has been optimized with respect to flow cell position and pump/probe beam alignment and the fluorescence optical windows have been chosen then simultaneous thermal lens/fluorescence detection can proceed. Figure 14 shows the deep UV (P = 150 mW) simultaneous thermal lens (Figure 14a) and fluorescence (Figure 14b) chromatograms of the standard PAH mixture. Fluorescence emission is collected over the bandpass shown in Figure 13a. All fluorescence chromatograms are inversely recorded above the thermal lens chromatograms to facilitate easier comparison of the two.

Initial observation of the thermal lens chromatogram indicates that chromatographic peak resolution has deteriorated upon switching from the Kratos flow cell to the square capillary tube. This arises from a volume discrepancy between the two flow cells. The Kratos flow cell volume, including the connecting tubing volume, is 1.1 μL compared to 4.6 μL for the square capillary (Refer to Appendix II for calculation). Thus, the larger volume of the square capillary promotes more band broadening resulting in poorer peak resolution. However, despite the less than optimum flow cell volume the square capillary yields resolution good enough to distinguish the nine components of the

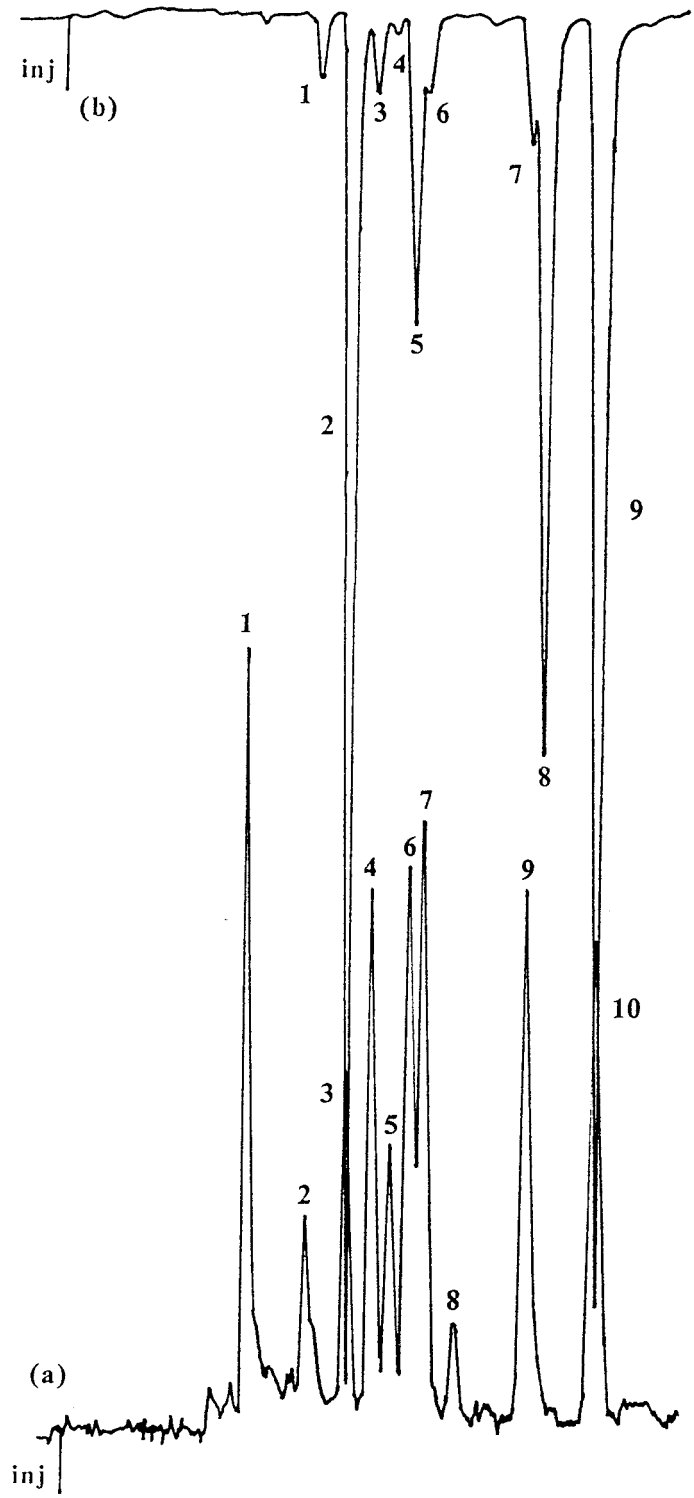

Figure 14. Deep UV simultaneous (a) thermal lens and (b) fluorescence chromatogram of the standard PAH mixture. Mobile phase: methanol (100%), flow rate: 30 μL/min, 20 ng or each component injected, P=150 mW.

Table 7. Peak Identities for the Deep UV Simultaneous Thermal Lens/Fluorescence Chromatograms of the Standard PAH Mixture

	Peak Number	
Compound	Thermal Lens Detection	Fluorescence Detection
toluene	1	----
phenanthrene	2	1
fluoranthene	3	2
pyrene	4	3
triphenylene	5	4
benzo[a]anthracene	6	5
chrysene	7	6
impurity	8	----
benzo[e]pyrene	9	7
perylene	----	8
benzo[a]pyrene	10	9

standard PAH mixture. Peak number 8 is an impurity since its retention time did not correspond to any of the singly injected PAH's.

Figure 14 illustrates an advantage inherent in the dual detector compared to conventional HPLC detectors in that thermal lens and fluorescence chromatograms can be recorded without resorting to two separate experiments. Also, since all of the thermal lens peaks have been previously identified peak assignment in the fluorescence chromatogram is merely an exercise in inspection. Of course, this is only an advantage if the sample components fluoresce at the chosen excitation wavelength. Injections of individual and spiked standards are not required for fluorescence peak identity confirmation. Table 7 lists the fluorescence peak identifications of the standard PAH mixture using the thermal lens profile as a reference standard. Peaks numbers in all dual chromatograms are assigned according to when the component elutes relative to the injection point.

In addition, simultaneous thermal lens and fluorescence detection allows for the identification of mixture components which would ordinarily be missed if only a single detection method were used. This is an obvious advantage however, the reason for it has more subtle origins and needs to be elaborated upon. The root of this advantage stems from the complementary nature which exists be-

tween the two techniques and is best demonstrated using perylene as an example. From Figure 11 it is known that perylene elutes between benzo[e]- and benzo[a]pyrene. However, despite the fact that perylene has extinction coefficient values of 2500 and 790 $Lmol^{-1}cm^{-1}$ (Refer to Appendix III), at 275 and 306 nm, respectively, a thermal lens peak is absent from Figures 10 and 14a. These extinction coefficient values indicate that perylene absorbs significantly at the two excitation wavelengths. Accordingly, this is confirmed by the presence of the perylene peak in the deep UV fluorescence chromatogram (Figure 14b, peak #8). If absorption did not occur then a fluorescence peak should not be present (assuming that fluorescence transmittance through the optical window is large). Taking these observations into consideration, the absence of a perylene peak in the thermal lens chromatogram indicates that $1-Q_f$ for perylene must be very small compared to Q_f meaning that fluorescence dominates over radiationless relaxation. Furthermore, a fluorescence quantum efficiency of 0.97 for perylene in cylcohexane has been reported (refer to Appendix III) which further supports the preceeding statement. Thus, even though a species absorbs significantly at the chosen excitation wavelength does not necessarily imply that a thermal lens signal will be produced. Consequently, simultaneously recording fluorescence

and thermal lens signals guarantees that compounds exhibiting such behavior do not go undetected.

The effect of changing the excitation wavelength, from the deep to the near UV laser line, on the appearance of the dual chromatogram is illustrated in Figure 15. Figure 15 represents the near UV thermal lens/fluorescence chromatogram of the standard PAH mixture. Each peak represents 20 ng of injected component detected using a laser power of 110 mW. Peak identities are listed in Table 8. Except for some slight peak broadening the thermal lens chromatogram is identical to that obtained with the Kratos flow cell (Figure 11). The fluorescence chromatogram contains only four peaks. However, this does not mean that only four components of the mixture fluoresce using the near UV laser line. The emission transmission optical window has been shifted to a longer wavelength range than that used for deep UV excitation. Other mixture components may have high enough fluorescence quantum efficiencies at the excitation wavelength but their emission could be blocked by the filters. In addition, as a result of the excitation wavelength change and the shifted optical window benzo[e]pyrene no longer appears as a shoulder on the perylene peak, thus making this compound easier to quantitate. Besides the different fluorescence optical windows used, differences in relative peak height observed for the near and deep UV simultaneous thermal lens/fluorescence

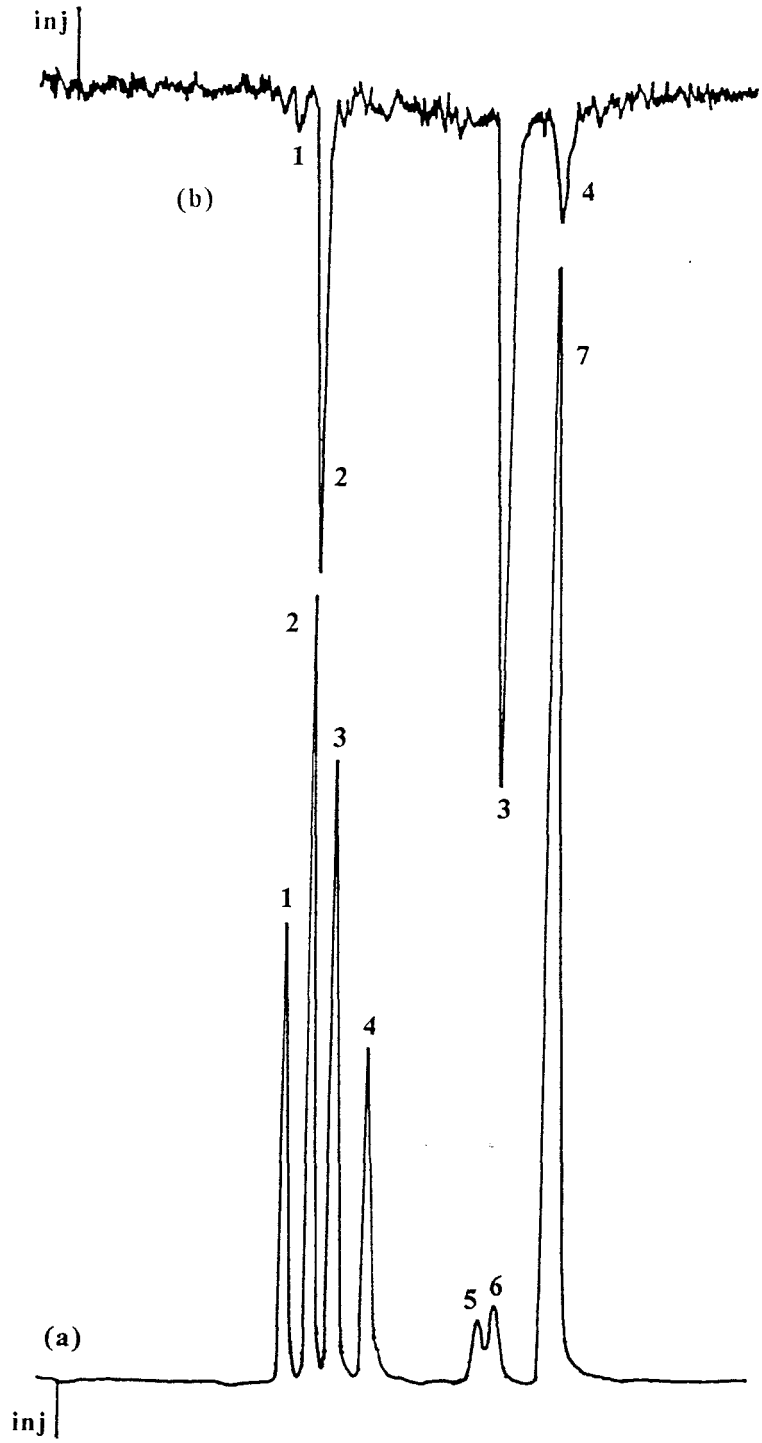

Figure 15. Near UV simultaneous thermal lens (a) and fluorescence (b) chromatogram of the standard PAH mixture Mobile phase: methanol (100%), flow rate: 30 μL/min, 20 ng of each component injected, P=110 mW.

Table 8. Peak Identities For the Near UV Simultaneous Thermal Lens/Fluorescence Chromatogram of the Standard PAH Mixture

Compound	Peak Number	
	Thermal Lens Detection	Fluorescence Detection
phenanthrene/ anthracene	1	1
fluoranthene	2	2
pyrene	3	----
benzo[a]anthracene	4	----
benzo[e]pyrene	5	----
perylene	6	3
benzo[a]pyrene	7	4

chromatograms reflect the dissimilar values of Q_f and $1-Q_f$ the mixture components have for the two excitation laser lines. By varying the excitation wavelength the overall absorbance:fluorescence ratio for each component changes thus producing chromatograms which are unique to the excitation wavelength employed.

Analysis of solvent refined coal. No where are the above advantages exemplified and the dual detector's utility more evident than in its ability to characterize the composition of an unknown complex mixture. Solvent refined coal (SRC) is an extremely complicated mixture of aliphatic hydrocarbons and neutral and heterocyclic aromatic hydrocarbons. Its diverse composition makes its analysis a time and labor intensive process plus prevents complete characterization using a single analytical method (85-88). Generally, prior to any instrumental analysis, a gross separation of SRC is performed dividing it into several fractions containing classes of compounds based on their solubility in various organic solvents. This separation is usually done on an alumina column or the SRC sample can be extracted directly (82, 89). In turn, each fraction, in and of itself, is a very complex mixture which requires gas chromatography or HPLC techniques in conjunction with the appropriate detectors to characterize it. Ideally, the chosen detector should provide the most information regarding the mixture composition in the least amount of time. Inspection of

Figures 16-18 demonstrates that the thermal lens/fluorescence dual detector accomplishes just that.

Figure 16 is recorded using the deep UV, Figure 17 the near UV and Figure 18 the 457.9 nm laser line. Each figure represents the comparison of SRC II neutral PAH fraction thermal lens and fluorescence chromatographic profiles simultaneously recorded using the designated wavelength and acquired with only a single injection. Alternatively, to obtain the same comparison using conventional detection systems one could record thermal lens and luminescence profiles separately and then overlay the chromatograms. However, this method requires setting up two different detection systems resulting in twice as much sample and mobile phase consumption as well as a doubling of analysis time. This last factor becomes very important when run times exceed 30 minutes for single injections. Also, a true comparison could not be obtained if a sample is unstable to the extent that its composition changes between recording of the separate chromatograms.

The deep UV thermal lens absorption profile, Figure 16a, indicates that the majority of the components in the SRC II mixture elute between 9 and 17 minutes indicating a composition composed of mainly 4 and 5 aromatic ring compounds when compared to the standard PAH mixture component retention times. Several unresolved components appear to elute between 6 and 7 minutes. These compounds should

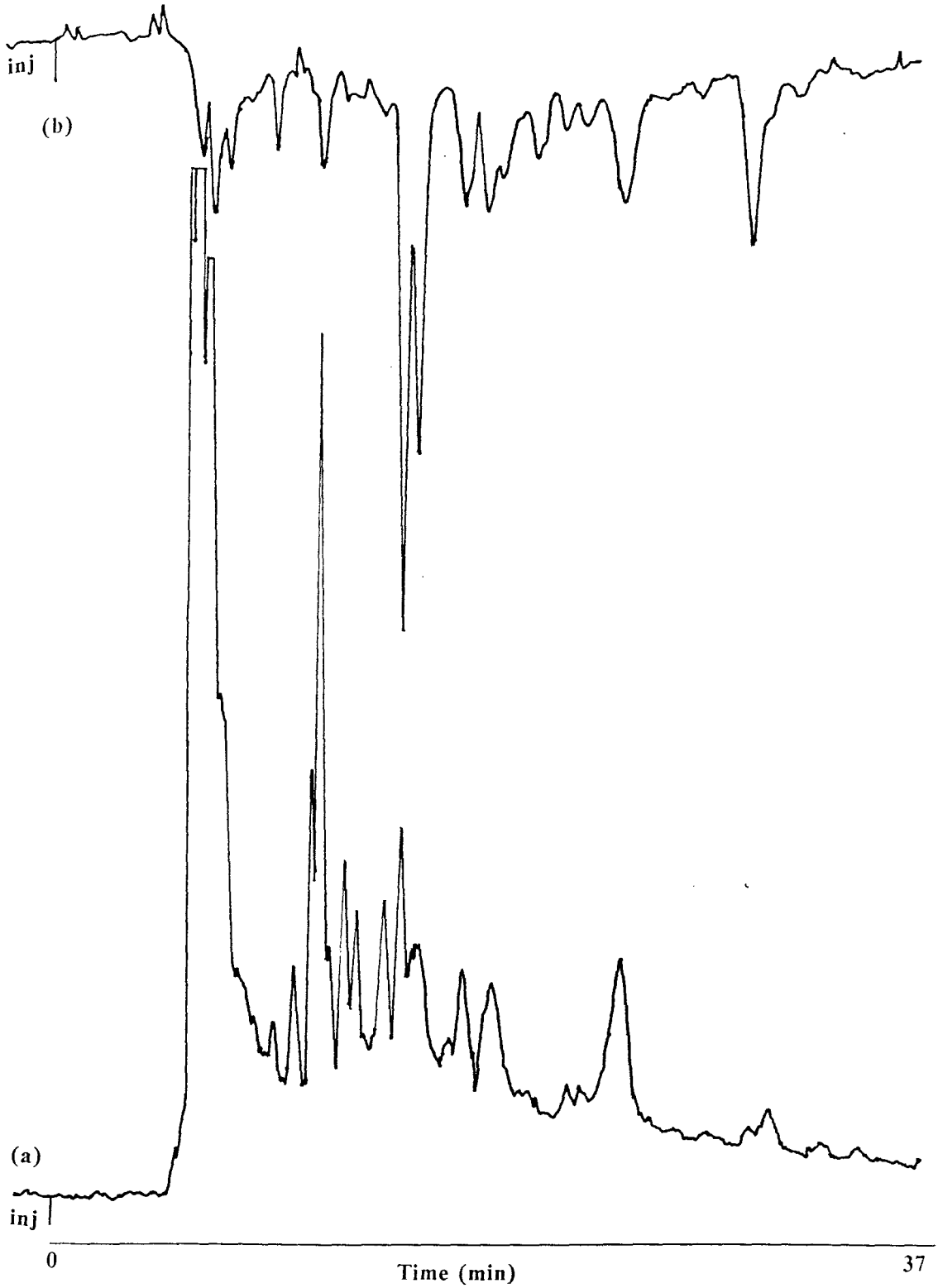

Figure 16. Deep UV simultaneous thermal lens (a) and fluorescence (b) chromatogram of the SRC II neutral PAH fraction. Mobile phase: methanol (100%), flow rate: 30 μL/min, P=200 mW.

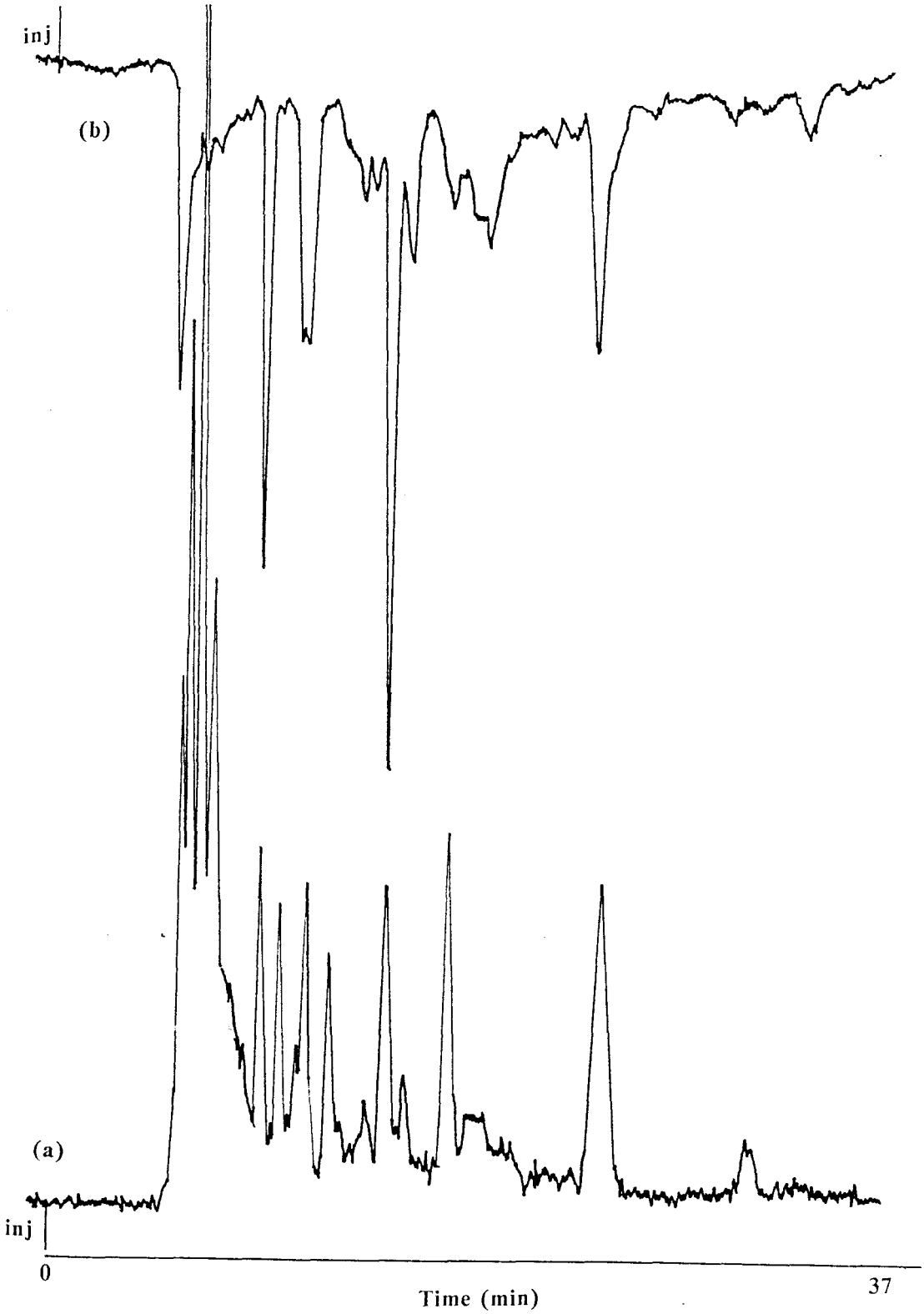

Figure 17. Near UV simultaneous thermal lens (a) and fluorescence (b) chromatogram of the SRC II neutral PAH fraction. Mobile phase: methanol (100%), flow rate: 30 μL/min, P=150 mW.

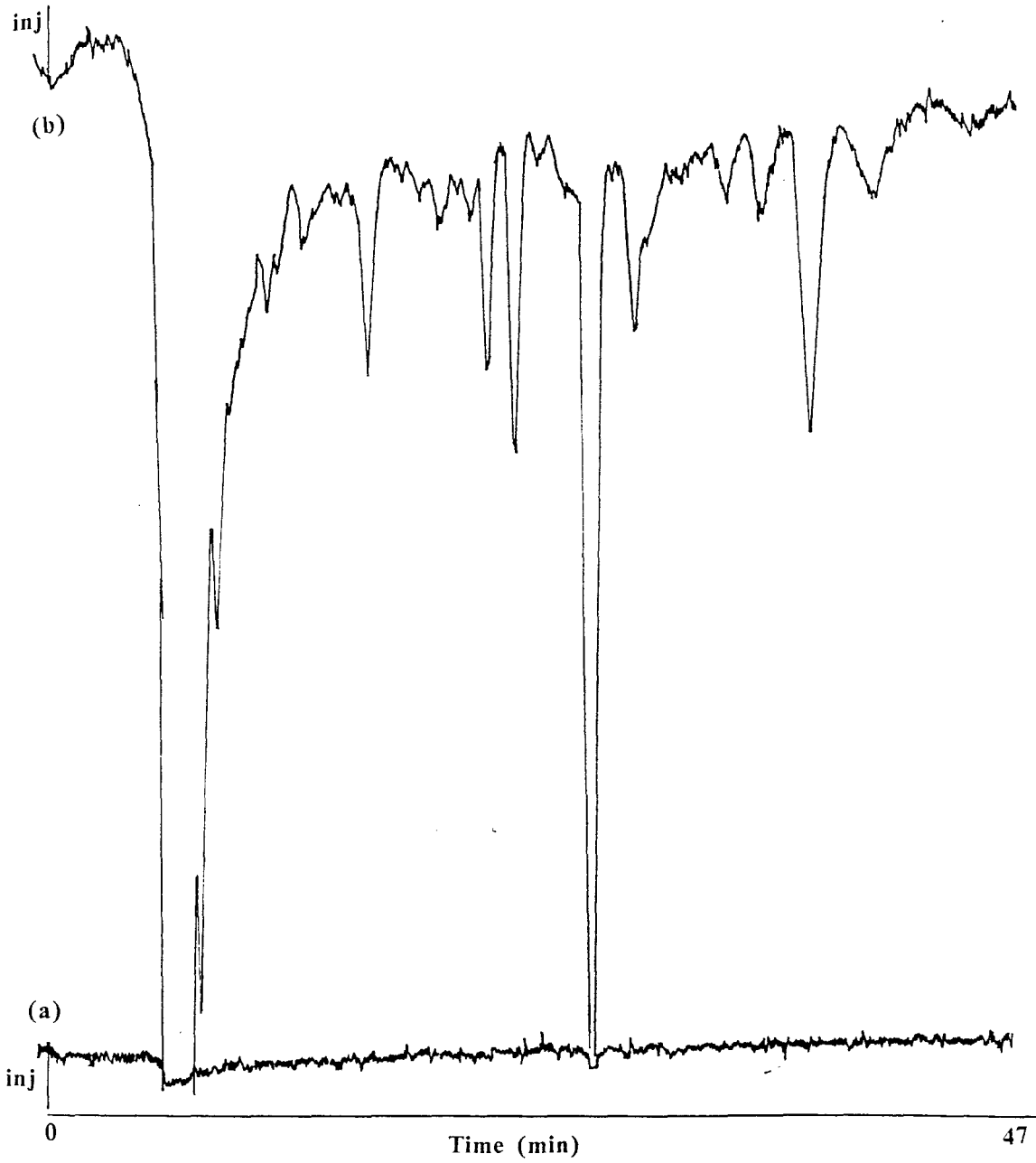

Figure 18. Simultaneous thermal lens (a) and fluorescence (b) chromatogram of the SRC II neutral PAH fraction obtained with 457.8 nm excitation. Mobile phase: methanol (100%), flow rate: 30 μL/min, P=150 mW.

contain 2 and 3 rings. The deep UV fluorescence profile, Figure 16b, reveals many fluorescing com-ponents in the mixture. Components which absorb as well as fluoresce at the given wavelength are easily identified by matching thermal lens peaks with the corresponding fluorescence peaks, if they exist. A few compounds containing more than five rings are present in the mixture indicated by the peaks appearing at retention times greater than 17 minutes. This is most noticeable in the fluorescence profile. Figures 17a and 17b, obtained with near UV excitation, again illustrate the effect that varying the excitation wavelength has on the thermal lens and fluorescence chromatographic profiles. As discussed earlier, the relative differences between the deep and near UV simultaneous chromatograms are a result of the complementary nature which exists between the thermal lens effect and fluorescence. To continue, Figure 18 illustrates the thermal lens and fluorescence profiles of the SRC II neutral PAH fraction, at three times the concentration used for the deep and near UV chromatograms, obtained at a wavelength of 457.9 nm. The most striking feature about this chromatogram is that the thermal lens profile contains no peaks while the fluorescence profile shows many components. Obviously, substantial absorption is taking place at this wavelength but is not being detected by the thermal lens effect.

This difference between the thermal lens and fluorescence chromatograms obtained at 457.9 nm excitation can be explained by one of two reasons. First, no thermal lens signal is observed because the probe beam is out of alignment. However, this is not the case since the pump/probe beam alignment is carefully optimized before any SRC II injections are made. The alignment is also re-checked after the chromatogram is recorded to insure that the alignment is maintained throughout the recording of the chromatogram. The second, and most likely, reason that no peaks are observed in the thermal lens chromatogram is that some mixture components do not possess extinction coefficients great enough to produce a thermal lens effect at 457.8 nm and the components which do absorb sufficiently relax primarily by radiant means. This example illustrates why it is so important that thermal lens detection be done in conjunction with fluorescence detection. If only thermal lens detection at 457.8 nm is used to characterize the SRC II PAH fraction then it would falsely be concluded that the mixture contains no components which absorb at that wavelength.

Another unexpected feature about Figure 18 is the relatively large amount of fluorescence observed due to unresolved components eluting between 5 and 9 minutes. This most likely results from unretained polar heterocyclic PAHs present in the mixture. Since the procedure used to separ-

ate the neutral PAH fraction from the SRC II sample is a gross one it is highly likely that these compounds are present to some extent.

Finally, to further demonstrate the applicability of the dual detector's wavelength variability for characterizing a complex mixture the SRC II neutral PAH fraction thermal lens profiles recorded with the deep UV, near UV and 457.9 nm laser lines are presented together in Figure 19. These chromatograms are obtained using the Kratos flow cell which explains the narrower peaks and sharper resolution compared to those recorded using the square capillary. A laser power of 200 mW is used for the deep and near UV chromatograms while 700 mW is used for the 457.9 nm profile.

Observing these chromatograms together reveals three important advantages of the detector's wavelength variability. First, as mentioned above only a single peak is observed in the 457.9 nm chromatogram. If the chromatogram is viewed alone it is questionable whether the observed peak reflects a real component of the mixture or an artifact. However, this component is shown not to be an artifact since peaks with identical retention times appear in the deep and near UV chromatograms. Second, the observed peak height differences for individual components which produce peaks in both UV chromatograms can aid in their identification. As a hypothetical example assume

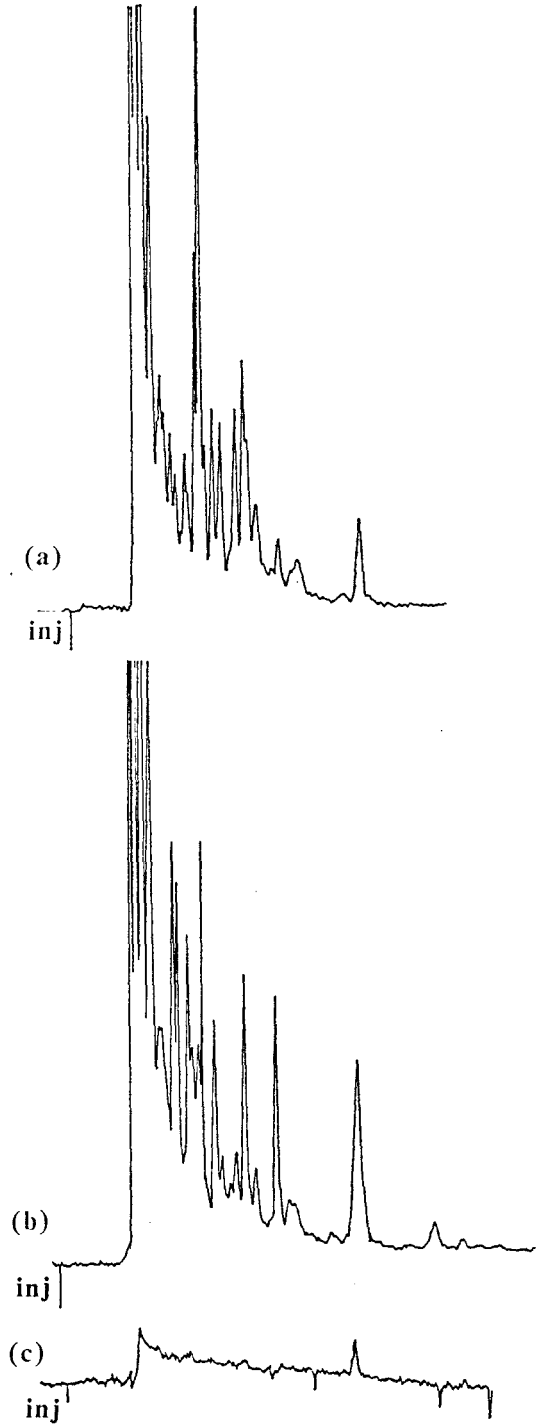

Figure 19. Deep UV (a), near UV (b), and 457.8 nm (c) thermal lens chromatograms of the SRC II neutral PAH fraction. Mobile phase: methanol (100%), flow rate: 30 μL/min.

that a component in the SRC II mixture which produces peaks in the deep and near UV chromatograms is thought to be due to chrysene. Assuming conditions are identical, except wavelength, during the recording of each chromatogram the difference in peak height between the two peaks is a reflection of the different extinction coefficients the component has at the two laser lines. If the component is chrysene then the ratio of the two peak heights should correspond to the extinction coefficient ratio of chrysene at the different laser lines. Third, a more comprehensive characterization of the mixture is obtained. Compounds in the mixture which do not absorb at one wavelength and would otherwise remain undetected are easily seen in chromatograms recorded at wavelengths at which the compounds do absorb.

Detection limit and linearity studies. The analytical thermal lens detection limits obtained with the dual detector are presented in Table 9. These studies are performed with the Kratos flow cell because of its smaller volume compared to the square capillary. Pyrene and benzo[a]anthracene are chosen for the deep and near UV studies, respectively. The lowest detection limits are obtained using the near UV laser line due to the higher beam powers available (Column 2). Using a near UV laser power of 1000 mW the lowest mass detection limit achievable is 9.3 pg, injected on column, corresponding to a concentration detec-

Table 9. Thermal Lens Detection Limits Obtained With the Dual Detector

Wavelength and Extinction Coefficient[a]	Power (mW)	Mass Detection Limit[b] (pg)	Concentration Detection Limit (M)	Absorbance Detection Limit (AU)
Deep UV[c] 4.4×10^4	70	390	1.7×10^{-6}	7.2×10^{-3}
	230	150	6.6×10^{-7}	2.9×10^{-3}
Near UV[d] 5.3×10^4	800	13	6.4×10^{-8}	3.4×10^{-4}
	1000	9.3	4.6×10^{-8}	2.4×10^{-4}

[a] The values listed are the sum of the individual extinction coefficient values, from Appendix III, that the designated compound has at each wavelength composing the laser line that was used. Units are $Lmol^{-1}cm^{-1}$.

[b] At S/N = 3.

[c] Compound used is benzo[a]anthracene.

[d] Compound used is pyrene.

tion limit of 4.6×10^{-8} M (S/N=3). This is equivalent to an absolute detection limit of 93 femtograms (0.46 femtomole or approximately 3×10^{8} molecules) of pyrene detected based on a calculated probe beam volume of 10 nL (Appendix IV). The absolute detection limit refers to the actual amount (mass, moles or molecules) detected at the designated signal-to-noise ratio. Figure 20 illustrates the thermal lens signal obtained for a 4 ng injection of benzo[a]anthracene using deep UV excitation at a power of 70 mW. The signal (peak #2) corresponds to approximately 6×10^{-3} AU with root mean square noise equivalent to approximately 2×10^{-4} AU.

The detection limits in terms of minimum detectable absorbance are poor compared to previously reported values of $2\text{-}4 \times 10^{-6}$ AU (46), 1×10^{-7} AU (47), and 2×10^{-5} AU (50). Two reasons could account for this. First, since benzo[a]-anthracene and pyrene have relatively large extinction coefficients and respective quantum efficiencies of 0.20 and 0.72 (refer to Appendix III) both compounds fluoresce significantly at the wavelengths used for the detection limit studies. This means that the fluorescence quantum efficiency magnitude plays a significant role in the thermal lens detection limit determination. The greater the fluorescence quantum efficiency the lesser amount of radiationless relaxation will take place and a smaller thermal lens signal is produced. Thus, the observed thermal lens detection limits for this study are poor if only radiation-

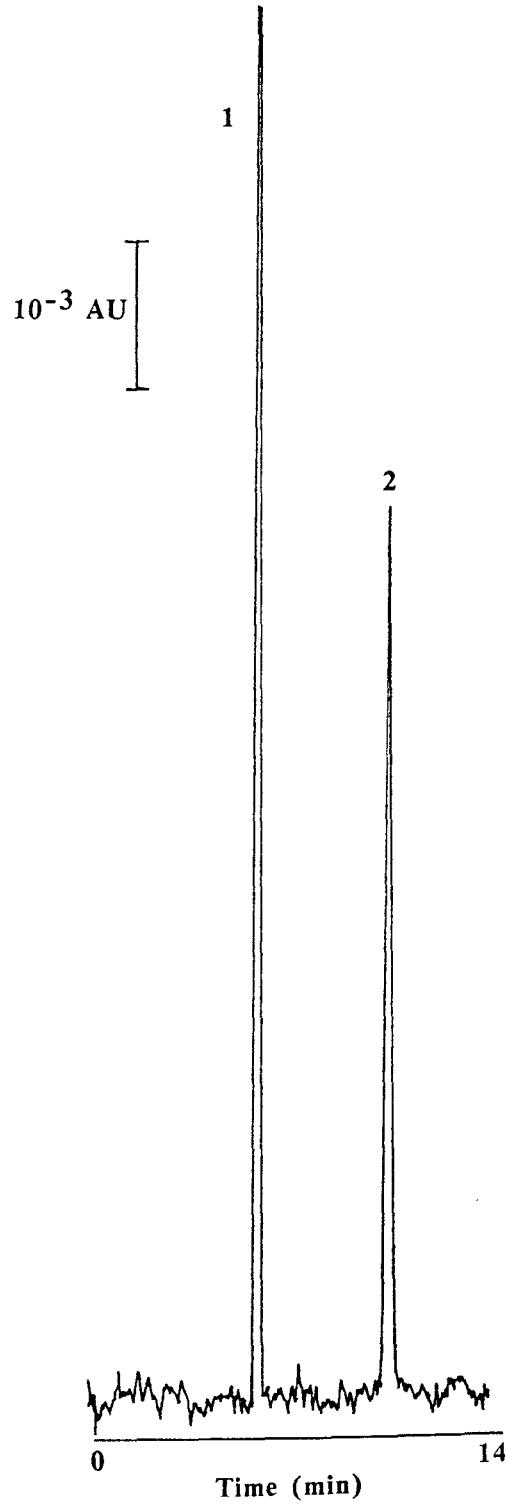

Figure 20. Deep UV thermal lens chromatogram of benzo[a]anthracene. Mobile phase : methanol (100%), flow rate: 30 uL/min, 4 ng injected, P=70 mW.

less relaxation is assumed. However, since this is not the case then the thermal lens detection limits must be viewed in the context that they reflect the degree to which fluorescence is occurring. Second, methanol is a relatively poor thermal lensing solvent because of its polarity. The thermal lens effect is strongest when nonpolar solvents possessing large dn/dT values are used. If a mobile phase more conducive to forming refractive index and temperature gradients could be found then lower thermal lens detection limits would be possible.

In Table 10 detection limits from various thermal lens HPLC detectors are listed. As expected, due to the microbore column's smaller internal diameter excellent mass detection limits are obtained with the dual detector compared to other thermal lens detectors which use an analytical column. The detection limits are in good agreement with those acquired with the listed microbore and capillary column systems. In addition, the thermal lens absolute detection limit is approximately three orders of magnitude better than those obtained, by Winefordner, et al, for a series of PAHs using laser-induced photoacoustic HPLC detection (90). The present dual detector thermal lens detection limits could be improved by using a shorter focal length lens which would deliver a higher power density to the sample. Alternatively, the optical configuration could be altered by placing the flow cell at the pump beam waist

Table 10. Comparison of Detection Limits Obtained With Various Thermal Lens HPLC Detectors

Wavelength (nm)	Power (mw)	Column Size	Compound Detected	Mass Detection Limit (pg)
deep UV	230	microbore	pyrene	150[a]
near UV	1000	microbore	benzo[a]anthracene	9.3[b]
488	300	microbore	DABS-gly	1.4[c]
458	800	capillary	o-nitroaniline	30[d]
458	80	analytical	o-nitroaniline	900[e]
458	190	analytical	o-nitroaniline	530[f]
515	500	microbore	benzopurpurin	3.0[g]

[a]This study.
[b]This study.
[c]Reference 91.
[d]The detection limit is reported as 30 pg at S/N=2 in Reference 92. The value listed in this table is adjusted to reflect S/N=3.
[e]Reference 42.
[f]Reference 40.
[g]Reference 49.

and using a separate lens to focus the probe beam at a distance beyond the pump beam waist equal to z_{opt}. This is the ideal configuration for a pump/probe thermal lensing system if maximum sensitivity is desired. Also, the thermal lens detection limits should be improved if compounds with negligible quantum efficiencies at the designated wavelengths are used.

Table 11 presents the fluorescence detection limits obtained with the dual detector using the square sided capillary flow cell. The lowest detection limit is obtained with near UV excitation and corresponds to an absolute detection limit of 29 fg (0.14 femtomole) or 8×10^7 molecules excited in a 12 nL pump volume. Table 12 lists the detection limits obtained with various laser fluorescence HPLC detectors. The current microbore system yields poorer fluorescence detection limits than those obtained with an analytical column. This could be explained by the fact that the microbore system does not allow for the excitation beam to be focussed into the sample as do the analytical column systems. Thus, a less than optimal power density delivered to the sample contributes to the marginal detection limits.

The dual detector fluorescence detection limits are approximately an order of magnitude better than the thermal lens detection limits when the amount of material detected per milliwatt of power is compared (refer to Tables 9 and

Table 11. Fluorescence Detection Limits Obtained With the Dual Detector

Excitation Wavelength (nm)	Power (mW)	Mass Detection[a] Limit (pg)	Concentration Detection Limit (M)
Deep UV[b]	100	3.8	1.5×10^{-8}
	200	3.3	1.3×10^{-8}
Near UV[c]	150	2.4	1.2×10^{-8}

[a]At S/N = 3. [b]Compound use is perylene.

[c]Compound used is fluoranthene.

Table 12. Comparison of Detection Limits Obtained With Various Laser Fluorescence HPLC Detectors

Excitation Wavelength (nm)	Power (mW)	Column Size	Compound Detected	Mass Detection Limit
deep UV	100	microbore	perylene	3.8 pg[a]
deep UV	200	microbore	perylene	2.4 pg[b]
near UV	150	microbore	fluoranthene	2.4 pg[c]
325	8	analytical	aflatoxins	1.1 pg[d]
325	8	analytical	zearalenone	300 pg[e]
488	100	analytical	MPDME[f]	53 pg[g]
488	1200	analytical	andriamycin	10 pg[h]
488	1200	analytical	daunorubin	15 pg[i]
351, 356	1000	analytical	fluoranthene	20 fg[j]
325	6.5	capillary	pyrene	24 fg[k]
325	10	capillary	coumarin 440	2.3 fg[l]

[a,b,c]This study.
[d]The detection limit is reported as 750 fg at S/N=2 in Reference 69. The value listed in this table has been adjusted to reflect S/N=3.
[e]Reference 71.
[f]mesoporphyrin IX dimethyl ester
[g]Reference 73.
[h,i]Reference 76.
[j]Reference 72.
[k]Reference 78.
[l]Reference 74.

11). This observation needs to be addressed. Thermal lensing is potentially as sensitive as fluorescence detection since the magnitude of both effects are directly proportional to pathlength and power delivered to the sample. However, additional variables, inherent in the manner in which the thermal lens signal is measured, contribute to the difference in thermal lens and fluorescence detection limits. Since flow is present inside the flow cell the pump beam region is constantly being cooled due to thermal transport causing a smaller thermal lens to be formed compared to a static situation (39). Also, turbulence as a result of mobile phase mixing inside the flowcell contributes noise to the background signal. Detection limits for flowing samples have been shown to be three times greater than those observed in static situations due to these two phenomena (39).

Another possible noise source stems from the fact that the blocking efficiency of the absorption filter used to reject the pump beam from the photodiode is not 100%. Thus, residual pump radiation strikes the detector and contributes to the background signal level as well as any optical interference produced by the overlapping pump and probe beams (29, 31). A possible means of reducing this noise would be to use a Glan-Thompson polarizer to reject the vertically polarized pump beam based on polarization. However, if this method is used then caution must be exer-

cised since the highest quality commercially available Glan-Thompson polarizers can pass residual pump radiation causing an intensity variation of the probe as high as 0.1% (31). To totally alleviate the problem one would have to resort to using a propagation-encoding optical configuration (31) which spatially isolates the pump and probe beams before the detector.

Methanolic benzo[a]anthracene solutions at different concentrations are used to study the linearity of the thermal lens system. Detector response is found to be linear from 7.5×10^{-6} to 1.4×10^{-4} M with a correlation coefficient of 0.993 using the deep UV line at an approximate power of 115 mW and corresponds to an on column mass detection range of 1.7 to 32 ng. The peak heights of three consecutive injections of the 27 ng standard gave a reproducibility of 2.7% relative standard deviation.

The narrow linear dynamic range obtained could possibly reflect the amount of fluorescence that occurs with benzo[a]anthracene using the deep UV laser line. As discussed earlier, if substantial fluorescence is occurring then the thermal lens peak heights will not be indicative of the specie's total absorption. If this is true, then the low end of the calibration curve would be extended if only radiationless relaxation were to take place. Presently though, the lower end of the linear dynamic range could

most likely be extended by using a higher laser power and a shorter focal length lens.

Figure 21 represents the thermal lens calibration curves obtained on five separate days. It illustrates how critical proper pump/probe beam alignment experience is to quantitation. Linear dynamic range varies widely from day to day as well as the sensitivity (slope) of each curve. However, with each successive day these two variables improve until on day 5 the steepest slope and largest linear dynamic range are obtained. The fact that both variables improved on a daily basis demonstrates the dependence of operator experience on quantitation. Thus, before quantitation is attempted it is imperative that the operator have substantial pump/probe beam alignment experience.

Additional deep UV thermal lens applications. Traditionally, depending on the type of laser used, the range of compounds detected with conventional thermal lens HPLC detection systems has been limited, often to compounds which absorb at a single visible wavelength. This restriction represents the technique's major impracticality since it excludes the analysis of multitudes of compounds that absorb in the ultraviolet. However, the present laser-based microbore detector overcomes this handicap with its ability to utilized wavelengths which span the ultraviolet through the green portion of the electromagnetic spectrum without having to result to more than one laser source. The avail-

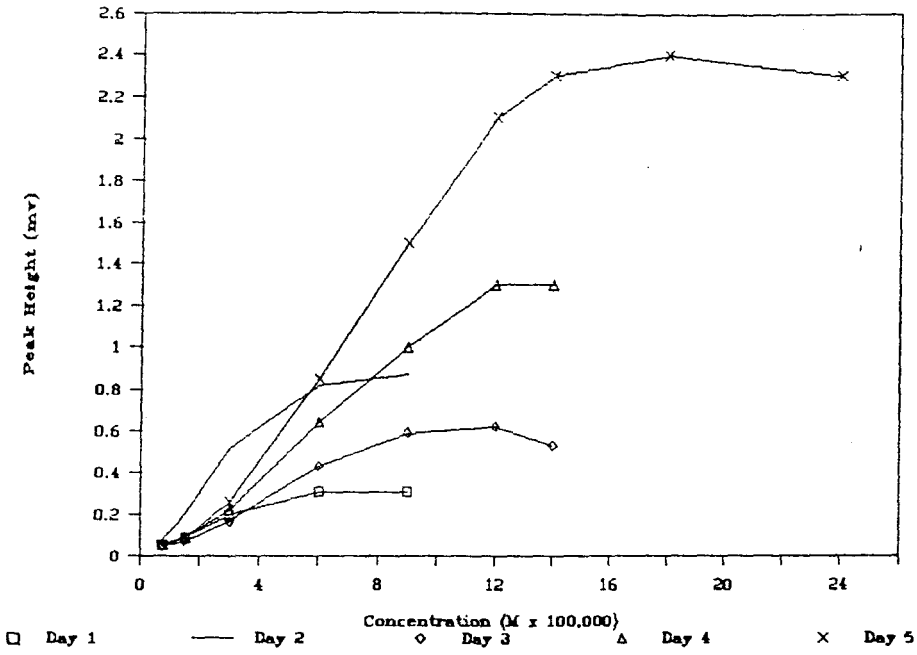

Figure 21. Thermal lens calibration curves obtained on five separate days.

ability of the deep UV line containing 275 and 306 nm makes the detector a more practical instrument since thermal lens detection can be extended to non-colored compounds. This is demonstrated in the following examples.

Figure 22 illustrates the deep UV (P = 100 mW) thermal lens isocratic separation of a mixture containing the seven substituted benzenes: phenol, benzaldehyde, acetophenone, nitrobenzene, methylbenzoate, anisole, and toluene. A mobile phase consisting of methanol/water, 70:30 (v/v) and flow rate of 30 μL/min are used. Table 13 lists the peak assignments, retention times and the amount of each compound injected. Baseline resolution is accomplished for nearly all components of the mixture and a mass detection limit of 580 pg (4.7×10^{-6} M, S/N=3) is calculated for nitrobenzene. In general, signal-to-noise ratios for all the components should increase as the laser power is increased. However, this is not always the case as is demonstrated in Figure 23. Figure 23 represents the deep UV thermal lens chromatogram of the substituted benzene mixture, at one half the concentration as that represented in Figure 22, recorded using a power of 310 mW. Comparing the two chromatograms shows that the relative peak heights for each component are different at the two powers. Most noticeable are the peak height increases for toluene and anisole (Peaks 6 and 7) and decreases for benzaldehyde and nitrobenzene (Peaks 2 and 4) in the 310 mW chromatogram

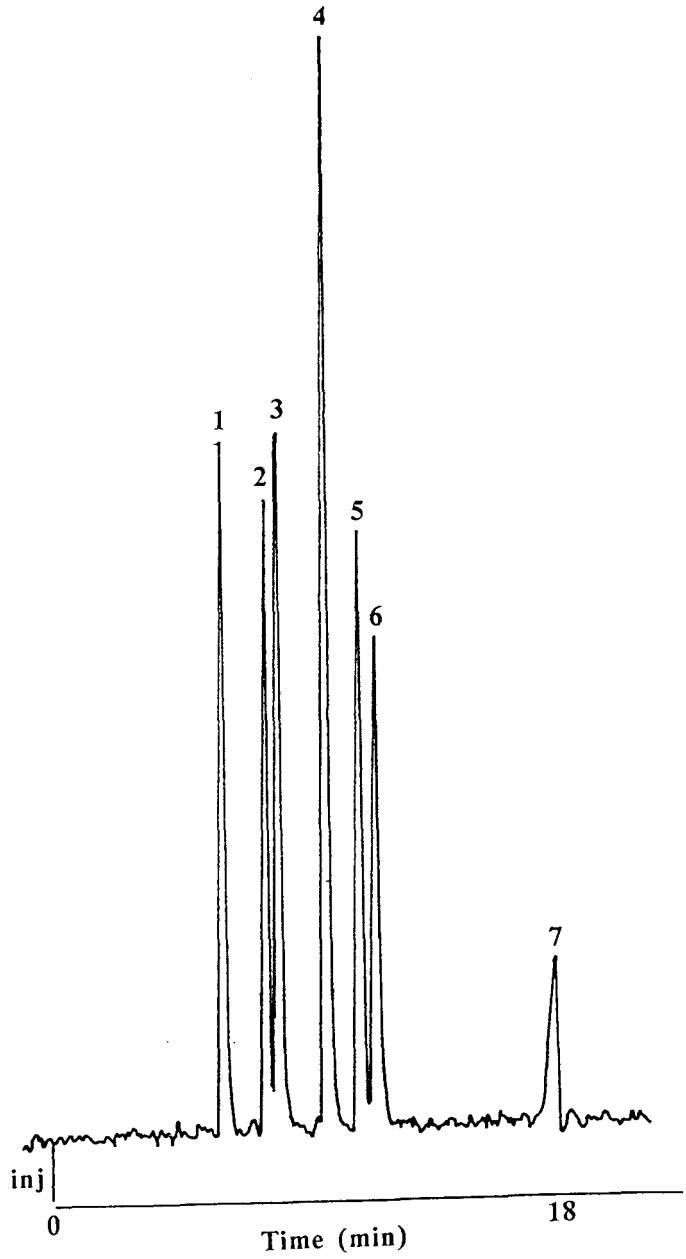

Figure 22. Deep UV thermal lens chromatogram of the substituted benzene mixture recorded using a laser power of 100 mW. Mobile phase: methanol/water (70:30, v/v), flow rate: 30 μL/min.

Table 13. Deep UV Thermal Lens Chromatogram Peak Assignments, Retention Times and Injected Quantities For the Substituted Benzenes Mixture Separation

Peak No.	Compound	Retention Time (min)	Quantity Injected (ng)
1	phenol	5.8	100
2	benzaldehyde	7.4	256
3	acetophenone	7.8	256
4	nitrobenzene	9.5	77
5	methylbenzoate	10.8	758
6	anisole	1	640
7	toluene	17.8	71,000

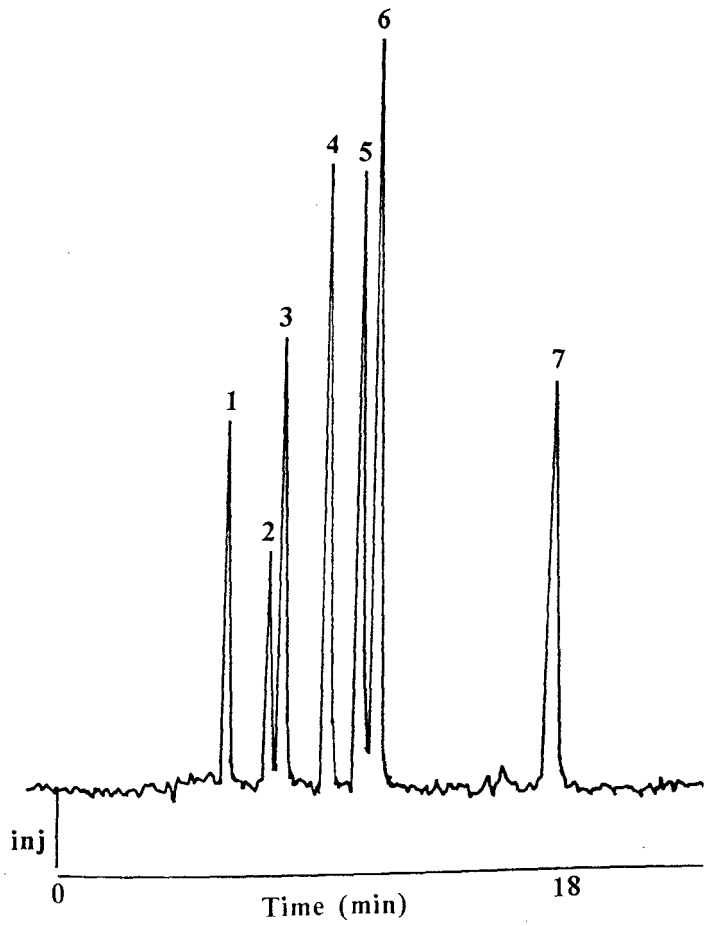

Figure 23. Deep UV thermal lens chromatogram of the substituted benzenes mixture recorded using a laser power of 310 mW. Refer to Table 13 for peak assignments and retention times.

Since all conditions remain the same during the recording of both chromatograms, excluding the laser power difference, the changes in peak height have to reflect a change in the proportions of the 275 and 306 nanometer content of the deep UV line as the current across the plasma tube is increased. Thus, caution must be exercised when trying to achieve lower thermal lens detection limits by increasing the laser power if a polychromatic line is used.

Another practical application of the deep UV thermal lens HPLC detection is shown in Figure 24. This figure represents the separation of a pharmaceutical mixture containing theophylline, caffeine, phenacetin, acetaminophen and acetylsalicylic acid recorded using a laser power of 100 mW. A mobile phase composed of methanol/water, 60:40 (v/v) and flow rate of 20 μL/min are used. Table 14 lists the peak assignments, retention times and detection limits for the five components. These substances are routinely analyzed for in blood and cold medications using analytical columns (93-96). However, gradients and mixed mobile phases involving acetate and phosphate buffers are often needed to separate the components resulting in much of the analysis time being spent re-equilibrating the column if multiple injections are made. Also, careful attention must be paid to insure that buffer salts do not precipitate on the column. Since the present detection system employs a microbore column the analysis is simplified in that an

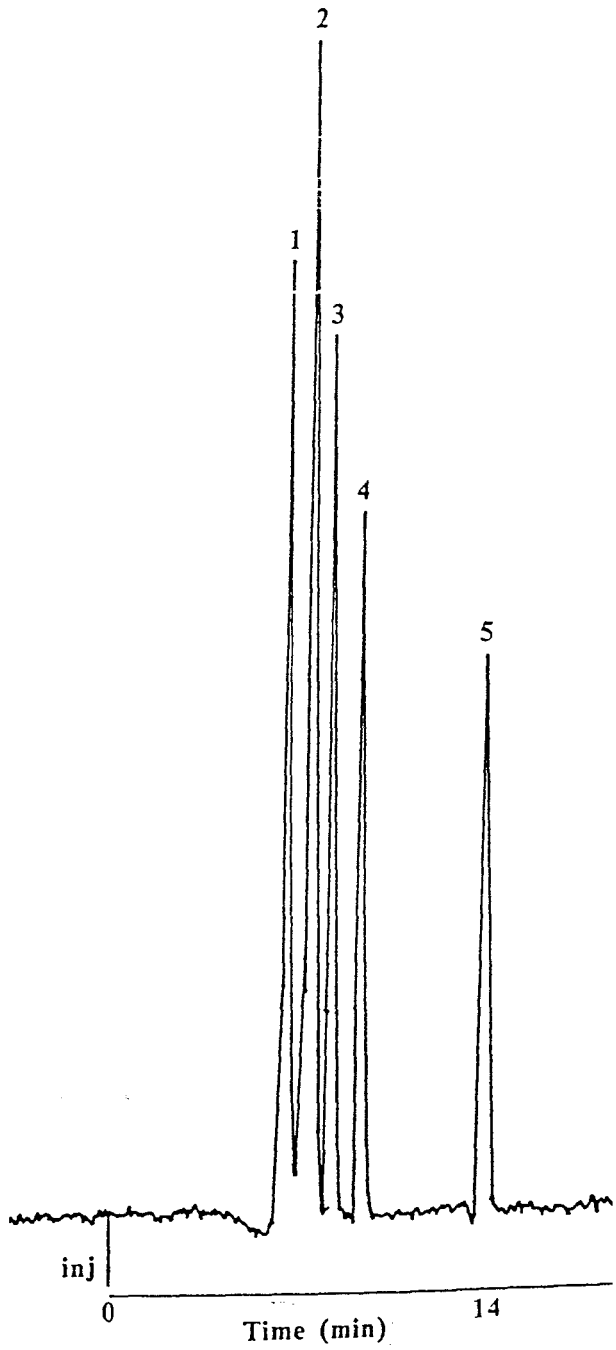

Figure 24. Deep UV thermal lens chromatogram of the pharmaceutical mixture. Mobile phase: methanol/water (60:40, v/v), flow rate: 20 μL/min, P = 100 mW.

Table 14. Deep UV Thermal Lens Chromatogram Peak Assignments, Retention Times and Detection Limits For the Pharmaceutical Mixture Separation

Peak No.	Compound	Retention Time (min)	Mass Detection Limit (ng)
1	acetylsalicyclic acid	6.4	2.9
2	acetaminophen	7.1	2.4
3	theophylline	7.8	1.2
4	caffeine	9.0	1.6
5	phenacetin	13.7	5.1

isocratic, near baseline separation of all five components is accomplished using a simple mobile phase of methanol and water in only 14 minutes. Furthermore, the observed concentration detection limits for theophylline, acetaminophen, and acetylsalicylic acid are comparable to those obtained by Kinberger and Holmen (93) in the determination of the three compounds in blood using a reverse phase analytical column and conventional UV detection at 280 nm. However, the mass detection limits achieved with the current system are an order of magnitude smaller than those reported by Kinberger and Holmen, most likely because a microbore column is used. A mass detection limit (S/N=2) of 150 pg of caffeine and 100 pg of theophylline in cocoa accomplished using a microbore column and conventional UV detection at 280 nm has been reported (97). The present detection limits were obtained with a laser power of only 100 mW and in theory, can be lowered to the picogram level by operating at higher laser powers.

CONCLUSIONS

A new type of laser-based microbore HPLC detector has been presented. By using a square sided capillary tube as a flow cell and positioning it at z_{opt} beyond the focussing lens simultaneous thermal lens and fluorescence chromatograms were obtained. The thermal lens signal is recorded by monitoring the beam center intensity of a HeNe probe laser which propagates collinear with the excitation beam while fluorescence is collected at 90 degrees from the excitation beam. The detector's versatility was demonstrated by recording simultaneous thermal lens/fluorescence chromatograms of a standard PAH mixture and the neutral PAH fraction of solvent refined coal using deep and near UV, as well as 457.8 nm excitation. Analysis of these chromatograms revealed that their overall appearance was a direct reflection of the complementary nature which exists between the thermal lens effect and fluorescence. In specific, the relative peak height differences between thermal lens and fluorescence chromatograms was governed by Q_f, $1\text{-}Q_f$, and the transmittance range, T, of the fluorescence optical window. The relative peak height difference between thermal lens chromatograms of the same mixture recorded at different wavelengths was governed by the extinction coefficient and $1\text{-}Q_f$ magnitudes the components had for each wavelength.

The best thermal lens detection limit achieved was 93 femtograms (0.46 femtomole) of pyrene using a near UV pump laser power of 1000 mW. Lower thermal lens detection limits most likely could be obtained by altering the optical configuration such that the pump beam is focussed into the flow cell and the probe beam is focussed at z_{opt}. Also, compounds having minimal fluorescence quantum efficiencies should be used. These changes could possibly expand the currently observed thermal lens linear dynamic range. The lowest fluorescence detection limit obtained was 29 femtograms (0.14 femtomole) of fluoranthene using a power of 150 mW. Better fluorescence detection limits would also be observed by focussing the excitation beam into the flow cell, using a higher laser power and maximizing the transmittance range of the fluorescence optical window.

The detector's versatility was further emphasized by demonstrating that thermal lens detection for liquid chromatography in the ultraviolet is now conveniently possible. Thermal lens detection is no longer restricted to compounds which absorb at visible wavelengths since continuous wave lasers are now commercially available which have the capability of producing low power ultraviolet beams. As a result, the range of compounds which can be detected by the thermal lens effect has been expanded. This was illustrated by recording chromatographic separations of a substituted benzenes and a pharmaceutical mixture.

CHAPTER 4

FUTURE RESEARCH

Rotoreflected double-beam thermal lens spectrometer: A method for transforming the current system into a multi-wavelength instrument is proposed. A major limitation of the present rotoreflected double-beam thermal lens spectrometer is its inability to operate at wavelengths other than 515.5 nm. This restriction is imposed by the retardation plates since the wavelength used and the desired state of polarization rotation dictates the thickness of each plate. Thus, if wavelengths other than 515.5 nm are to be used with the current spectrometer separate half-wave and quarter-wave plates would be required for each wavelength employed. This is very impractical since every time the wavelength is changed the retardation plates would also have to be changed requiring substantial realignment of the entire optical configuration. However, this handicap can be circumvented if a Soleil-Babinet compensator and a Pockels cell are incorporated into the present system.

A Soleil-Babinet compensator is an optical device that functions as a retardation plate which can be adjusted

to achieve a specific retardation at any wavelength between 250 nm and 3.5 micrometers (98, 99). It is composed of two wedge shaped pieces of crystalline quartz which are placed on top of each other. One wedge is fixed while the other's movement is controlled by means of a micrometer. In this manner the total thickness of quartz that the light travels through can be varied. Thus, the compensator can be adjusted to produce a chosen retardation for any wavelength within the specified range.

A Pockels cell is an electrooptic instrument which can be used to modulate a laser beam by encoding it with alternate states of orthogonal polarization (99, 100). It consists of a crystalline birefringent material to which an electric field is applied which induces a change in the materials birefringence. Thus, a laser beam passing through the material while the electric field is applied will undergo a change in polarization. The magnitude of the electric field applied across the crystal dictates the degree to which the polarization of the laser beam will be altered. By controlling the frequency at which the electric field is turned on and off, with a waveform generator, polarization modulated beams can be produced with modulation frequencies on the order of megahertzs.

If the half-wave plate and chopper are replaced by a Pockels cell and quarter-wave plates are replaced with Soleil-Babinet compensators then the present configuration

would be transformed into a multiwavelength spectrometer. To accomodate a laser wavelength change the only manipulations required would be to adjust the Soleil-Babinet compensator micrometers and the applied voltage to the Pockels cell. The need to purchase separate half-wave and quarter-wave plates for each laser wavelength would be eliminated as would the necessity of gross realignment at every wavelength change. More significant would be the spectrometer's potential to function in the ultraviolet allowing a much greater range of samples to be analyzed. In addition, a sensitivity enhancement should be realized as a result of replacing the chopper with the Pockels cell. This would result from modulation frequencies on the order of megahertzs producing a much stronger steady state thermal lens in the sample compared to that obtained at 1.5 kHz. Also, noise due to chopper blade cutting imperfections and chopper vibration would be eliminated since a mechanical chopper would no longer be a part of the configuration.

Another way to lower the noise in the system is to incorporate a spatial filter into the configuration prior to the limiting aperture (101). Dust and dirt on the lenses and mirrors interact with the beam to cause interference patterns which are responsible for the speckle observed when the laser spot is observed in the far-field. There is a finite amount of noise associated with laser speckle which, if eliminated, could lower the present de-

tection limits. The spatial filter is comprised of a very short focal length lens and a pinhole, whose diameter is slightly less than that of the focussed beam, which is placed at the lens focal point. The beam is positioned such that only the beam center is allowed to pass through the pinhole. Since the beam interferences associated with dust and dirt on the optics are concentrated at the outer portions of the beam, they will not pass through the pinhole and the emerging beam will be devoid of speckle.

Microbore HPLC thermal lens/fluorescence detector: A method for improving the thermal lens and fluorescence detection limits of the current detector is proposed.

Ultimate detection limits in fluorescence determinations are limited by the magnitude of background noise present in the system. In theory, drastic signal-to-noise ratio enhancement can be achieved by eliminating, from the fluorescence of interest, the two largest contributors to signal background: solvent Raman scatter and scattered excitation radiation. Generally, extraneous excitation radiation is reduced to a minimum through careful baffling of the emission collection optics and by using appropriate interference filters or a monochromator positioned before the photomultiplier tube. However, reduction of solvent Raman scatter poses a more difficult challenge since overlap of Raman emission with the fluorescence region usually is the case. Often the overlap is so severe that it is impossible

to extract a portion of the fluorescence that does not contain any solvent Raman emission using conventional collection optics. A method called phase resolved background suppression has been developed, by Demas and Keller (102), using principles of phase resolved spectroscopy to circumvent this problem.

Demas and Keller developed this technique to resolve severely overlapping fluorescence from Raman scatter. Others have used the technique to resolve heterogeneous emissions (103-107). The theory of phase-resolved spectroscopy relies on the premise that heterogenous emission can be resolved into its component emissions assuming that the lifetimes of the luminescent species are different (102, 108). Specifically, if sinusoidally modulated light is used to excite a mixture containing components A and B the resulting emission will also be sinusoidally modulated and the emission phase will be shifted relative to the excitation. If the emission lifetime of component A is greater than that of component B, the emission of component A will lag behind that of B. In other words, a difference in the phase angles of the two emissions results from the corresponding difference in their emission lifetimes. Successful resolution of two overlapping emissions exploits the phase angle difference between the two components. An emissive component's phase angle, ϕ_i depends on the life-

time of the component, τ_i and the excitation modulation frequency, f according to the following relationship:

$$\phi_i = \arctan(2\pi f\tau_i) \qquad (16)$$

To achieve appreciable phase differences between components whose lifetimes are on the order of nanoseconds requires modulation frequencies in the megahertz regime (102). Modulation of laser beams at such high frequencies are accomplished by using an acoustooptic modulator.

Resolution of the component emissions is achieved by using a phase sensitive detector (lock-in amplifier). The lock-in amplifier output, I, for two emissive components is defined by the following equation (104, 105):

$$I = 2^{-\frac{1}{2}}[K_A\cos(\phi_A-\phi_D) + K_B\cos(\phi_B-\phi_D)] \qquad (17)$$

where ϕ_A and ϕ_B are the component phase angles, ϕ_D is the detector phase angle and K_A and K_B are constants which depend on the observation wavelength, concentrations, demodulation factors, extinction coefficients, and quantum yields of the components (102, 108). If component A corresponds to unwanted solvent Raman emission then by inspection of equation 17 this component can be suppressed if $\phi_A-\phi_D=90°$. In practice this is accomplished by setting the lock-in detector phase such that it is 90° out of phase with respect to component A. Only emission due to component B will be detected with a reduction corresponding to a factor of $\sin(\phi_B-\phi_A)$ of its original intensity (102).

An improvement in the fluorescence detection limits obtained with the present detector might be possible since this phase resolution offers a way to suppress mobile phase Raman scatter. First, the lifetime of the sample emission would have to be experimentally determined. Established techniques for determining emissive lifetimes exist in the literature (51, 109, 110). Once the sample emission lifetime is known, the phase angle shift relative to the excitation phase can be calculated from equation 16. Knowing the value for the sample emission phase angle shift would allow the lock-in amplifier phase to be set accordingly to null out the Raman scatter.

Application of the phase resolve background suppression technique to the thermal lens/fluorescence liquid chromatography detector would present a situation where thermal lens detection limits could also be improved over those currently observed. However, modification of the optical configuration would be necessary since modulation at megahertz frequencies would produce a steady state thermal lens making the pump/probe approach useless. The magnitude of the steady state thermal lens produced in the sample cell would have to be compared to a reference signal using a differential configuration similar to that developed by Skogerboe and Yeung (50). An illustration of the modified dual detector is presented in Figure 25. After exiting the laser cavity the beam passes through an acous-

tooptic modulator driven by a waveform generator. The emerging zeroth-order and first-order beams would be used as respective sample and reference beams. A lens placed after the Bragg cell would direct the sample beam into the flow cell positioned at z_{opt}. An aperture is placed in the sample beam path so that the beam center intensity change can be monitored. Both sample and reference beams strike a photodiode and a differential output is produced by lock-in amplifier #2. Fluorescence emission would be collected perpendicular to the sample cell using an appropriate lens and filter system before a photomultiplier tube. The signal from the photomultiplier tube would be sent to lock-in amplifier #1 which would be set at the proper phase to null out the mobile phase Raman scatter.

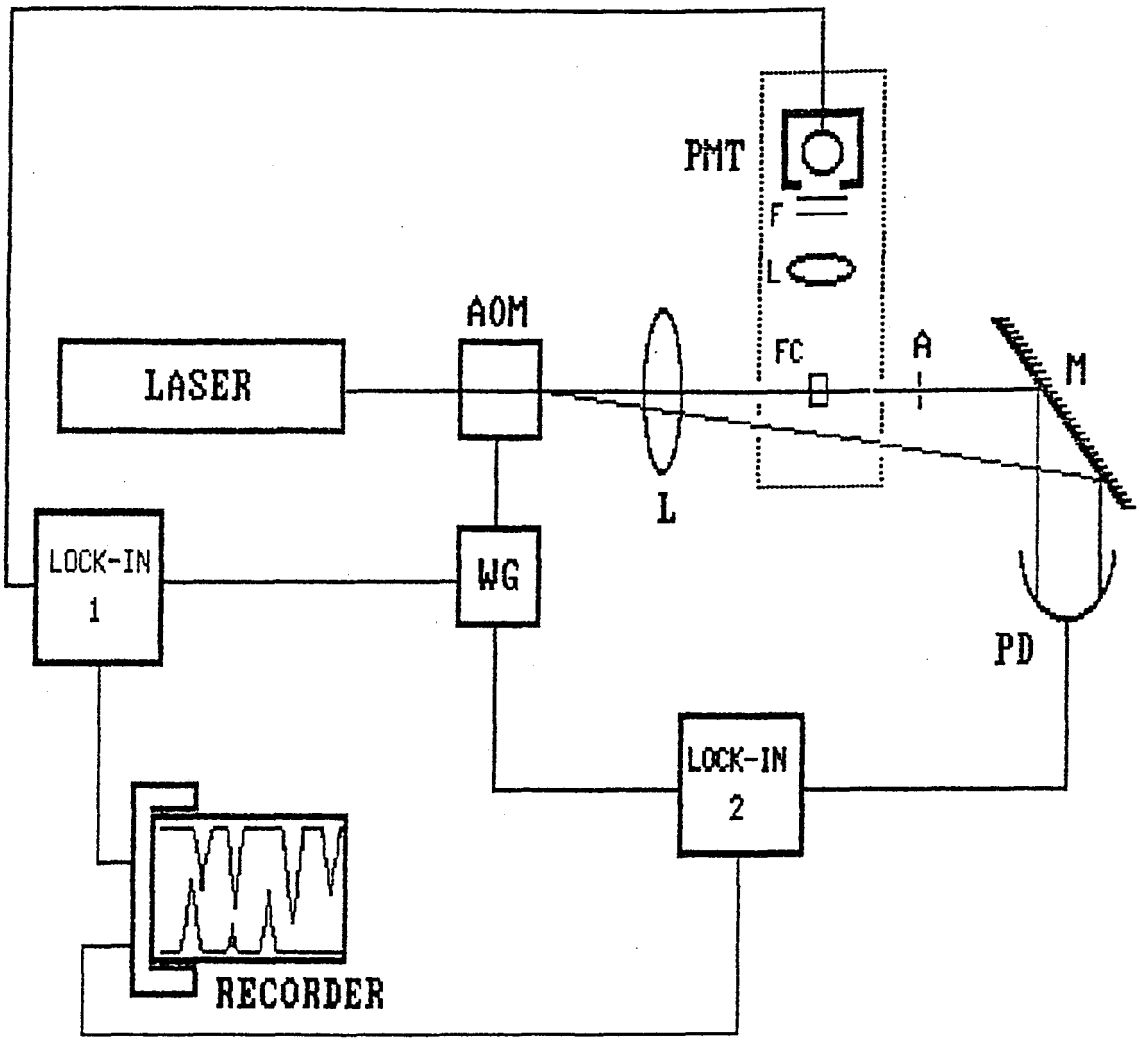

Figure 25. Modified dual detector: AOM, acoustooptic modulator; WG, waveform generator; PMT, photomultiplier tube; L, lens; FC, flow cell; F, filter; M, mirror; PD, photodiode.

REFERENCES

1. Gordon, J. P.; Leite, R. C. C.; Moore, R. S.; Porto, S. P. S.; Whinnery, J. R. J. Appl. Phys., **1964**, 36, 3.

2. Harris, J. M.; Dovichi, N. J. Anal. Chem., **1980**, 52, 695A.

3. Leite, R. C. C.; Moore, R. S.; Whinnery, J. R. Appl. Phys. Lettr., **1964**, 5, 141.

4. Solimini, D. J. J. Appl. Phys., **1966**, 37, 3314.

5. Stone, J. J. Opt. Soc. Amer., **1972**, 62, 327.

6. Dabby, F. W.; Gustafson, T. K.; Whinnery, J. R.; Kohnzadeh, Y. Appl. Phys. Lettr., **1970**, 16, 362.

7. Hu, C.; Whinnery, J. R. Appl. Opt., **1973**, 12, 72.

8. Swofford, R. L.; Long, M. E.; Albrecht, A. C. J. Chem. Phys., **1976**, 65. 179.

9. Long, M. E.; Swofford, R. L.; Albrecht, A. C. Science, **1979**, 191, 183.

10. Swofford, R. L.; Morrell, J. A. J. Appl. Phys. **1976**, 49, 3667.

11. Swofford, R. L.; Long, M. E.; Albrecht, A. C. J. Chem. Phys., **1976**, 65, 179.

12. Twarowski, A. J.; Kliger, D. S. Chem. Phys., **1977**, 20, 253.

13. Vaida, V.; Turner, R. E.; Casey, J. L.; Colson, S. D. Chem. Phys. Lett., **1978**, 20, 25.

14. Dovichi, N. J.; Harris, J. M. Anal. Chem., **1979**, 51, 728.

15. Imasake, T.; Kazuhiko, M.; Ishibashi, N. Anal. Chemi. Act., **1980**, 115, 407.

16. Kazuhiko, M.; Imasake, T.; Ishibashi, N. Anal. Chemi. Act., **1981**, 124, 381.

17. Fujiwara, K.; Wei, L.; Uchiki, H.; Shimokisishi, F.; Kobayashi, T. Anal. Chem., 1982, 54, 2026.

18. Mori, K.; Imasaka, T.; Ishibashi, N. Anal. Chem., 1983, 55, 1075.

19. Carter, C. A.; Brady, J. M.; Harris, J. M. Appl. Spectrosc., 1982, 36, 309.

20. Higashi, T.; Imasaka, T.; Ishibashi, N. Anal. Chem. 1983, 55, 1907.

21. Sheldon, S. J.; Knight, L. V.; Thorne, J. M. Appl. Opt., 1982, 21, 1663.

22. Carter, C. A.; Harris, J. M. Appl. Spectrosc., 1983, 37, 166.

23. Berthoud, T.; Delorme, N.; Mauchien, P. Anal., Chem., 1985, 57, 1216.

24. Dovichi, N. J.; Harris, J. M. Anal. Chem., 1980, 52, 2338.

25. Grishko, V. I.; Yudelevich, I. G.; Grishko, V. P. Anal. Chim. Act., 1985, 176, 51.

26. Berthoud, T.; Delorme, N. Appl. Spectrosc., 1987, 41, 15.

27. Termae, M.; Winefordner, J. S. Appl. Spectrosc., 1987, 41, 164.

28. Jansen, K. L.; Harris, J. M. Anal. Chem., 1985, 57, 2434.

29. Yang. Y. Anal. Chem., 1984, 56, 2336.

30. Pang, T. J.; Morris, M. D. Appl. Spectrosc., 1985, 39, 90.

31. Yang, Y.; Hall, S. C.; De La Cruz, M. S. Anal. Chem., 1986, 58, 758.

32. Yang, Y. Anal. Chem., 1986, 58, 1420.

33. Erskine S. R.; Foley, M. C.; Bobbit, D. R. Appl. Spectrosc., 1987, 41, 1189.

34. Yang, Y.; Hairrell, R. E. Anal. Chem., 1984, 56, 3002.

35. Dovichi, N. J.; Nolan, T. G.; Weimer, W. A. Anal. Chem., 1984, 56, 1700.

36. Nolan, T. G.; Weimer, W. A.; Dovichi, N. J. Anal. Chem., 1984, 56, 1704.

37. Ishibashi, N.; Imasade, T.; Miyaishi, K. Anal. Chem., 1982, 54, 2039.

38. Jansen, K. L.; Harris, J. M. Anal. Chem., 1985, 57, 1698.

39. Dovichi, N. J.; Harris, J. M. Anal. Chem., 1981, 53, 689.

40. Leach, R.; Harris, J. M. J. Chromatogr., 1981, 218, 15.

41. Carter, C. A.; Harris, J. M. Anal. Chem., 1981, 53, 106.

42. Buffett, C. E.; Morris, M. D. Anal. Chem., 1982, 54, 1824.

43. Pang, J. T.; Morris, M. D. Anal. Chem., 1984, 56, 1467.

44. Pang, T. J.; Morris, M. D. Anal. Chem., 1985, 57, 2153.

45. Pang. T. J.; Morris, M. D. Anal. Chem., 1985, 57, 2700.

46. Buffett, C. E.; Morris, M. D. Anal. Chem., 1983, 55, 378.

47. Nolan, T. G.; Hart, B. K.; Dovichi, N. J. Anal. Chem., 1985, 57, 2703.

48. Nolan, T. G.; Dovichi, N. J.; Anal. Chem., 1987, 59, 2803.

49. Nolan, T. G.; Bornhop, D. J.; Dovichi, N. J. J. Chromatogr., 1987, 384, 189.

50. Skogerboe, K. J.; Yeung, E. S. Anal. Chem., 1986, 58, 1014.

51. Lakowicz, J. R. "Principles of Fluorescence Spectroscopy; Plenum Press: New York, 1983.

52. Berlman, I. B. "Handbook of Fluorescnece Spectra of Aromatic Molecules"; Academic Press: New York, 1971.

53. Gooijer, C.; Baumann, R. A.; Hofstraat, J. W. J. Chrom Sci., 1986, 24, 361.

54. Willard, H. H.; Merritt, L. L.; Dean, J. H. "Instrumental Methods of Analysis", 5th ed.; D. Van Nostrand Co.: New York, 1974.

55. Lawrence, J. F.; Frei, R. W. "Chemical Derivatization in Liquid Chromatography"; Elsevier: Amsterdam, 1976.

56. Blau, K.; King, G. "Handbook of Derivatives for Liquid Chromatography"; Heyden and Smith: London, 1977.

57. Knapp, D. R. "Handbook of Analytical Derivatization Reagents"; Wiley: New York, 1979.

58. Imai, K; Toyo'oka, T.; Miyano, H. Analyst, 1986, 109, 1365.

59. Lingeman, H.; Underberg, W. J. M.; Takadate, A.; Hulshoff, A. J. Liq. Chromatogr., 1985, 8, 789.

60. Lawrence, J. F. J. Chromatogr. Sci., 1985, 23, 484.

61. Yeung, E. S.; Sepaniak, M. J. Anal. Chem., 1980, 52, 1465A.

62. Imasaka, T.; Ogawa, T.; Ishibashi, N. Anal. Chem., 1979, 51, 502.

63. Hieftje, G. "New Applications of Lasers to Chemistry"; American Chemical Society: Washington D. C., 1978.

64. Topp, M. R. Appl. Spectrosc. Rev., 1979, 14, 1.

65. Wirth, M. J.; Lytle, F. E. Anal. Chem., 1977, 49, 2054.

66. Folestad, S.; Galle, B.; Josefsson, B. J. Chromatogr. Sci., 1985, 23, 273.

67. Kucera, P. "Microbore High-Performance Liquid Chromatography"; Elsevier: Amsterdam.

68. Guthrie, E. J.; Jorgenson, J. W.; Dluzneski, P. R. J. Chromatogr. Sci., 1984, 22, 171.

69. Diebold, G. J.; Zare, R. N. Science, 1977, 196, 1439.

70. Lidofsky, S. D.; Imasake, T.; Zare, R. N. Anal. Chem., 1979, 51, 1602.

71. Diebold, G. J.; Karny, N.; Zare, R. N. Anal. Chem., 1979, 51, 67.

72. Folestad, S.; Johnson, L.; Joseffson, B. Anal. Chem., 1982, 54, 925.

73. Hershberger, L. W.; Callis, J. B.; Christian, G. H. Anal. Chem., 1979, 51, 1444.

74. McGuffin, V.; Zare, R. N. Appl. Spectrosc., 1985, 39, 847.

75. Sepaniak, M. J.; Yeung, E. S. Anal. Chem., 1977, 49, 1554.

76. Sepaniak, M. J.; Yeung, E. S. J. Chromatogr., 1980, 190, 377.

77. Gluckman, J.; Shelly, D.; Novotny, M. J. Chromatogr., 1984, 317, 443.

78. Roach, M. C.; Harmony, M. D. Anal. Chem., 1987, 59, 411.

79. Sepaniak, M. J.; Yeung, E. S. J. Chromatogr., 1981, 211, 95.

80. Mho, Sun-Il; Yeung, E. S. Anal. Chem., 1985, 57, 2253.

81. Carter, C. A.; Harris, J. M. Anal. Chem., 1984, 56, 922.

82. Vassilaros, D. L.; Later, D. W.; Lee, M. L.; Bartle, K. D.; Kong, R. C. Anal. Chem., 1981, 53, 1612.

83. Least squares fit of the data is performed using a template developed by M. De La Cruz with LOTUS 123 software.

84. Reference chromatogram supplied with standard PAH mixture, Supelco, Inc.

85. Novotny, M.; Hirose, A.; Wiesler, D. Anal. Chem., 1984, 56, 1243.

86. Blumer, M. Scientific American, 1976, 234, 35.

87. Andreolini, F.; Borra, C.; Wiesler, D.; Novotny, M. J. Chromatogr., 1987, 406, 375.

88. Allen, T. W.; Hurtubise, R. J.; Silver, H. F. Anal. Chimi. Acta, 1982, 141, 411.

89. Schweighardt, F. K.; Thames, B. M. Anal. Chem., 1978, 50, 1381.

90. Lai, E. P.C.; Su, S. Y.; Voigtman, E., Winefordner, J. D. Chromatographia, 1982, 15, 645.

91. Nolan, T. G.; Hart, B. K.; Dovichi, M. J. Anal. Chem., 1985, 57, 2703.

92. Sepaniak, M. J.; Vargo, J. D.; Kettler, C. N.; Maskarinec, M. P. Anal. Chem. 1984, 56, 1252.

93. Kinberger, B; Holmen, A. J. Chromatogr. 1982, 229, 492.

94. Mineshita, S.; Eggers, R.; Kitteringham, N. R.; Ohnhaus, E. E. J. Chromatogr. 1986, 380, 407.

95. Matsushima, Y.; Nagata, Y.; Takakusagi, K.; Niyomura, M. J. Chromatogr. 1985, 332, 265.

96. Dulitzky, M.; De La Teja, E.; Lewis, H. F. J. Chromatogr. 1985, 318, 403.

97. Hurst, W. J.; Snyder K. P.; Martin, Jr., R. A. J. Chromatogr. 1985, 318, 408.

98. "Optics Guide 4", Melles Griot, 1988, 15-29.

99. Driscoll, W. G.; Vaughan, W. "Handbook of Optics", McGraw-Hill: New York, 1978.

100. Siegman, A. E. "Lasers", University Science Books: Mill Valley, California, 1986.

101. Conversation with R. Haidle, 3-27-89.

102. Demas, J. N.; Keller, R. A. Anal. Chem., 1985, 57, 538.

103. Lakowicz, A. R.; Cherek, H.; Keating-Nakamoto, S. M. Anal. Chem., 1987, 59, 271.

104. McGown, L. B.; Bright, F. V. Anal. Chim. Act., 1985, 169, 117.

105. McGown, L. B.; Bright, F. V. Anal. Chem., 1985, 57, 2877.

106. McGown, L. B.; Bright, F. V. Anal. Chem., 1985, 57, 55.

107. Lakowicz, J. R.; Cherek, H.; Keating-Nakamoto, S. Anal. Biochem., 1985, 148, 349.

108. Jameson, D. M.; Graffton, E.; Hall, R. D. Appl. Spectrosc. Rev., 1984, 20, 55.

109. Dalbey, R. E.; Weiel, J.; Perkins, W. J.; Yount, R. J. Biochem. Biophys. Methods, 1984, 9, 251.

110. Hieftje, G. M.; Ramsey, J. M.; Haugen, G. R. ACS Symp. Symp., 1978, 85, 118.

111. Friedel, R. A.; Orchin, M. "Ultraviolet Spectra of Aromatic Compounds" John Wiley and Sons: New York, 1951.

112. Lang, L. "Absorption Spectra in the Ultraviolet and Visible Region" Academic Press: New York, 1966.

113. Serial Number 61, "Selected Ultraviolet Spectral Data" Thermodynamics Research Center Hydrocarbon Project, College Station, Texas, 1964.

114. Schwarz, F. P.; Wasik, S. P. Anal. Chem., 1976, 48, 524.

115. Dawson, W. R. J. Opt. Soc. Amer., 1968, 58, 222.

APPENDIX I

APPENDIX I

The equation describing the differential signal produced by the rotoreflected double-beam thermal lens spectrometer is derived below using the following diagram and definitions:

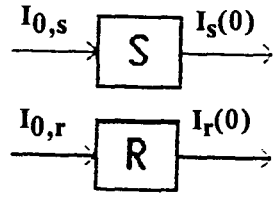

where $I_{o,s}$ = beam center intensity before the sample cell
$I_s(0)$ = sample beam center intensity after exiting the cell at t=0
$I_{o,r}$ = beam center intensity before the reference cell
$I_r(0)$ = reference beam center intensity after exiting the cell at t=0.

The derivation starts with the equation for the steady state thermal lens: $\Delta I/I(0) = 2.303EA$ where $\Delta I = I(0)-I(\infty)$. This equation can be used to describe the thermal lens signals produced in the sample and reference cells of the rotoreflected double-beam configuration. For the sample cell thermal lens

$$[I_s(0)-I_s(\infty)]/I_s(0) = 2.303EA_s \qquad (1)$$

or

$$I_s(0)-I_s(\infty) = 2.303EA_sI_s(0) \qquad (2)$$

Similarly, for the reference cell thermal lens

$$[I_r(0)-I_r(\infty)]/I_r(0) = 2.303EA_r \qquad (3)$$

and

$$I_r(0)-I_r(\infty) = 2.303EA_rI_r(0). \quad (4)$$

The lock-in amplifier measures the difference between the sample and reference cells. Thus, equation 3 is subtracted from equation 2 to give the following:

$$I_s(0)-I_s(\infty)-I_r(0)+I_r(\infty) = 2.303E[A_sI_s(0) - A_rI_r(0)] \quad (5).$$

If an offset is present between the sample and reference beams then $I_s(0)$ does not equal $I_r(0)$. By rearranging and letting $\Delta I(0)=I_s(0)-I_r(0)$ equation 5 can be expressed as

$$I_s(\infty)-I_r(\infty) = -2.303E[A_sI_s(0) - A_rI_r(0)] + \Delta I(0) \quad (6).$$

The signal that is actually measured corresponds to the difference between the beam center intensities produced by the steady-state thermal lenses in the sample and reference cells or $\Delta I=I_s(\infty)-I_r(\infty)$ so

$$\Delta I = -2.303E[A_sI_s(0) - A_rI_r(0)] + \Delta I(0) \quad (7).$$

If there is an offset between the sample and reference beams then $I_s(0)-I_r(0)$ will be a function of the intensity difference between sample and reference beams <u>before</u> they enter the cells as well as the difference in the sample and reference beam center intensities due to the difference in absorbance between cells, ΔI_{abs}. This relationship is described by equation 8:

$$I_s(0)-I_r(0) = \Delta I_o + \Delta I_{abs} \quad (8)$$

where $\Delta I_o = I_{o,s} - I_{o,r}$.

If $A_s - A_r$ is defined as ΔA and Beer's Law is applied then

$$\Delta I_{abs} = 2.303 I_o \Delta A \quad (9).$$

Substituting equation 9 into equation 8 and rearranging gives

$$I_s(0) = \Delta I_o + 2.303 I_o \Delta A + I_r(0) \quad (10).$$

Substitution of equation 10 into equation 7 gives

$$\Delta I = -2.303E[A_s(\Delta I_o + 2.303 I_o \Delta A + I_r(0)) - A_r I_r(0)] + \Delta I(0) \quad (11)$$

$$= -2.303E[A_s \Delta I_o + 2.303 I_o A_s \Delta A + I_r(0)\Delta A] + \Delta I(0) \quad (12).$$

Since $I_0 \sim I_r(0)$ then the differential signal can be expressed as

$$\Delta I = -2.303E[A_s \Delta I_o + 2.303 I_o A_s \Delta A + \Delta A I_o] + \Delta I(0) \quad (13).$$

If no offset is present between the sample and reference beams then $\Delta I_o = 0$ and $\Delta I(0) = 0$ and equation 13 reduces to

$$\Delta I = -2.303E(2.303 I_o A_s \Delta A + \Delta A I_o) \quad (14).$$

Equation 14 can be rewritten as

$$\Delta I = -2.303 E I_o \Delta A(2.303 A_s + 1) \quad (15).$$

Since A_s is very small then $(2.303A_s + 1)$ is approximately equal to unity and the equation reduces to

$$\Delta I = -2.303EI_o\Delta A \qquad (16).$$

APPENDIX II

Appendix II

The total volume, V_T, that a component experiences upon elution from the column is comprised of the volume of the tubing connecting the column to the flow cell, V_t, and the volume of the flow cell, V_c or

$$V_T = V_t + V_c \quad (1)$$

where

$$V_t = Pr^2l \quad (2)$$

with r = tube radius = 6.4×10^{-3} cm
l = tube length = 5.0 cm.

For the Kratos flow cell:

$V_c = 0.5\ \mu L$ (see reference 46)

$V_t = (P)(6.4 \times 10^{-3}\ cm)^2(5.0\ cm)(10^{-3}\ L/mL)(10^6\ \mu L/1) = 0.6 \mu L$

and

$V_T = 0.6\ \mu L + 0.5\ \mu L = 1.1\ \mu L.$

For the capillary flow cell:

$$V_c = lwh \quad (3)$$

with $l = 0.05$ cm
$w = 0.05$ cm
$h = 1.5$ cm.

$V_c = (0.05\ cm)^2(1.5\ cm)(10^{-3}\ L/mL)(10^6\ \mu L/L) = 4.0\ \mu L$

$V_t = 0.6\ \mu L$

and

$V_T = 4.0\ \mu L + 0.6\ \mu L = 4.6\ \mu L.$

APPENDIX III

APPENDIX III

Extinction Coefficient, ϵ, Values For Mixture Components at 275 and 306 Nanometers

Compound	ϵ275	ϵ306	Solvent	Ref.
toluene	100	----*	cyclohexane	111
anisole	1000	----*	cyclohexane	111
phenol	10,000	----*	cyclohexane	111
nitrobenzene	5610	7610	ethanol	112
benzaldehyde	1650	820	ethanol	112
methylbenzoate	796	2	methanol	**
acetophenone	920	69	methanol	**
acetylsalicyclic acid	820	360	methanol	113
phenacetin	3330	240	ethanol	112
caffeine	9520	1560	ethanol	112
theophylline monohydrate	9250	10	water	112
acetaminophen	2780	277	methanol	**
phenanthrene	16,000	250	cyclohexane	111
anthracene	320	630	cyclohexane	111
fluoranthene	25,000	3200	95% ethanol	111
pyrene	10,000	13,000	95% ethanol	111
triphenylene	16,000	1800	ethanol	111
benzo[a]anthracene	40,000	4000	95% ethanol	111
chrysene	16,000	13,000	95% ethanol	111
benzo[e]pyrene	40,000	18,000	ethanol	111
benzo[a]pyrene	32,000	35,000	ethanol	111
perylene	2500	790	95% ethanol	111

*no appreciable absorbance at 306 nanometers

**experimentally determined

Extinction Coefficient, ϵ, Values For PAHs at 334, 351 and 363 Nanometers

Compound	ϵ334	ϵ351	ϵ363
phenanthrene	112	----*	----*
anthracene	3600	4000	1600
fluoranthene	5000	6300	1600
pyrene	45,700	420	300
triphenylene	350	71	----*
benzo[a]anthracene	4500	3300	2800
chrysene	630	320	250
benzo[e]pyrene	11,200	1600	501
benzo[a]pyrene	5600	10,000	22,000
perylene	1100	1800	4200

*no appreciable absorbance

Solvents and references are the same as listed in the preceeding table.

Quantum Efficiency, Q_f, Values For PAHs

Compound	Q_f	Solvent	Reference
anthracene	0.30	ethanol	114
pyrene	0.72	ethanol	114
benzo[e]pyrene	0.42	ethanol	114
fluoranthene	0.21	ethanol	114
perylene	0.97	cyclohexane	52
chrysene	0.14	cyclohexane	52
triphenylene	0.08	cyclohexane	52
benzo[a]anthracene	0.20	hexane	115

APPENDIX IV

APPENDIX IV

The radius of the focussed probe beam at its waist is determined by the following equation:

$$\omega_f = \frac{\lambda f}{\pi \omega_o} = 0.01 \text{ mm}$$

Where :

λ = laser wavelength = 632.8 nm

f = lens focal length = 200 mm

ω_o = $1/e^2$ radius of probe laser beam = 0.4 mm.

To determine the probe beam radius at z_{opt} the following diagram is used:

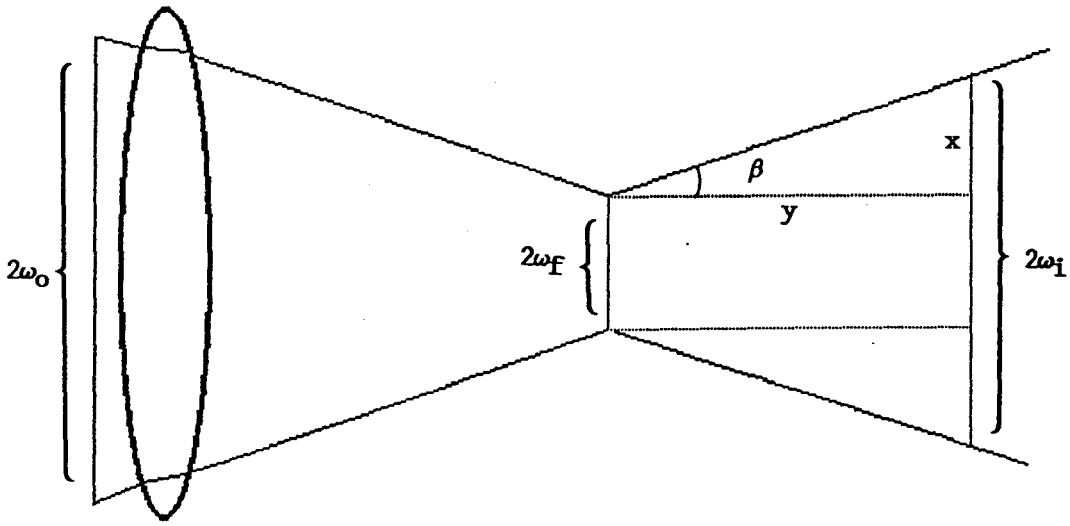

$$\beta = \sin^{-1}\left[\frac{\omega_o - \omega_f}{f}\right] = 0.11^\circ$$

$$x = y\tan\beta = 0.05 \text{ mm}$$

$$\omega_i = \omega_f + x = 0.06 \text{ mm}$$

$$\text{probe volume at } z_{opt} = \pi r^2 h = 10 \text{ nL}$$

where:

$r = \omega_i = 0.06$ mm and h = flow cell pathlength = 0.1 mm.

The pump beam volume at z_{opt} is calculated using the same procedure. However, since the deep and near UV laser lines are not monochromatic ω_o is calculated as the average ω_o of the individual wavelengths composing each line.

APPROVAL SHEET

The dissertation submitted by Steven C. Hall has been read and approved by the following committee:

Dr. Yen Yang, Director
Associate Professor, Chemistry, Loyola

Dr. Alanah Fitch
Assistant Professor, Chemistry, Loyola

Dr. David Crumrine
Associate Professor, Chemistry, Loyola

Dr. Bruno Jaselskis
Professor, Chemistry, Loyola

Mr. Rudy Haidel
Manager, Fiber Optics Lab, Northwestern University

The final copies have been examined by the director of the dissertation and the signature which appears below verifies the fact that any necessary changes have been incorporated and that the dissertation is now given final approval by the Committee with reference to content and form.

The dissertation is therefore accepted in partial fulfillment of the requirements for the degree of Doctor of Philosophy.

4-14-89
Date

Director's Signature